ELECTROSTATIC ACTUATORS FOR PORTABLE MICROFLUIDIC SYSTEMS

BY

JOSHUA TICE

DISSERTATION

Submitted in partial fulfillment of the requirements
for the degree of Doctor of Philosophy in Chemical Engineering
in the Graduate College of the
University of Illinois at Urbana-Champaign, 2012

Urbana, Illinois

Doctoral Committee:

Professor Paul J.A. Kenis, Chair
Professor Christopher A. Apblett
Professor Edmund G. Seebauer
Assistant Professor Charles M. Schroeder

Abstract

Both developed and developing nations have an urgent need to diagnose disease cheaply, reliably, and independently of centralized facilities. Microfulidic platforms are well-positioned to address the need for portable diagnostics, mainly due to their obvious advantage in size. However, most microfluidic methods rely on equipment outside of the chip either for driving fluid flow (*e.g.*, syringe pumps) or for taking measurements (*e.g.*, lasers or microscopes). The energy and space requirements of the whole system inhibit portability and contribute to costs. To capitalize on the strengths of microfluidic platforms and address the serious needs of society, system components need to be miniaturized. Also, miniaturization should be accomplished as simply as possible, considering that *simplicity* is usually requisite for achieving truly transformative technology.

Herein, I attempt to address the issue of controlling fluid flow in portable microfluidic systems. I focus on systems that are driven by elastomer-based membrane valves, since these valves are inherently simple, yet they are capable of sophisticated fluid manipulation. Others have attempted to modify pneumatic microvalves for portable applications, *e.g.*, by transitioning to electromagnetic, thermopneumatic, or piezoelectric actuation principles. However, none of these strategies maintain the proper balance of simplicity, functionality, and ease of integration. My research centers on electrostatic actuators, due to their conceptual simplicity and the efficacy of electrostatic forces on the microscale. To ensure easy integration with polymer-based systems, and to maintain simplicity in the fabrication procedure, the actuators were constructed solely from poly(dimethylsiloxane) and multi-walled carbon nanotubes. In addition, the actuators were fabricated exclusively with soft-lithographic techniques. A mathematical model was developed

to identify actuator parameters compatible with soft-lithography, and also to minimize actuation potentials while eliminating stiction. Two strategies were developed to overcome challenges with electrode screening in the presence of aqueous fluids. First, instead of using the electrostatic actuators to interact directly with aqueous solutions, the actuators were used to regulate pressurized control lines for pneumatic microvalves. Secondly, by adopting a normally-closed architecture, the actuators were converted into microvalves capable of directly interacting with aqueous solutions. The two strategies are complementary, and together should enable sophisticated microfluidic systems for applications ranging from point-of-care diagnostics to portable chemical detection. To conclude the dissertation, I demonstrate a proof-of-principle microfluidic system that contained sixteen independently-operated electrostatic valves, operated with battery-operated electrical ancillaries in a hand-held format.

Acknowledgments

I would like to express my deepest gratitude to my family, friends, and colleagues who have walked with me on this journey, and made it all the more worthwhile. I thank my advisor, Prof. Paul Kenis, for his invaluable insight, encouragement, and patience as I labored on this project. Thanks to Prof. Christopher Apblett who allowed me to borrow from his wealth of experience, and also to Prof. Rustem Ismagilov, who introduced me to the world of scientific research when I was an undergraduate student.

To fully acknowledge the help that I received from my fellow students and scientists during the course of this work would itself entitle a publication of lengthy proportions. I hope I will be forgiven for inadvertently omitting anyone from this list of contributions. Thanks to the members of the Kenis research group for help in both the small and great matters of research – for trouble-shooting my experiments, critiquing my presentations, and simply going out to get coffee. Specifically, I thank Dr. Matthew Cole and Dr. Michael Toepke for getting me started in the Kenis Research Group. Thanks to Dr. Sarah Perry for her collaboration on microfluidic platforms for membrane protein crystallization, as well as Griffin Roberts, who made invaluable contributions to that project. Thomas Bassett spent many long hours working with me to improve the design and fabrication procedure for electrostatic actuators, while Dr. Amit Desai spent just as much time on the theoretical aspects of the project. Thanks to Dr. Benjamin Schudel for working on the initial stages of the normally-closed electrostatic microvalve, and to Ritika Mohan, Chotitath Sanpitakseree, and Jae-bum Lee for assistance during the remainder of the project. Thanks to Prof. Fikile Brushett, Dr. Tobias Wheeler, and Dr. Daria Khvostichenko for productive talks and inspiration.

Others from the University of Illinois whom I would like to thank include Dr. James Wentz and John Rosheck for help in developing electrical ancillaries for the electrostatic actuators, Dane Sievers for assistance in measuring the sheet resistance of carbon nanotube electrodes, Li Gao for performing scanning electron microscopy of the cross-sections of the actuators, and Dr. Melikhan Tanyeri for helpful suggestions. I'd also like to thank Prof. Charles Schroeder and Prof. Edmund Seebauer for serving on my committee, and Sarah-Ellen Leonard, Christine Bowser, Kay Moran, and Catherine Paceley for assistance in administrative matters.

From Sanida National Laboratories, I thank Dr. Greg Ten Eyck, who provided valuable input at the early stages of the electrostatic actuator project, and Dr. Richard Givler, who modeled the initial design of the actuator. From the University of New Mexico, I thank Christopher Hamlin and Andrew Collard, who performed initial characterization of carbon nanotube electrodes.

I gratefully acknowledge financial support from Sandia National Laboratories, funded by the DOE through grant LDRD PR#922327; the Center for Nanoscale Chemical Electrical Mechanical Manufacturing Systems (Nano-CEMMS) at the University of Illinois, funded by the NSF through grant DMI-0328162; and the Center for Microanalysis of Materials in the Frederick Seitz Materials Research Laboratory Central Facilities at the University of Illinois.

Finally, I thank my family for always being there for me, no matter where I go or what I decide to do. Thanks to my mother and father, for their unconditional love and support, and to my siblings, for always cheering me on. Lastly, I would like to thank Ritika Mohan again, but this time for her enduring love and encouragement.

Table of Contents

Chapter 1
Introduction

1.1 Motivation

1.1.1 The future of miniaturized chemical and biological systems in portable applications

Since emerging over thirty years ago, the study of miniaturized chemical and biological systems has grown increasingly sophisticated, beginning with relatively modest accomplishments such as a microfabricated gas chromatography column[1], and progressing to include far more intricate platforms capable of, *e.g.*, multi-step chemical syntheses[2-4], high-throughput crystallization screening[5-12], and gene expression profiling[13]. Considering the strides that have already been made, researchers widely predict that chip-based microfluidic platforms will eventually displace conventional automated fluid-handling paradigms (*e.g.*, robotics), and perhaps even replace whole laboratories. However, despite the predictions, "lab-on-a-chip" systems have not been widely commercialized. As a result, many question how to proceed forward[14]. Most critics agree that the difficulty is not a short-coming inherent in the technology, but rather an issue of where the technology is being applied. Many argue that researchers need to realistically assess where society's needs are and adapt problem-centered approaches, rather than technology-centered approaches, to meet these needs. In other words, questions of "why" should come before questions of "what" or "how", and demonstrating scientific prowess should be balanced with addressing pragmatic challenges.

As to the question of "why," currently both developed and developing nations have an urgent need to diagnose disease cheaply, reliably, and independently of centralized facilities. In

resource-poor areas where clinics are sparse, portable diagnostics could bridge the gap between doctor and patient. In developed nations, particularly the United States, more technology and treatment options may be available, but the costs of those advances are unsustainable. As it is, the cost of health insurance is staggering and prevents millions of people from access to medical care. Therefore, as we move toward personalized and preventative medicine, we will likely require medical testing that is more routine, cheap, and portable.

Microfulidic systems are well-positioned to address the need for portable diagnostics, mainly due to their obvious advantage in size. Conceptually, a whole chip could easily fit into a person's pocket. However, most microfluidic platforms rely on equipment outside of the chip either for driving fluid flow (*e.g.*, syringe pumps) or for taking measurements (*e.g.*, lasers or microscopes). The energy and space requirements of the whole system inhibit portability and contribute to costs. To capitalize on the strengths of microfluidic platforms and address the serious needs of society, system components would need to be miniaturized, and ideally, as simply as possible.

1.1.2 The importance of simplicity

For microfluidics or any technological sector, it could be argued that *simplicity* is absolutely essential for creating sustainable growth. According to a recent lecture by Whitesides[15], technological simplicity consists of four major criteria including the following: (i) functionality – the ability to perform a straight-forward, yet valuable task; (ii) reliability – the ability to perform the task in a repeatable, predictable fashion; (iii) low cost; and (iv) "stackability" – the ability to interconnect simple building blocks in such a way to add functionality while retaining reliability. An example of a simple innovation in the microelectronics industry is the transistor. Transistors possess a useful function as switches for electric current. They operate much more reliably than

their predecessor – the vacuum tube – and they can be mass-produced much more cheaply. Moreover, "stacking" transistors enables sophisticated logic operations that add value. Integrating transistors into microchips, inserting microchips into computers, and then "stacking" computers to form networks have led to the remarkable materialization of the Internet, showing how much impact a seemingly simple idea can have.

1.1.3 Simple innovations in microfluidics: soft-lithography and pneumatic microvalves

A close examination of the history of lab-on-a-chip technology shows that major advances have also been driven primarily by simple innovations. Two especially relevant examples include soft-lithography and pneumatic microvalves.

When the field of microfluidics was in its infancy, most devices were fabricated by etching glass or silicon, processes that were available only to researchers with access to specialized microfabrication facilities. However, beginning in the early 1990's, Whitesides *et al.* pioneered a new set of microfabrication techniques, collectively known as soft-lithography, which utilized moldable elastomeric stamps to create microstructures and micropatterns[16-18]. The elastomer can also be molded to create devices for manipulating fluids, and the process for making the devices does not require the typical deposition, patterning, or deposition processes mentioned above. Using soft-lithography, a well-trained researcher can design, fabricate, and test a microfluidic design in the span of a single day, making the process both time and cost efficient. As a result, soft-lithographic techniques are now ubiquitous in academic research (including the fields of biology[19], tissue engineering[20-21], and nanotechnology[22]), and they have been characterized to the extent that they are highly predictable. Consequently, according to Whitesides' criteria, soft-lithography can be considered a "simple" technological innovation.

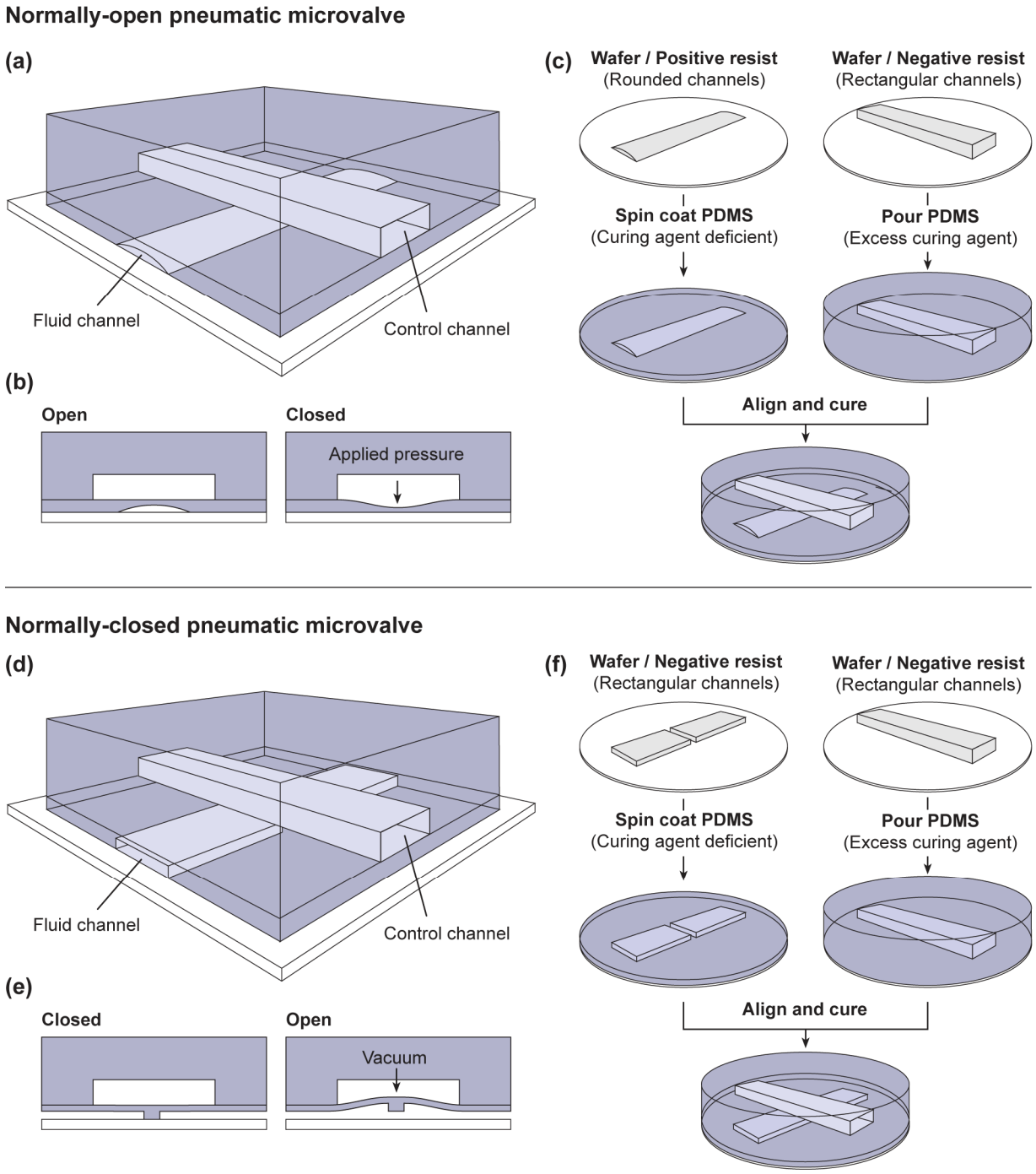

Figure 1.1 Pneumatic microvalves. (a) A perspective view of an assembled normally-open microvalve. (b) An illustration of the operation principle of a normally-open microvalve. (c) A typical soft-lithographic fabrication procedure for a normally-open microvalve. (d-f) Same as (a-c), but for a normally-closed microvalve.

While soft-lithography enabled rapid prototyping of fluidic networks, fluid manipulation in these early devices was mainly limited to pressure-driven, electroostmotic, or electrophoretic

flow. More versatile flow control became available with another simple innovation – the pneumatic micromechanical valve introduced by Quake *et al.* in 2000[23] (Figure 1.1a). The valve consists of two orthogonal channels, one above the other, separated by a thin elastomeric membrane. When the upper channel (referred to as the "control channel") is pressurized, the membrane impinges on the non-pressurized channel (referred to as the "fluid channel"), which obstructs fluid flow (Figure 1.1b). The fluid channel may be rounded such that when the membrane deflects, a hermetic seal develops between the membrane and the floor of the channel. The fabrication procedure for the microvalve is straightforward (Figure 1.1c). Molds for both channels are made from photoresist on silicon wafers using photolithography. Liquid elastomer precursors, most commonly poly(dimethylsiloxane) (PDMS) mixed with a cross-linking agent, are deposited onto both molds and then vulcanized by heating. Afterwards, the molded elastomeric channels can be removed from their respective molds, aligned, and sealed together by taking advantage of mismatched concentrations of cross-linker in each layer. The valves have been actuated for millions of cycles without failure[23], and the probability of defects is low, meaning that thousands of the microvalves can be integrated on a monolithic device with full fidelity[24]. By "stacking" the valves into integrated microfluidic circuits, impressive fluid handling capabilities emerge. Combining three valves together, for instance, creates a peristaltic pump that can drive fluid flow.

While Quake's initial design had a normally-open configuration, normally-closed configurations are possible as well (Figure 1.1d-f)[25-28]. For normally-closed pneumatic microvalves, instead of increasing the pressure of the control channel, a vacuum is applied so that the membrane lifts away from the fluid channel, allowing the working fluid to flow around a barrier that normally obstructs the channel. Several different designs have been presented, some

with glass channels combined with an elastomeric membrane[25] and others with all-PDMS construction[26-28]. Also, the barrier can be attached to the membrane[27-28] or alternatively affixed to the floor of the fluid channel[25-26].

Unfortunately, operating pneumatic microvalves typically requires an external source of pressure or vacuum, an external array of solenoid valves to direct the pressure to individual control channels, a computer to send instructions to the solenoid valves, and tubing to connect the solenoid valves to the chip. In addition, long term processes are usually powered by a stationary source (*e.g.*, a wall receptacle); so, although the microvalves are highly versatile, they are not widely used in portable applications.

1.1.4 Required simple innovations to address portability

To create microfluidic systems that are portable, new simple innovations are needed. Researchers are currently investigating new paradigms such as paper-based platforms[29] or hand-powered devices[30] that can detect highly relevant analytes with minimalist approaches. These platforms have great potential for low-cost, high-volume commercialization aimed at resource poor areas. However, for certain applications, they may be too simple. In systems that require multi-step chemistry, flexible programmability, or remote-controllability, pneumatic microvalves are preferable. Consequently, developing simple miniaturized ancillaries for pneumatic microsystems could serve a vast array of applications.

In the next section, I review strategies for controlling pneumatic microvalves in portable formats that have been reported in the literature. However, I further suggest that none has the proper balance of simplicity *and* functionality. In fact, none have made widespread impact. Therefore, I will introduce my solution, which centers on an electrostatic actuator that I have engineered to be as "simple" as possible.

1.2 A literature review of strategies for increasing the portability of pneumatic microsystems

Three main strategies have emerged to address the innate portability issues of pneumatic microsystems. The first is to reduce the number of required ancillary actuators by implementing multiplexing schemes or on-chip signal processing. The second strategy, which complements the first, is to adopt ancillary actuators that are more compact and less energy-intensive. The last approach is to forgo pneumatic actuation altogether and transition to microvalves that operate with different principles, yet remain as versatile as pneumatic microvalves. Below, I briefly summarize the work that has been done in each thrust.

1.2.1 Methods for decreasing the number of pneumatic inputs

In the most rudimentary form of sending flow control signals to pneumatic microvalves, an external solenoid valve is attached to only one set of synchronously-actuated microvalves, meaning that as the number of independent valve lines increases, the external solenoid valve array scales proportionally, which rapidly increases the size of the whole system. Methods for decreasing the number of pneumatic inputs required for pneumatic microsystems were recently reviewed by Takayama and Burns, *et al.*[31], but for completeness are included here as well.

To address an array of N fluid channels, Quake *et al.* designed a microfluidic multiplexer that operated similar to a binary tree, requiring $2 \log_2 N$ control channels for full functionality (Figure 1.2a)[24]. The researchers demonstrated the power of this method by selectively accessing an array of 1000 chambers using only 22 control interconnects. However, the number of external actuators still increases as the number of valves on chip increases, and this issue remain for other examples of multiplexing as well.

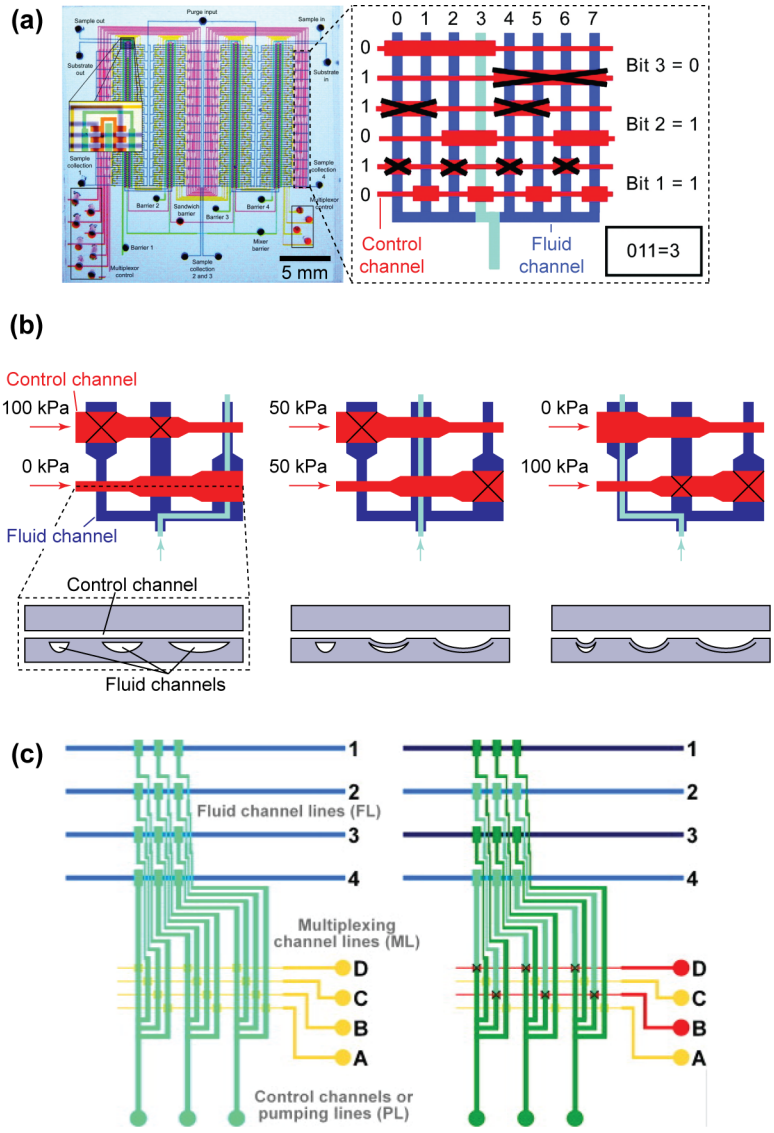

Figure 1.2 Multiplexing schemes for integrated pneumatic microvalve systems. (a) A micrograph and an illustration of a binary-tree multiplexor[24]. (From T. Thorsen, S.J. Maerkl and S.R. Quake, *Science,* 2002, 298, 580-584. Reprinted with permission of AAAS.) (b) A scheme for a ternary multiplexer that takes advantage of pneumatic microvalves with different threshold pressures for actuation[32]. (c) An illustration of a method for multiplexing independent sets of peristaltic pumps[34]. (Reprinted from M.C. Cole, A.V. Desai and P.J.A. Kenis, *Sensors and Actuators B: Chemical,* 2011, 151, 384-393, with permission from Elsevier.)

Cho *et al.* showed that by using pneumatic microvalves with different actuation thresholds (*i.e.*, the minimum pressure required to completely close a pneumatic microvalve), one can increase the capacity of Quake's basic multiplexer design (Figure 1.2b)[32-33]. In their preliminary results, they were able to demonstrate control of N fluid channels with 2 $\log_3 N$ or 2 $\log_4 N$

control channels for ternary and quaternary multiplexors, respectively. (For a comparison of the scaling of Cho's method with Quake's method and a method with no multiplexing, see Figure 1.3). The disadvantage of this approach, however, is that additional equipment is required to modulate the pressure of the control lines.

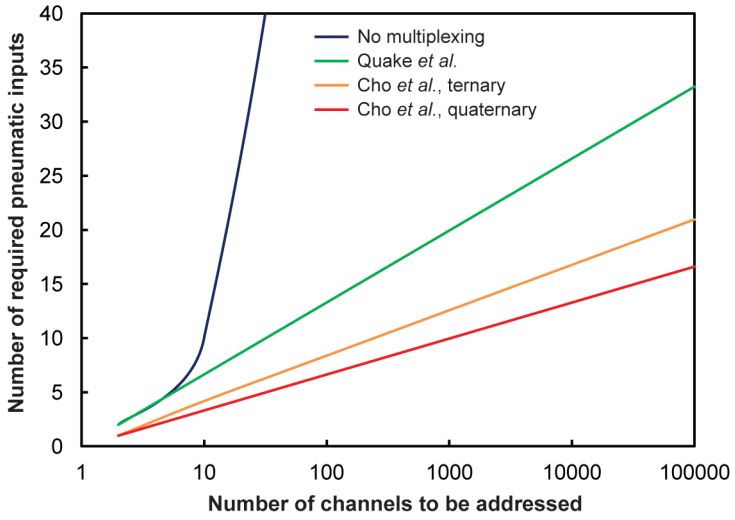

Figure 1.3 A comparison of the scaling of published methods for multiplexing flow channels with pneumatic microvalves[24,32-33].

Finally, realizing that independently-operating peristaltic pumps are typically one of the main contributors to the overall number of valves on-chip, Kenis *et al.* developed a scheme where the control channels were multiplexed in addition to the fluid channels (Figure 1.2c)[34]. In this case, M independent peristaltic pumps can be operated with $3 + 2 \log_2 M$ inputs (or N pumping valves, in sets of three, can be operated with $3 + \log_2 3N$ inputs).

Multiplexing falls into a category of instruction methods referred to as "parallel", where one electrical signal from the controls translates into one mechanical actuation event in the ancillaries and then one fluid actuation event enacted on-chip. Recently, a new paradigm has emerged for integrated microfluidic circuits where a sequence of pressure pulses are generated by the ancillaries and then translated by on-chip fluidic circuits before being routed to pneumatic

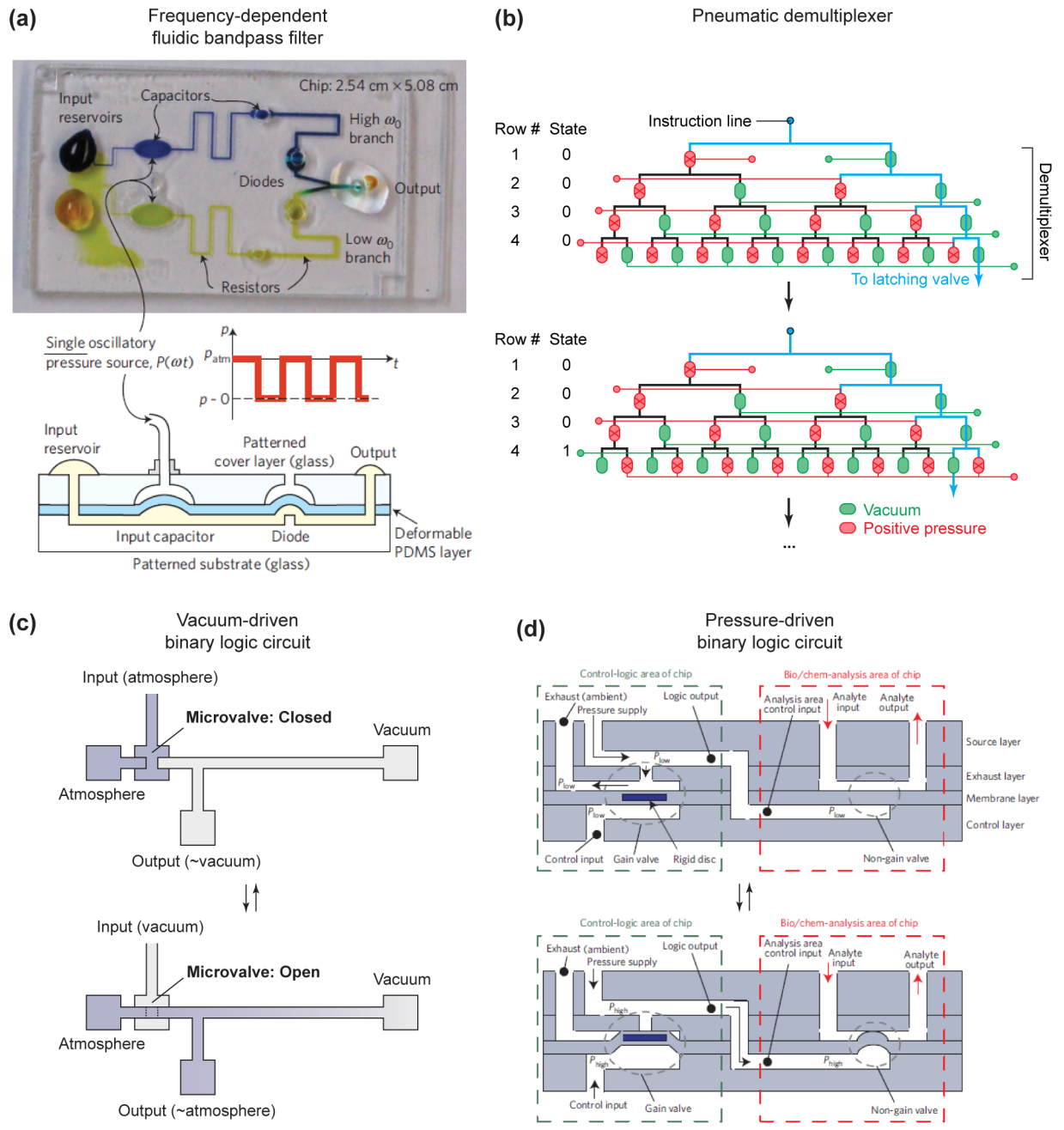

Figure 1.4 A summary of "serial" methods available for instructing pneumatic microvalves. (a) A circuit comprising fluidic resistors, capacitors, and flow rectifying valves that acts as a band-pass filter[35]. (Reprinted by permission from Macmillan Publishers Ltd: Nature Physics (D.C. Leslie, C.J. Easley, E. Seker, J.M. Karlinsey, M. Utz, M.R. Begley and J.P. Landers, *Nature Physics,* 2009, 5, 231-235), copyright 2009.) (b) A binary-tree demultiplexer that uses a single signaling line to instruct an array of latching pneumatic valves[36]. (c) Vacuum-driven[37] and (d) pressure-driven[38] microfluidic binary logic circuits. (Reprinted by permission from Macmillan Publishers Ltd: Nature Physics (J.A. Weaver, J. Melin, D. Stark, S.R. Quake and M.A. Horowitz, *Nature Physics,* 2010, 6, 218-223), copyright 2010.)

microvalves. This strategy has been labeled "serial" instruction because of the similarities to instructional delivery methods in modern electronic circuits[31]. As an example, Landers *et al.* created a circuit comprising fluidic capacitors (chambers with flexible membranes), resistors (microfluidic channels), and diodes (normally-closed valves) that acted as a frequency-responsive band-pass filter (Figure 1.4a)[35]. Low frequency pressure pulses forced fluid through one normally-closed microvalve while high frequency pressure pulses actuated another. In principle, the system requires only one pneumatic input; however, the frequency-response range was broad, meaning that sharp transitions between actuation states were difficult to produce, and consequently, instructing large numbers of valves would be problematic.

Mathies *et al.* introduced a microfluidic demultiplexer, consisting of a binary tree structure of normally-closed pneumatic microvalves that cycled access to an array of latching pneumatic microvalves (Figure 1.4b)[36]. For N latching valves, the binary tree structure required $\log_2 N$ inputs to cycle access to the latching valves, and only one input line for sending instructions. Although the number of total pneumatic inputs scaled similarly to parallel multiplexing approaches, the concept of only using one line for sending instructions categorizes this strategy as a "serial" approach.

Perhaps the most powerful example of a serial approach involves the implementation of cascading binary logic structures to create fluidic processors on-chip. These processors can, in principle, translate instructions from a single input line into an arbitrary number of independent fluid actuation events. Burns *et al.* constructed a fluidic NOT gate by fabricating a microfluidic channel with a normally-closed pneumatic microvalve near the outlet (Figure 1.4c)[37]. A peripheral channel was integrated directly upstream of the valve. Vacuum was applied to the inlet, and the outlet was vented to atmosphere. With atmosphere applied to the microvalve (logic

state “0”), the output in the peripheral channel was vacuum (logic state “1”), and with vacuum applied to the microvalve, the output of the peripheral channel was atmosphere, due to the ensuing development of a pressure gradient. With the NOT gate as the basic building block, Burns was able to construct clock generators, autonomous triggers, and shift registers – all the elements needed to successfully convert one serial input into an arbitrary number of parallel instructions. In practice, most of Burns’ examples (including a 4-bit digital pneumatic processor and a 3-bit multiplexer) were operated with four separate inputs, one for relaying serial instructions, one for transmitting a clock signal generated off-chip, and a third for triggering data transfer from the shift register to the microvalves of interest. A vacuum was also applied separately to provide the driving force for fluid flow through the circuits. This highlights one of the main disadvantages of the fluidic processor paradigm – circuit designs for relaying “serial” instructions are not always as intuitive or as compact as the on-chip plumbing for relaying “parallel” instructions. Regardless, the ability to operate a (theoretically) limitless number of independent microvalves with 2-4 inputs is impressive.

Quake *et al.* implemented a strategy similar to that of Burns, except they used pressurized gas, rather than a vacuum, to drive the operation of the fluidic processor (Figure 1.4d)[38]. Quake fabricated a microfluidic channel with the inlet pressurized and the outlet vented to atmosphere. A specially-designed normally-open microvalve with a disc made from photoresist embedded in the membrane acted as a pressure-gain valve near the outlet, and a peripheral channel was placed directly upstream of the valve. With no pressure applied to the pressure-gain valve, fluid flow persisted through the main channel, resulting in a pressure gradient that output a low pressure to the peripheral channel. With pressure applied to the gate, flow was blocked, resulting in a build-up of pressure in the peripheral channel. The pressure-gain valve could also be located further

upstream and the peripheral channel moved downstream of the gate, resulting in a NOT gate. In principle, these circuits can accomplish the same processing capabilities as Burns' example, although Quake only demonstrated a two-input to four-output decoder.

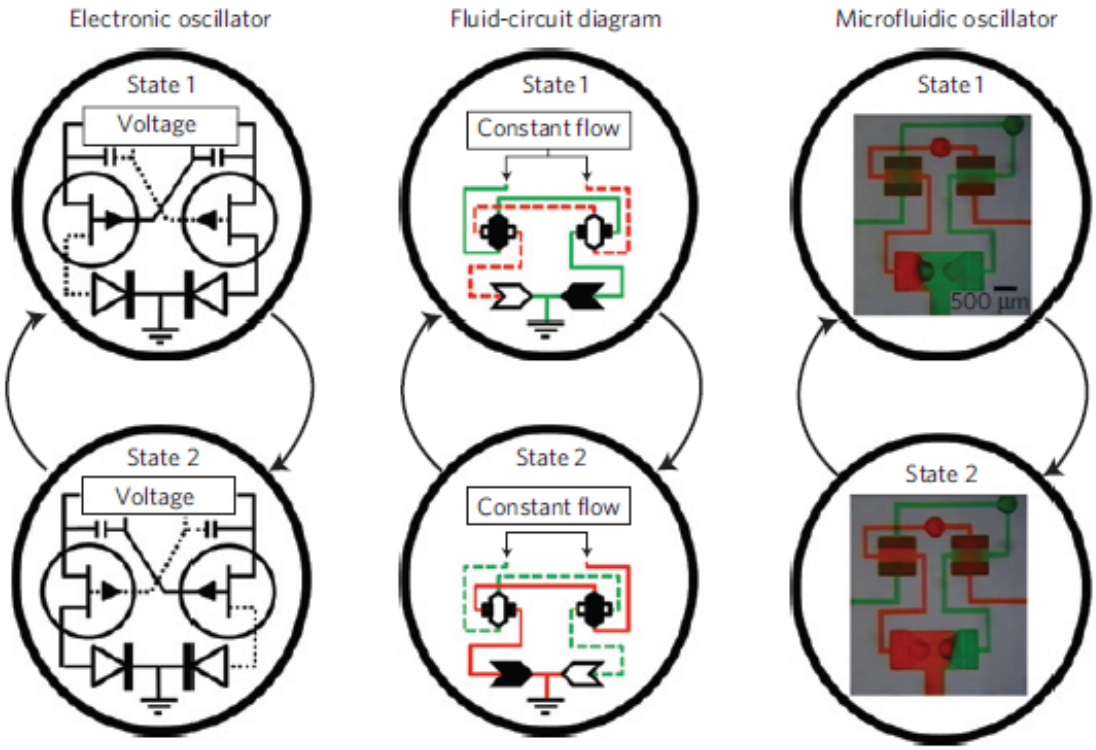

Figure 1.5 An "embedded" instruction method for pneumatic microsystems[40]. After passing through the fluidic circuit, two aqueous streams infused at constant flow rates transform into oscillatory laminar flow. (Reprinted by permission from Macmillan Publishers Ltd: Nature Physics (B. Mosadegh, C.-H. Kuo, Y.-C. Tung, Y.-s. Torisawa, T. Bersano-Begey, H. Tavana and S. Takayama, *Nature Physics,* 2010, 6, 433-437), copyright 2010.)

The final class of instruction methods that has emerged for pneumatic microsystems is referred to as "embedded" because of the auto-regulatory nature of the circuits utilized[31]. The demonstration by Takayama *et al.* used similar components to those mentioned above: fluidic capacitors, resistors, and normally-closed valves, but in a combination that precluded any need for an outside signaling line (Figure 1.5)[39-40]. Instead, all the necessary instructions for fluid direction were embedded in the circuit by means of carefully designed feed-back and feed-forward loops. The only input required was a constant perfusion of reagents, which could be

supplied either with a syringe pump, a pipette, or a hand-held syringe. Currently, Takayama has only demonstrated circuits that create oscillatory flow between two reagents. More sophisticated devices will inevitably be more difficult to design, given that operation is sensitive to fluctuations in flow, and "analog" fluidic circuits are less intuitive to design than the "digital" methods mentioned above.

Overall, none of the methods above can effectively address every challenge encountered with instructing pneumatic microsystems. Instead, future microsystems will likely rely on combinations of the methods working together synergistically, much as modern electronics also rely on parallel, serial, and embedded instruction approaches simultaneously. Hence, the issue of converting electronic signals into pneumatic actuation in an energy-efficient and space-conscious manner remains a critical challenge for portable microsystems. Accordingly, I now shift my attention to recent strategies for accomplishing this crucial task.

1.2.2 Portable actuators for generating pressure pulses

The most common approach for generating pressure pulses without a pressure reservoir and an array of solenoid valves has been to create small fluid reservoirs on-chip connected to the control lines of pneumatic microvalves, and then to compress the fluid reservoirs with an outside actuator. Sia *et al.* created a portable battery-operated platform that was capable of actuating four solenoid valves for this very purpose (Figure 1.6a)[41]. Springs were incorporated into the solenoid actuators so that at rest, the actuators compressed the fluid reservoirs, resulting in normally-closed pneumatic microvalves. Actuation of the solenoids was necessary only when the valves needed to be opened, an intelligent energy-saving strategy. The springs could

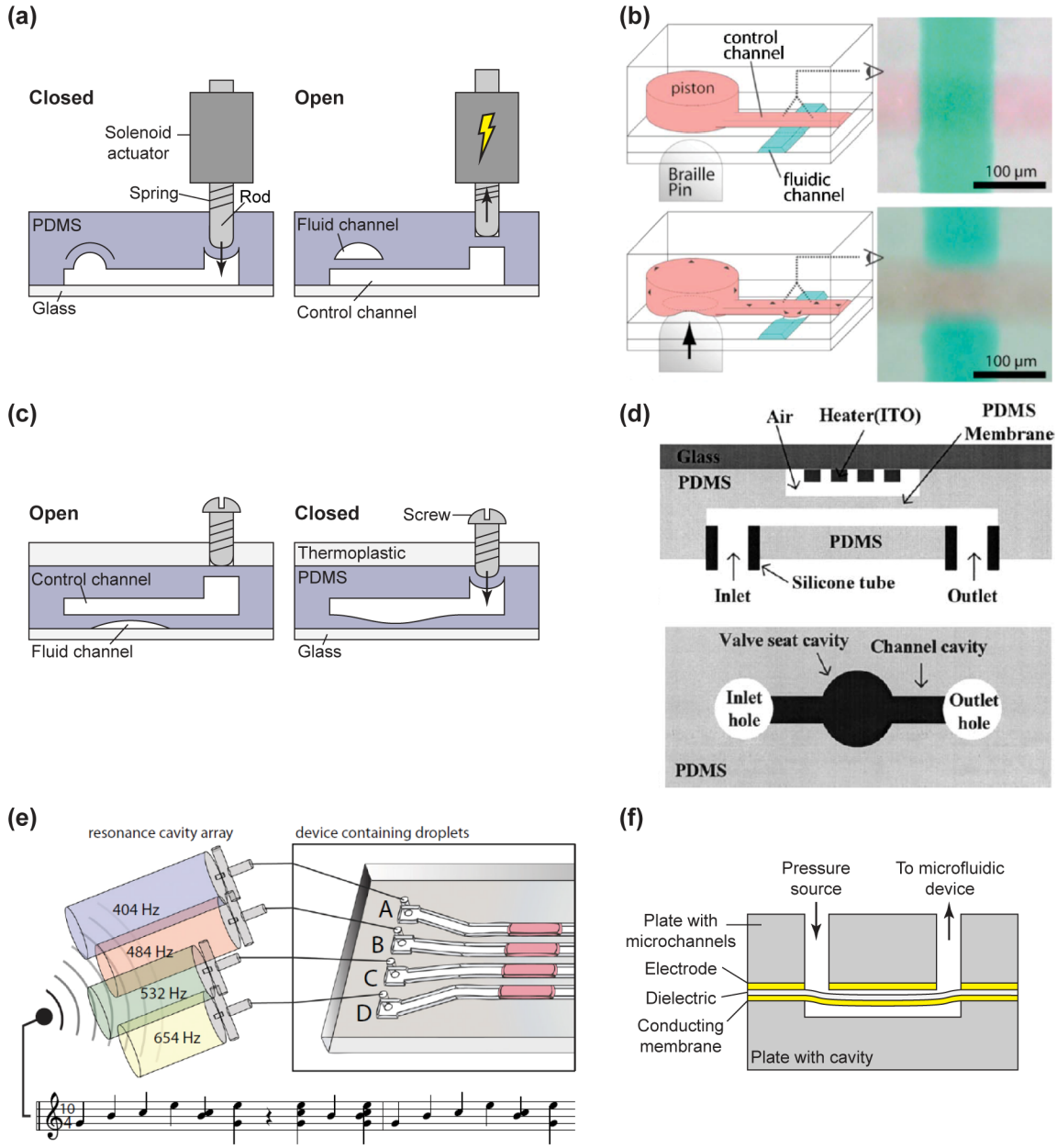

Figure 1.6 Strategies for creating pressure pulses for pneumatic microsystems using compact ancillaries. (a) Compressing a fluid reservoir with a solenoid valve[41]. (b) Compressing a fluid reservoir with Braille pins[42]. (Reprinted with permission from W. Gu, H. Chen, Y.-C. Tung, J.-C. Meiners and S. Takayama, *Applied Physics Letters,* 2007, 90, 033505-3. Copyright 2007, American Institute of Physics.) (c) Compressing a fluid reservoir with a manually operated screw[43]. (d) A thermopneumatic method where a resistive heater heats a reservoir of air that compresses a microfluidic channel[44]. (Reprinted from J.-H. Kim, K.-H. Na, C.J. Kang, D. Jeon and Y.-S. Kim, *Microelectronic Engineering,* 2004, 73–74, 864-869, with permission from Elsevier.) (e) A method for pressurizing fluids in microsystems that utilizes cavities driven by acoustic signals[45]. (Reproduced with permission from S.M. Langelier, D.S. Chang, R.I. Zeitoun and M.A. Burns, *Proceedings of the National Academy of Sciences,* 2009, 106, 12617-12622) (f) An electrostatic valve for controlling pressure flow to a microfluidic device[46].

be removed if it would be more energy-efficient to have the pneumatic microvalves normally-open. An issue with this approach, however, is that while solenoid actuators can be purchased with relatively small dimensions, they still remain large when compared to the size of microfluidic chips. Consequently, it remains to be seen whether arrays of these actuators could be scaled out effectively. Takayama *et al.* utilized refreshable Braille displays to compress their fluid reservoirs (Figure 1.6b)[42]. Each piezoelectric actuator on the Braille display occupied an area with a diameter of about 1 mm, making their approach more scalable than that of Sia. However, refreshable Braille displays are expensive, typically costing thousands of dollars, so platforms incorporating this approach would have to have a high value to be practically commercialized. Moreover, the actuators in Braille displays have a smaller range of motion than offered with solenoid actuators, so the fluid displacement is lower, making signal transduction less effective over long distances. Alternatively, Wu *et al.* used a screw to compress fluid reservoirs, but for automated purposes, the approach is not relevant (Figure 1.6c)[43].

Other strategies for generating pressure pulses without fluid reservoirs include that of Kim *et al.*, who heated small gas reservoirs with resistive heating elements (Figure 1.6d)[44]. With their particular geometry, the valves took more than ten seconds to cycle using 300 mW of power. In another strategy, recently reported by Burns *et al.*, although not explicitly for instructing pneumatic microvalves (Figure 1.6e)[45], the researchers attached acoustic resonators to the inlets of a microfluidic device such that sound alone was able to drive fluid flow through the device. So far in their research, the pressures generated by the acoustic cavities have not been high enough for most common pneumatic microvalve configurations, and the acoustic cavities were not directly integrated on-chip. In addition, the sound source was neither portable nor integrated, although further work may make the system amenable to systems with pneumatic microvalves.

Finally, Gale *et al.* created a manifold of external electrostatic valves to control the flow of pressurized gas to microfluidic systems (Figure 1.6f)[46]. The array of electrostatic valves was smaller than external solenoid arrays and required less power. One challenge with that system, however, was preventing drift in the electric potential needed to actuate the valves, because after 20 actuation cycles, the potential drifted upwards by as much as 300 V.

1.2.3 Alternatives to pneumatic microvalves

Instead of simultaneously developing methods for decreasing pneumatic inputs and increasing the energy efficiency and integration capabilities of ancillary actuators, many researchers have opted to develop micromechanical valves that operate with principles other than pneumatic forces. The literature addressing the development of microvalves is vast, with many examples originating from the field of microelectromechanical systems (MEMS). Valves in MEMS devices mainly consist of stiff materials such as silicon, glass, oxides, and metals and usually require intensive fabrication processes including photolithography, high-vacuum deposition, chemical etching, and thermal annealing. Consequently, integrating large numbers of the valves onto a single platform with minimal defects is challenging.

In this section, I will highlight non-pneumatic microvalves that still incorporate a flexible, polymeric membrane similar to Quake's seminal design. The examples below have largely arisen in response to the challenges posed by pneumatic ancillaries. (For a more general summary of microvalve technology, see the recent review by Kwang and Chong[47].)

Multiple groups have published methods of impinging a rigid rod into the membrane of a valve as a means of actuation. Whitesides *et al.* incorporated a screw into their device that was tightened to shut a valve and loosened to open it (Figure 1.7a)[48]. Eddington *et al.* demonstrated a

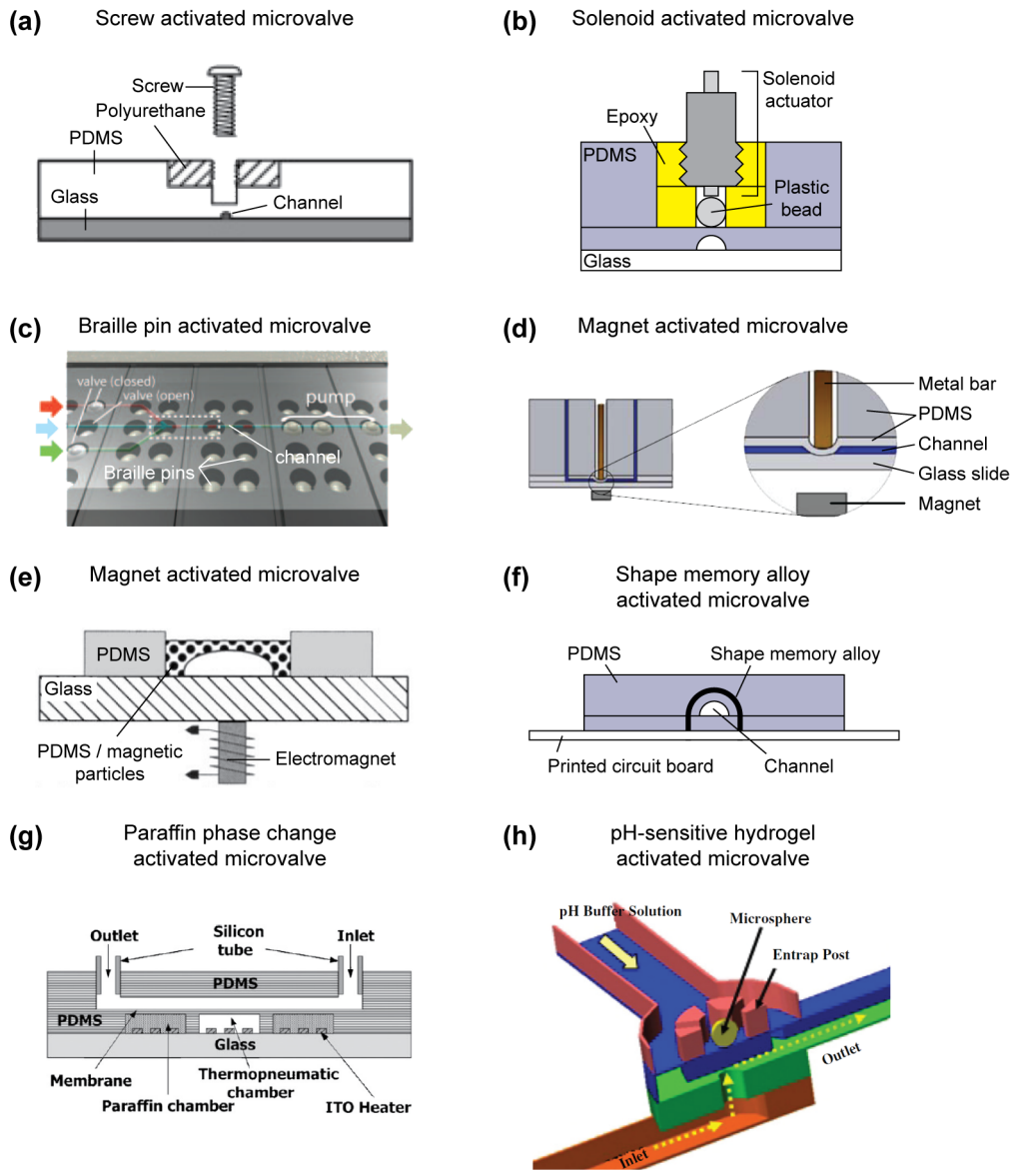

Figure 1.7 Actuation methods for activating elastomeric membrane microvalves using (a) manually operated screws[48] (Reproduced with permission from D.B. Weibel, M. Kruithof, S. Potenta, S.K. Sia, A. Lee and G.M. Whitesides, *Analytical Chemistry,* 2005, 77, 4726-4733. Copyright 2005, American Chemical Society), (b) solenoid actuators[50], (c) Braille display pins[51] (Reproduced with permission from W. Gu, X. Zhu, N. Futai, B.S. Cho and S. Takayama, *Proceedings of the National Academy of Sciences of the United States of America,* 2004, 101, 15861-15866.), (d) external permanent magents with metallic pins[53] (Reproduced from A. Gaspar, M. Piyasena, L. Daroczi and F. Gomez, *Microfluidics and Nanofluidics,* 2008, 4, 525-531, with kind permission from Springer Science and Business Media. Copyright 2008 Springer Science and Business Media), (e) external electromagnets with a PDMS membrane infused with magnetic particles[55] (Reproduced with permission from W.C. Jackson, H.D. Tran, M.J. O'Brien, E. Rabinovich and G.P. Lopez, *Journal of Vacuum Science & Technology B,* 2001, 19, 596-599. Copyright 2001, American Vacuum Society.), (f) shape memory alloy[56], (g) the phase-change properties of paraffin wax[57] (Reprinted from J.-C. Yoo, Y.J. Choi, C.J. Kang and Y.-S. Kim, *Sensors and Actuators A: Physical,* 2007, 139, 216-220, with permission from Elsevier), and (h) the swelling properties of a pH-sensitive hydrogel[58] (Reproduced from P. Ji Young, O. Hyun Jik, K. Duck Joong, B. Ju Yeoul and L. Sang Hoon, "A polymeric microfluidic valve employing a pH-responsive hydrogel microsphere as an actuating source" *Journal of Micromechanics and Microengineering,* 2006, 16, 656, with permission of IOP publishing).

similar approach using metal pins[49]. For simple cases, these types of valves are an easy solution, but not for devices containing high densities of valves or applications that require automation. Whitesides *et al.* also embedded solenoid actuators in PDMS devices as a means of actuating membrane valves (Figure 1.7b)[50]. However, the actuators were 10 mm in diameter, meaning that they also could not be integrated into dense arrays of valves. Takayama *et al.* used a Braille display to directly actuate the elastomeric membrane of a microvalve (Figure 1.7c) [51-52], but this approach was limited due to the fact that the spatial arrangement of actuators in the Braille display was fixed, and also, the display was not transparent.

Several groups have attempted to actuate elastomeric membrane valves with magnetism. In these methods, either a permanent magnet was placed just above a PDMS membrane (Figure 1.7d)[53-54] or the PDMS membrane was impregnated with magnetic particles (Figure 1.7e)[55], and then an external permanent magnet or electromagnet was used to actuate the embedded magnetic element. Issues could arise when attempting to fabricate large arrays of the magnetic valves, as large numbers of permanent magnets would have to be placed precisely. External magnets used to drive actuation also tend to be relatively large, so dense arrays of valves are not practical, and cross-talk between valves would be likely. To surmount these issues, one could attempt to integrate small electro magnets directly on-chip, but this would be challenging.

Scherer *et al.* used a shape-memory alloy (SMA) as an actuator for elastomeric microvalves (Figure 1.7f)[56]. A SMA wire was placed in close proximity to a PDMS membrane, and passing a current through the wire caused it to shorten, resulting in constriction of the channel. Cooling the wire allowed the valve to re-open. Similar to the case of magnetic microvalves, placement of the actuators was done serially in this approach, and every SMA wire needed to be individually soldered to an electrical board, making the overall fabrication arduous.

Other phase change materials may also be used, often with on-chip heaters, to actuate elastomeric membrane microvalves. The most commonly used material is paraffin wax, which expands in volume when heated above its glass-transition temperature (Figure 1.7g)[57]. Similar to systems that utilize heated air, paraffin systems typically require at least several seconds for actuation.

A change in volume can also be induced with stimuli other than heat. Lee *et al.* placed a sphere of pH-responsive, volume-changing hydrogel above an elastomeric membrane and initiated actuation by raising the pH (Figure 1.7h)[58]. Interestingly, the researchers were able to mass produce the spheres using a microfluidic method, although each sphere needed to be placed manually on the device. A disadvantage of this system is that, again, the time scale for actuation was on the order of decades of seconds[58].

1.2.4 Polymer-based electrostatic actuators

This final section discusses membrane microvalves actuated with electrostatic forces. I will pay special attention to this category of actuator because it informs the remainder of the work in my dissertation. Conceptually, electrostatic actuators only require a simple modification to Quake's initial design. By embedding one electrode in the elastomeric membrane and another in the channel floor, one may actuate the membrane simply by applying an electric potential between them. However, several significant challenges make the strategy more difficult to implement than implied by this simplistic description.

The first challenge is related to fabrication and stems largely from incorporating electrically conductive electrodes into the microvalve structure. Most researchers have gravitated towards

	Schematic diagram	Reference	Fabrication processes	Fluids	Electric potential
(a)	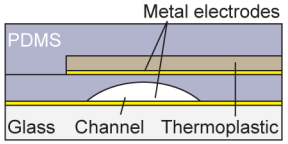	Quake *et al.*[59]	Metal deposition Photolithography Chemical etching Plasma treatment Soft lithography	Air	> 1000 V
(b)	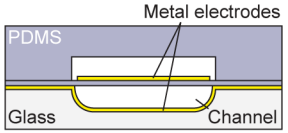	Juncker *et al.*[60]	Metal deposition Photolithography Chemical etching Plasma treatment Soft lithography	Air	300 V
(c)	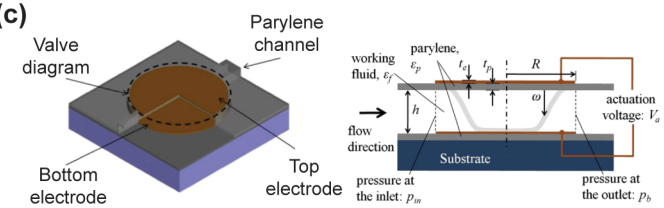	Yildirim *et al.*[65*]	Metal deposition Photolithography Chemical etching Parylene deposition	Air Oil	60-300 V
(d)	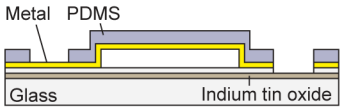	Maharbiz *et al.*[67-68]	Metal deposition Photolithography Chemical etching Oxide deposition High temperature annealing	Aqueous solutions	15-25 V
(e)	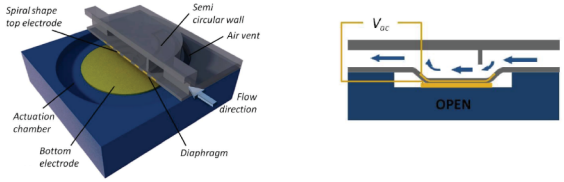	Yildirim *et al.*, [70**]	Metal deposition Photolithography Chemical etching Parylene deposition	Aqueous solutions	50-80 V

Figure 1.8 Polymer-based electrostatic microvalves. *Reproduced from E. Yıldırım and H. Külah, "Analysis and characterization of an electrostatically actuated in-plane parylene microvalve" *Journal of Micromechanics and Microengineering*, 2011, 21, 105009 **Reprinted from E. Yıldırım, M.A.S. Arıkan and H. Külah, *Sensors and Actuators A:Physical*, doi: 10.1016/j.sna.2012.05.008, with permission from Elsevier.

metallic thin films for the electrodes. Quake *et al*. molded a microfluidic channel out of PDMS with a thin membrane suspended above (Figure 1.8a)[59]. Then, the researchers patterned a gold electrode onto a sheet of polyimide, and laminated the electrode to the top of the PDMS membrane. Finally, they set the two layers on top of another gold electrode patterned on glass. While the fabrication was relatively simple, the electrodes required sputtering and patterning steps, and more significantly, the electric potentials needed to close the valves were greater than 1 kV. Also, the transparency available with pneumatic microvalves was lost.

Others have attempted to sputter gold electrodes directly onto the PDMS membrane, eliminating the need for a thermoplastic support. Juncker *et al.* published a patent where they deposited gold onto a PDMS membrane, patterned the gold, and then suspended the membrane above a microfluidic channel etched into glass (Figure 1.8b)[60]. A second gold electrode was deposited onto the floor of the channel. While not reported in the patent, Bowden *et al*. have observed that depositing metal films onto PDMS substrates typically cause the films to buckle[61]. Buckling is not necessarily an issue, as it can confer a degree of "stretchability" to the electric circuit[62]. Graudejus *et al*. have also shown that buckling can be eliminated with precise control of parameters such as deposition temperature, film thickness, elastic modulus, thickness of the adhesion layer, and mechanical pre-strain[63]. For Juncker's valve, however, large strains caused the gold film to crack, so a specially-tailored channel cross-section was required to reduce the stresses applied to the electrode[64].

Another factor that makes fabrication difficult for polymer-based electrostatic microvalves is avoiding premature collapse of membranes. While PDMS is easily molded with soft-lithographic techniques, the most common formulations have a low elastic modulus. Although a low modulus is beneficial for reducing the electrical potential needed to actuate a membrane, it

also leaves the membrane more susceptible to Laplace-Young pressure-driven collapse. In addition, adhesion with rigid substrates tends to be high. For instance, in Juncker's case, the membrane was not capable of releasing from the channel floor under its own strength. An external pressure source was needed to delaminate the membrane after it closed. Other polymers, such as parylene[65-66] and photo-curable PDMS[67-68], have been used to circumvent these issues, and can also be used to limit the buckling of metallic films. However, incorporating these polymers either complicates fabrication or requires specialized equipment.

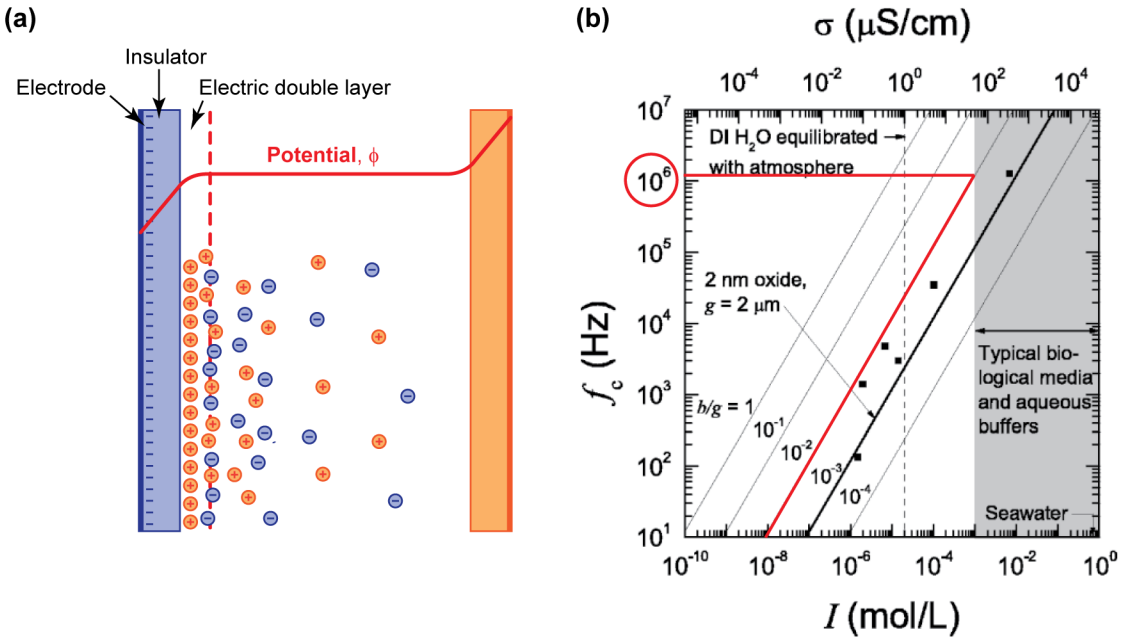

Figure 1.9 The frequency dependence of electrostatic actuators when actuating in aqueous environments. (a) An illustration of electrode screening. (b) Frequencies required by oscillating electric fields to prevent electrode screening as a function of ionic strength[69]. *b*: thickness of an insulating oxide layer over the electrode. *g*: the gap or distance separating the electrodes. (© 2005 IEEE. Reprinted with permission from T.L. Sounart, T.A. Michalske and K.R. Zavadil, *Journal of Microelectromechanical Systems*, 2005, 14, 125-133.)

Perhaps the most significant problem faced by electrostatic microvalves arises from charged solutes passing between electrodes. When exposed to an electric field, the charges migrate to the surfaces of the electrodes, forming an electric double layer that effectively screens the electric field, preventing the valve from actuating (Figure 1.9a). This phenomenon may be prevented by using rapidly oscillating electric fields that switch polarity on timescales more rapidly than

charge migration[69]. The required frequency of the field, though, is sensitive to the ionic strength of the working fluid and also the ratio of the thickness of the insulating layer to the distance between electrodes (*b*/*g* in Figure 1.9b). Therefore, if the valve is fabricated using only soft-lithographic techniques, the thickness of the insulating layer will be ~0.1 μm at best, and in most precedents, the gap between electrodes was between 2-10 μm. Hence, with biologically relevant media and buffers, Zavadil *et al.* predict that the frequency required will be at least 10^6 Hz (Figure 1.9b)[69]. To accommodate frequencies this high, the electric potential must be low; otherwise, sophisticated electronics will be needed, making portability unreasonable and cost of the system excessive.

Maharbiz *et al.* are the only researchers who have reported a polymer-based electrostatic microvalve that can accommodate aqueous solutions passing between the electrodes[67-68]. They maintained a thin insulating layer over the electrode, and they used a photo-curable form of PDMS, stiffer than typical formulations, to prevent Laplace-Young pressure-driven collapse. Their microvalve actuated with potentials as low as 15 V, allowing them to easily drive actuation with high-frequency electric fields. However, to keep the insulating layer extremely thin (0.45 μm thick), the fabrication procedure necessitated a chemical-vapor deposition step and a thermal annealing process. In addition, the entire fabrication process required several other sputtering, photoresist patterning, chemical etching, and thermal annealing steps. Ultimately, in this case, the issue of electrode screening negatively influenced the complexity of fabrication.

Another means of circumventing electrode screening was demonstrated by Yildirim *et al.*[70], who switched to a normally-closed microvalve architecture. In their approach, one electrode remained embedded in the membrane, and the other was moved to a position above the membrane such that charged solutes no longer passed between the electrodes. In the rest

position, a barrier prevented flow through the channel; when the membrane was actuated, fluid flowed around the barrier. Although this approach still required arduous micromachining protocols, oscillating electric fields were no longer required to operate in aqueous environments.

1.3 Objective: *Simple* polymer-based electrostatic actuators

In summary, more work needs to be done to bring sophisticated microfluidic capabilities to portable analytical platforms. This work involves (i) improving pneumatic microsystems by reducing the number of inputs needed, and transitioning to more compact and energy efficient ancillary actuators, or (ii) switching to microvalve technologies with actuation principles more amenable to portable system components (*i.e.*, non-pneumatic). Electrostatic actuators are especially promising due to their conceptual simplicity and their ability to be directly integrated with electronics. However, truly simple and effective solutions have not yet emerged for any strategy. Either fabrication is too complicated, implementation is not straight-forward, or the functionality is reduced compared with the pneumatic microvalve precedent.

In this dissertation, I describe simple electrostatic actuators that are fabricated exclusively with soft-lithographic techniques and operated with energy efficient, compact ancillaries. I show that these actuators can be used either to generate pressure pulses for instructing pneumatic microsystems or to actuate microvalves directly. My goal and desire is that the framework provided here will contribute valuable insight, and eventually lead to the widespread use of these actuators in portable microfluidic applications, especially in point-of-care devices where society's need is great (*e.g.*, healthcare). In Chapter 2, I discuss initial investigations into the design and fabrication of the actuators, including a semi-analytical model that guided their development. Chapter 3 addresses microfluidic pressure-amplifier circuits that utilize

electrostatic gates as a means of generating pressure pulses. In Chapter 4, I report a normally-closed electrostatic microvalve. Finally, in Chapter 5, I summarize the work and provide suggestions for future research.

1.4 References

1. S.C. Terry, J.H. Jerman and J.B. Angell, "Gas-chromatographic air analyzer fabricated on a silicon-wafer" *IEEE Transactions on Electron Devices,* 1979, 26, 1880-1886.

2. C.C. Lee, G.D. Sui, A. Elizarov, C.Y.J. Shu, Y.S. Shin, A.N. Dooley, J. Huang, A. Daridon, P. Wyatt, D. Stout, H.C. Kolb, O.N. Witte, N. Satyamurthy, J.R. Heath, M.E. Phelps, S.R. Quake and H.R. Tseng, "Multistep synthesis of a radiolabeled imaging probe using integrated microfluidics" *Science,* 2005, 310, 1793-1796.

3. H.R. Sahoo, J.G. Kralj and K.F. Jensen, "Multistep continuous-flow microchemical synthesis involving multiple reactions and separations" *Angewandte Chemie-International Edition,* 2007, 46, 5704-5708.

4. I. Shestopalov, J.D. Tice and R.F. Ismagilov, "Multi-step synthesis of nanoparticles performed on millisecond time scale in a microfluidic droplet-based system" *Lab on a Chip,* 2004, 4, 316-321.

5. M.J. Anderson, C.L. Hansen and S.R. Quake, "The use of microfluidic devices towards protein crystallography" *Biophysical Journal,* 2005, 88, 55A-55A.

6. C.L. Hansen, E. Skordalakes, J.M. Berger and S.R. Quake, "A robust and scalable microfluidic metering method that allows protein crystal growth by free interface diffusion" *Proceedings of the National Academy of Sciences,* 2002, 99, 16531-16536.

7. M.J. Anderson, C.L. Hansen and S.R. Quake, "Phase knowledge enables rational screens for protein crystallization" *Proceedings of the National Academy of Sciences,* 2006, 103, 16746-16751.

8. B. Zheng, J.D. Tice, L.S. Roach and R.F. Ismagilov, "A droplet-based, composite PDMS/glass capillary microfluidic system for evaluating protein crystallization conditions by microbatch and vapor-diffusion methods with on-chip X-ray diffraction" *Angewandte Chemie-International Edition,* 2004, 43, 2508-2511.

9. S.L. Perry, G.W. Roberts, J.D. Tice, R.B. Gennis and P.J.A. Kenis, "Microfluidic generation of lipidic mesophases for membrane protein crystallization" *Crystal Growth & Design,* 2009, 9, 2566-2569.

10. L. Li and R.F. Ismagilov, Protein crystallization using microfluidic technologies based on valves, droplets and slipChip. In *Annual Review of Biophysics, Vol 39*, D. C. D. K. A. W. J. R. Rees, Ed. 2010; Vol. 39, pp 139-158.

11. L. Li, D. Mustafi, Q. Fu, V. Tereshko, D.L. Chen, J.D. Tice and R.F. Ismagilov, "Nanoliter microfluidic hybrid method for simultaneous screening and optimization validated with crystallization of membrane proteins" *Proceedings of the National Academy of Sciences of the United States of America,* 2006, 103, 19243-19248.

12. B. Zheng, C.J. Gerdts and R.F. Ismagilov, "Using nanoliter plugs in microfluidics to facilitate and understand protein crystallization" *Current Opinion in Structural Biology,* 2005, 15, 548-555.

13. M. Diehn, R.W. Cho, N.A. Lobo, T. Kalisky, M.J. Dorie, A.N. Kulp, D.L. Qian, J.S. Lam, L.E. Ailles, M.Z. Wong, B. Joshua, M.J. Kaplan, I. Wapnir, F.M. Dirbas, G. Somlo, C. Garberoglio, B. Paz, J. Shen, S.K. Lau, S.R. Quake, J.M. Brown, I.L. Weissman and M.F. Clarke, "Association of reactive oxygen species levels and radioresistance in cancer stem cells" *Nature,* 2009, 458, 780-U123.

14. G.M. Whitesides, "The origins and the future of microfluidics" *Nature,* 2006, 442, 368-373.

15. G.M. Whitesides. (2010, February). "George Whitesides: Toward a science of simplicity" [Video file]. Retrieved from http://www.ted.com/talks/lang/en/george_whitesides_toward_a_science_of_simplicity.html.

16. J.C. McDonald, D.C. Duffy, J.R. Anderson, D.T. Chiu, H.K. Wu, O.J.A. Schueller and G.M. Whitesides, "Fabrication of microfluidic systems in poly(dimethylsiloxane)" *Electrophoresis,* 2000, 21, 27-40.

17. Y.N. Xia and G.M. Whitesides, "Soft lithography" *Angewandte Chemie-International Edition,* 1998, 37, 551-575.

18. Y.N. Xia and G.M. Whitesides, "Soft lithography" *Annual Review of Materials Science,* 1998, 28, 153-184.

19. G.M. Whitesides, E. Ostuni, S. Takayama, X.Y. Jiang and D.E. Ingber, "Soft lithography in biology and biochemistry" *Annual Review of Biomedical Engineering,* 2001, 3, 335-373.

20. R. Gauvin and A. Khademhosseini, "Microscale technologies and modular approaches for tissue engineering: Moving toward the fabrication of complex functional structures" *ACS Nano,* 2011, 5, 4258-4264.

21. A. Khademhosseini, R. Langer, J. Borenstein and J.P. Vacanti, "Microscale technologies for tissue engineering and biology" *Proceedings of the National Academy of Sciences of the United States of America,* 2006, 103, 2480-2487.

22. D. Qin, Y. Xia and G.M. Whitesides, "Soft lithography for micro- and nanoscale patterning" *Nature Protocols,* 2010, 5, 491-502.

23. M.A. Unger, H.P. Chou, T. Thorsen, A. Scherer and S.R. Quake, "Monolithic microfabricated valves and pumps by multilayer soft lithography" *Science,* 2000, 288, 113-116.

24. T. Thorsen, S.J. Maerkl and S.R. Quake, "Microfluidic large-scale integration" *Science,* 2002, 298, 580-584.

25. W.H. Grover, A.M. Skelley, C.N. Liu, E.T. Lagally and R.A. Mathies, "Monolithic membrane valves and diaphragm pumps for practical large-scale integration into glass microfluidic devices" *Sensors and Actuators B: Chemical,* 2003, 89, 315-323.

26. K. Hosokawa and R. Maeda, "A pneumatically-actuated three-way microvalve fabricated with polydimethylsiloxane using the membrane transfer technique" *Journal of Micromechanics and Microengineering,* 2000, 10, 415-420.

27. J. Kim, M. Kang, E.C. Jensen and R.A. Mathies, "Lifting gate polydimethylsiloxane microvalves and pumps for microfluidic control" *Analytical Chemistry,* 2012, 84, 2067-2071.

28. R. Mohan, B.R. Schudel, A.V. Desai, J.D. Yearsley, C.A. Apblett and P.J.A. Kenis, "Design considerations for elastomeric normally closed microfluidic valves" *Sensors and Actuators B: Chemical,* 2011, 160, 1216-1223.

29. A.W. Martinez, S.T. Phillips, G.M. Whitesides and E. Carrilho, "Diagnostics for the developing world: Microfluidic paper-based analytical devices" *Analytical Chemistry,* 2009, 82, 3-10.

30. C.D. Chin, T. Laksanasopin, Y.K. Cheung, D. Steinmiller, V. Linder, H. Parsa, J. Wang, H. Moore, R. Rouse, G. Umviligihozo, E. Karita, L. Mwambarangwe, S.L. Braunstein, J. van de Wijgert, R. Sahabo, J.E. Justman, W. El-Sadr and S.K. Sia, "Microfluidics-based diagnostics of infectious diseases in the developing world" *Nature Medicine,* 2011, 17, 1015-1019.

31. B. Mosadegh, T. Bersano-Begey, J.Y. Park, M.A. Burns and S. Takayama, "Next-generation integrated microfluidic circuits" *Lab on a Chip,* 2011, 11, 2813-2818.

32. D.W. Lee and Y.-H. Cho, "High-radix microfluidic multiplexer with pressure valves of different thresholds" *Lab on a Chip,* 2009, 9, 1681-1686.

33. D.W. Lee and Y.-H. Cho, "A digital dilution chip using inter-well valves controlled by a ternary microfluidic multiplexer" *Sensors and Actuators B: Chemical,* 2011, 155, 380-387.

34. M.C. Cole, A.V. Desai and P.J.A. Kenis, "Two-layer multiplexed peristaltic pumps for high-density integrated microfluidics" *Sensors and Actuators B: Chemical,* 2011, 151, 384-393.

35. D.C. Leslie, C.J. Easley, E. Seker, J.M. Karlinsey, M. Utz, M.R. Begley and J.P. Landers, "Frequency-specific flow control in microfluidic circuits with passive elastomeric features" *Nature Physics,* 2009, 5, 231-235.

36. W.H. Grover, R.H.C. Ivester, E.C. Jensen and R.A. Mathies, "Development and multiplexed control of latching pneumatic valves using microfluidic logical structures" *Lab on a Chip,* 2006, 6, 623-631.

37. M. Rhee and M.A. Burns, "Microfluidic pneumatic logic circuits and digital pneumatic microprocessors for integrated microfluidic systems" *Lab on a Chip,* 2009, 9, 3131-3143.

38. J.A. Weaver, J. Melin, D. Stark, S.R. Quake and M.A. Horowitz, "Static control logic for microfluidic devices using pressure-gain valves" *Nature Physics,* 2010, 6, 218-223.

39. S.-J. Kim, R. Yokokawa, S.C. Lesher-Perez and S. Takayama, "Constant flow-driven microfluidic oscillator for different duty cycles" *Analytical Chemistry,* 2011, 84, 1152-1156.

40. B. Mosadegh, C.-H. Kuo, Y.-C. Tung, Y.-s. Torisawa, T. Bersano-Begey, H. Tavana and S. Takayama, "Integrated elastomeric components for autonomous regulation of sequential and oscillatory flow switching in microfluidic devices" *Nature Physics,* 2010, 6, 433-437.

41. K.A. Addae-Mensah, Y.K. Cheung, V. Fekete, M.S. Rendely and S.K. Sia, "Actuation of elastomeric microvalves in point-of-care settings using handheld, battery-powered instrumentation" *Lab on a Chip,* 2010, 10, 1618-1622.

42. W. Gu, H. Chen, Y.-C. Tung, J.-C. Meiners and S. Takayama, "Multiplexed hydraulic valve actuation using ionic liquid filled soft channels and Braille displays" *Applied Physics Letters,* 2007, 90, 033505-3.

43. Y. Zheng, W. Dai and H. Wu, "A screw-actuated pneumatic valve for portable, disposable microfluidics" *Lab on a Chip,* 2009, 9, 469-472.

44. J.-H. Kim, K.-H. Na, C.J. Kang, D. Jeon and Y.-S. Kim, "A disposable thermopneumatic-actuated microvalve stacked with PDMS layers and ITO-coated glass" *Microelectronic Engineering,* 2004, 73–74, 864-869.

45. S.M. Langelier, D.S. Chang, R.I. Zeitoun and M.A. Burns, "Acoustically driven programmable liquid motion using resonance cavities" *Proceedings of the National Academy of Sciences,* 2009, 106, 12617-12622.

46. A. Douglas, A.L. Gregory and K.G. Bruce, "An electrostatic microvalve for pneumatic control of microfluidic systems" *Journal of Micromechanics and Microengineering,* 2012, 22, 025019.

47. W.O. Kwang and H.A. Chong, "A review of microvalves" *Journal of Micromechanics and Microengineering,* 2006, 16, R13.

48. D.B. Weibel, M. Kruithof, S. Potenta, S.K. Sia, A. Lee and G.M. Whitesides, "Torque-actuated valves for microfluidics" *Analytical Chemistry,* 2005, 77, 4726-4733.

49. M.-E. Brett, S. Zhao, J. Stoia and D. Eddington, "Controlling flow in microfluidic channels with a manually actuated pin valve" *Biomedical Microdevices,* 2011, 13, 633-639.

50. S. Elizabeth Hulme, S.S. Shevkoplyas and G.M. Whitesides, "Incorporation of prefabricated screw, pneumatic, and solenoid valves into microfluidic devices" *Lab on a Chip,* 2009, 9, 79-86.

51. W. Gu, X. Zhu, N. Futai, B.S. Cho and S. Takayama, "Computerized microfluidic cell culture using elastomeric channels and Braille displays" *Proceedings of the National Academy of Sciences of the United States of America,* 2004, 101, 15861-15866.

52. N. Futai, W. Gu, J.W. Song and S. Takayama, "Handheld recirculation system and customized media for microfluidic cell culture" *Lab on a Chip,* 2006, 6, 149-154.

53. A. Gaspar, M. Piyasena, L. Daroczi and F. Gomez, "Magnetically controlled valve for flow manipulation in polymer microfluidic devices" *Microfluidics and Nanofluidics,* 2008, 4, 525-531.

54. T. Pan, E. Kai, M. Stay, V. Barocas and B. Ziaie, "A magnetically driven PDMS peristaltic micropump" *Conference proceedings : Annual International Conference of the IEEE Engineering in Medicine and Biology Society. IEEE Engineering in Medicine and Biology Society.,* 2004, 4, 2639-42.

55. W.C. Jackson, H.D. Tran, M.J. O'Brien, E. Rabinovich and G.P. Lopez, "Rapid prototyping of active microfluidic components based on magnetically modified elastomeric materials" *Journal of Vacuum Science & Technology B,* 2001, 19, 596-599.

56. S. Vyawahare, S. Sitaula, S. Martin, D. Adalian and A. Scherer, "Electronic control of elastomeric microfluidic circuits with shape memory actuators" *Lab on a Chip,* 2008, 8, 1530-1535.

57. J.-C. Yoo, Y.J. Choi, C.J. Kang and Y.-S. Kim, "A novel polydimethylsiloxane microfluidic system including thermopneumatic-actuated micropump and Paraffin-actuated microvalve" *Sensors and Actuators A: Physical,* 2007, 139, 216-220.

58. P. Ji Young, O. Hyun Jik, K. Duck Joong, B. Ju Yeoul and L. Sang Hoon, "A polymeric microfluidic valve employing a pH-responsive hydrogel microsphere as an actuating source" *Journal of Micromechanics and Microengineering,* 2006, 16, 656.

59. B.S. Driggs, M.M. Enzelberger and S.R. Quake, "Electrostatic valves for microfluidic devices" U. S. Patent 7232109, 2002.

60. D. Juncker, M. Nannini and V. Logiudice, "Electrical microvalve and method of manufacturing thereof" I. Patent 12513381, 2007.

61. N. Bowden, S. Brittain, A.G. Evans, J.W. Hutchinson and G.M. Whitesides, "Spontaneous formation of ordered structures in thin films of metals supported on an elastomeric polymer" *Nature,* 1998, 393, 146-149.

62. J.A. Rogers, T. Someya and Y. Huang, "Materials and mechanics for stretchable electronics" *Science,* 2010, 327, 1603-1607.

63. O. Graudejus, P. Görrn and S. Wagner, "Controlling the morphology of gold films on poly(dimethylsiloxane)" *ACS Applied Materials & Interfaces,* 2010, 2, 1927-1933.

64. N. Pekas, Q. Zhang, M. Nannini and D. Juncker, "Wet-etching of structures with straight facets and adjustable taper into glass substrates" *Lab on a Chip,* 2010, 10, 494-498.

65. E. Yıldırım and H. Külah, "Analysis and characterization of an electrostatically actuated in-plane parylene microvalve" *Journal of Micromechanics and Microengineering,* 2011, 21, 105009.

66. J. Xie, J. Shih, Q. Lin, B. Yang and Y.-C. Tai, "Surface micromachined electrostatically actuated micro peristaltic pump" *Lab on a Chip,* 2004, 4, 495-501.

67. T. Bansal, M.-P. Chang and M.M. Maharbiz, "A class of low voltage, elastomer-metal 'wet' actuators for use in high-density microfluidics" *Lab on a Chip,* 2007, 7, 164-166.

68. M.-P. Chang and M.M. Maharbiz, "Electrostatically-driven elastomer components for user-reconfigurable high density microfluidics" *Lab on a Chip,* 2009, 9, 1274-1281.

69. T.L. Sounart, T.A. Michalske and K.R. Zavadil, "Frequency-dependent electrostatic actuation in microfluidic MEMS" *Journal of Microelectromechanical Systems,* 2005, 14, 125-133.

70. E. Yıldırım, M.A.S. Arıkan and H. Külah, "A normally-closed electrostatic parylene microvalve for micro total analysis systems" *Sensors and Actuators A: Physical,* 2012, 181, 81-86.

Chapter 2

Design, modeling, and characterization of an electrostatic actuator fabricated with soft-lithographic techniques*

2.1 Introduction

Based on the precedents of polymer-based electrostatic microvalves summarized in the previous chapter, the most significant obstacle facing widespread adoption of electrostatic actuators in portable microsystems seemed to be the complicated nature of established fabrication procedures. Ideally, the actuators would be fabricated predominantly (or even exclusively) with soft-lithographic techniques, precluding the need for specialized microfabrication equipment and decreasing the time needed for prototyping. Soft-lithographic methods also have more potential to translate over to cost-effective mass manufacturing methods for polymers (*e.g.*, extrusion molding or embossing) compared with traditional MEMS micromachining methods.

2.1.1 Challenges associated with using soft-lithography to fabricate electrostatic actuators

However, switching to soft-lithographic methods has inherent challenges, also evident in several of the precedents. The most commonly used soft-lithographic techniques are limited to larger length-scales than traditional microfabrication techniques, usually by at least an order of magnitude. For example, oxides used for insulating electrodes can be deposited as monolayers

*Part of the work presented in this chapter has been previously published: A.V. Desai, J.D. Tice, C.A. Apblett and P.J.A. Kenis, "Design considerations for electrostatic microvalves with applications in poly(dimethylsiloxane)-based microfluidics" *Lab on a Chip*, 2012, 12, 1078-1088. Reproduced with permission from the Royal Society of Chemistry. A.V.D developed the model, and J.D.T designed, fabricated, and tested the actuators. The figures shown here were created by J.D.T with input from A.V.D.

with atomic layer deposition methods, whereas the thicknesses of spin-coated elastomer films are limited to several hundred nanometers, and are more commonly reported with thicknesses between one micrometer and several hundred micrometers. (Note, however, that a number of soft-lithographic approaches have been adopted for patterning nanostructures for myriad applications, and this is an area of rapid progress[1-3]. The specific techniques that I used for fabricating actuators, however, are limited to approximately micron size features.) The forces exerted by electric fields scale unfavorably with increasing distance between electrodes, so actuators made with soft-lithographic techniques will likely require higher electric potentials to operate than MEMS devices. The two examples of polymer-based electrostatic microvalves listed previously with poly(dimethylsiloxane) (PDMS) membranes[4-5] (excluding the example with a special photo-curable formulation[6-7]) required between 300-1500 V to actuate. Even presuming small length-scales could be attained, elastomeric structures with extreme aspect ratios (*e.g.*, thin membranes, shallow channels, or narrow posts) tend to buckle, collapse, or otherwise distort in detrimental ways. The high surface energies of elastomers easily overwhelm other mechanical forces, which are crucial for effective operation. Consequently, designing soft-lithographic electrostatic actuators requires a challenging balancing-act of choosing dimensions that increase the efficacy of electric fields and yet prevent surface forces from dominating the system.

2.1.2 Methods for modeling electrostatic actuation

In this chapter, I will describe a semi-analytical model to help guide the design of an elastomeric actuator such that the electric potential needed for actuation can be minimized while simultaneously preventing unwanted collapse or adhesion. Two approaches are most commonly used in the modeling of electrostatic actuation of microscale structures: (i) numerical techniques,

and (ii) analytical and semi-analytical approaches. In the former approach, finite element analysis (FEA) or numerical analysis of the governing differential equations has been used to examine various phenomena during electrostatic actuation, including dynamics of pull-in behavior[8], effect of large deformation and non-linear material properties[9], and Casimir forces[10]. However, the non-explicit representation of the design parameters and the complexity of these computational procedures limit their utility when designing new electrostatic actuator configurations. In contrast, analytical and semi-analytical approaches describe the physical relationships between all the geometrical, material and operational parameters explicitly. These approaches have been used to model electrostatic actuation of microelectromechanical systems (MEMS) in liquids[11] and the effect of actuation on material properties[12], and I also utilize these approaches here.

2.1.3 Objectives

We extended analytical models reported in the literature to our polymer-based actuator system by considering several issues that are typically ignored in electrostatic actuation of microscale structures, such as the use of multi-layer components, collapse of actuator membranes, and dynamic actuation in pressurized liquids. We specifically focused on the design of microfluidic actuators fabricated out of PDMS, although the analytical model is described within a generic framework and can be extended to electrostatic actuators fabricated out of other materials (*e.g.*, silicon, glass, or other polymers). The analytical model explicitly identifies the critical design parameters from which a set of design guidelines were derived to address the challenges mentioned previously.

In parallel with the model, we also developed a preliminary actuator design fabricated predominantly with soft-lithographic techniques. The preliminary design allowed us to compare our model predictions with experimental results, which informed the remainder of my work.

2.2 Materials and methods

2.2.1 Soft-lithographic fabrication of electrostatic actuators

Molds for channels and actuator chambers were made by patterning SU-8 5 photoresist (Microchem Corp.) onto silicon wafers using standard photolithographic techniques in accordance with the manufacturer's specifications. Molds for the support layer were similarly fabricated using SU-8 50 (Microchem Corp.). To reduce adhesion between poly(dimethlysiloxane) (PDMS) and the molds, a surface treatment was performed by placing the molds in a vacuum desiccator along with several drops of (tridecafluoro-1,1,2,2-tetrahydrooctyl)trichlorosilane (Gelest, Inc.), and then applying vacuum overnight.

To construct the upper layers of the actuator, including the membrane with an embedded electrode, a thin layer of PDMS (20:1 ratio of monomer to cross-linking agent by weight; General Electric RTV 615, Hisco, Inc.) was first spin-coated onto the mold at 10,000 rpm for 50, 120, or 300 seconds (corresponding to molds with approximately 2, 4, and 7 μm tall features, respectively) such that a thin film covered the features on the mold. The film was cured in an oven at 70 °C for 1 hour and then allowed to cool to room temperature.

To form a thin film of multi-walled carbon nanotubes, an aqueous suspension of multi-walled carbon nanotubes (MWNTs) (20-30 nm outer diameter, 10-30 μm length, > 95 wt% purity, ash < 1.5 wt%; Cheaptubes, Inc.) with a ratio of 1 g MWNTs : 10 g sodium dodecyl sulfate : 1 mL deionized water was prepared and sonicated (Vibra-Cell VCX130PB, Sonics & Materials, Inc.)

for approximately 30 minutes to solubilize the MWNTs. A 0.5 mL sample was then diluted into approximately 20-30 mL deionized water and stirred briefly. The dilute suspension was filtered through a membrane filter (Whatman Anopore™ inorganic membrane, Anodisc™, 0.1 or 0.2 μm pore size, 47 mm diameter) that had been wet with ethanol. After the aqueous suspension had fully passed through the membrane, the MWNTs that remained on the membrane were washed with ethanol until the filtrate was free of bubbles. A PDMS stamp (20:1 ratio of monomer to cross-linking agent by weight) was molded and brought into contact with the MWNT film. Areas in contact with the stamp were lifted off the membrane filter and then applied to the PDMS film formed previously. Pressure was applied by hand, and after lifting off the PDMS stamp, most of the MWNT film transferred to the PDMS film. Some residual MWNTs remained on the stamp. Electrical contacts were made from a mixture of PDMS (5:1 ratio of monomer to cross-linking agent by weight) with 10 wt% MWNTs, which was applied at two corners of the MWNT film and subsequently cured in an oven at 70 °C for 15 minutes.

To encapsulate the MWNT electrode, a second layer of PDMS (20:1 ratio of monomer to cross-linking agent by weight) was spin-coated on top of the electrode at 2400 rpm (for membranes 35 ± 6 μm thick) or 3,000 rpm (for membranes 25 ± 6 μm thick) for 30 seconds and allowed to cure until tacky in an oven at 70 °C for 20-40 minutes. A PDMS support layer (5:1 ratio of monomer to cross-linking agent by weight) that contained 50 μm tall cylindrical cavities with diameters that matched the underlying actuator chambers was aligned onto the membrane. The recesses in the support layer also contained posts scaled to have diameters 20 % of the underlying actuator's diameter. After aligning the support layer, uncovered regions of the mold were filled in with liquid PDMS (5:1 ratio of monomer to cross-linking agent by weight) and the whole assembly was cured overnight in an oven at 70 °C. The support layer sealed permanently

to the membrane due to the mismatch of curing agent concentration between the layers. The actuators were removed from the mold and holes were punched to the inlets of the microchannels using a sharpened 20 gauge steel needle. To complete the actuator assembly, the PDMS layers were set onto a glass slide coated with a thin film of indium tin oxide (ITO), which served as the lower electrode. The ITO film was thermally evaporated onto the glass substrate at a rate of ~1.5 Å s^{-1} for a total thickness of 2500 Å. The coated glass slides were then annealed for one hour at 550 °C, resulting in a transparent, slightly colored film. In cases where oil was tested between the membrane and the lower electrode, fluorinated oil (3M™ Fluorinert™ FC-40) was dispensed first onto the ITO-covered glass slide, and then the PDMS layers were set on top. The PDMS layers formed a reversible bond with the lower electrode upon contact.

2.2.2 Characterization of carbon nanotube films

Films of MWNTs were formed with solution-based processes as described in the fabrication. Sheet resistance was measured with a custom-made four point probe while the films were still on the membrane filters. The films were then transferred to featureless PDMS stamps (20:1 ratio of monomer to cross-linking agent by weight, cured at 70 °C overnight) without leaving observable residue on the filtration membranes. The optical absorbance of MWNT films with known densities were measured with a Perkin Elmer Lambda 650 UV/Vis spectrometer at a wavelength of 400 nm (while still on the PDMS stamps) to produce a calibration curve of optical absorbance relative to film density.

Finally, MWNT films (initially 40 μg cm^{-2}) were transferred from stamps to PDMS membranes, and then encapsulated with another layer of PDMS. The calibration curve was then used to extrapolate the final densities of MWNT films.

2.2.3 Determination of actuation potentials

To test the potentials needed to shut the actuators, an electrical potential was applied between the upper and lower electrodes with a DC power supply (Hewlett Packard model 6209B). One lead from the power source was attached to a wire that was inserted into an electrical contact made of PDMS and MWNT, and the second lead was attached to the film of ITO. The upper electrode was negatively polarized. The potential was increased slowly until the membrane touched the lower electrode. After all the actuators on a device had been actuated, the potential was released and the device was visually inspected to see whether actuators re-opened. Before repeating the experiment, the upper PDMS layers were removed from the ITO-coated glass slide and heated at 70 °C for one hour. A total of three actuators were tested for each geometrical configuration, and each actuator was actuated a minimum of five times to determine average values of actuation potentials.

2.2.4 Measuring actuator dimensions

To determine critical actuator dimensions, the actuators were cut in half to expose the cross-sections and then observed with a scanning electron microscope (JEOL 6060LV SEM). Channel depths were measured with a profilometer (Dektak 3030).

2.3 Results and discussion

2.3.1 An analytical model for guiding the development of electrostatic actuators

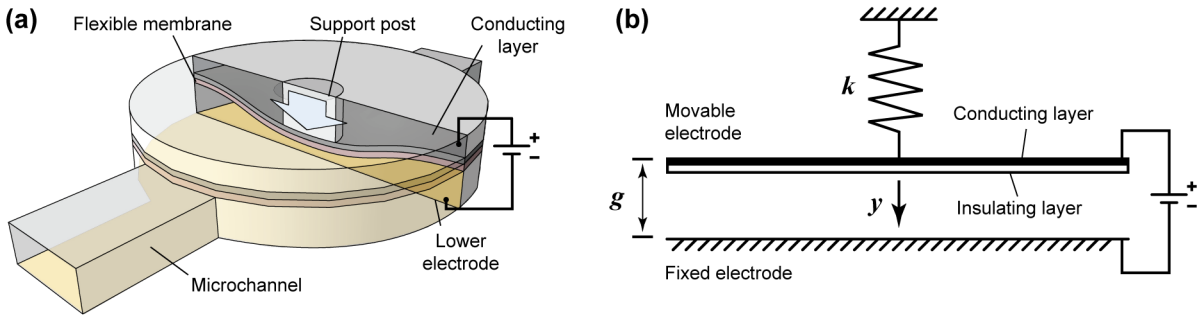

Figure 2.1 (a) A schematic illustration of a contemplated electrostatic actuator in a microfluidic channel. (b) A parallel-plate capacitor model for the electrostatic actuator, with electrode gap / channel height g, spring constant / stiffness of the membrane k, and moveable plate / membrane displacement y.

The electrostatic actuator configuration we initially envisioned consisted of a thin, flat, and elastomeric membrane suspended above a microfluidic channel and clamped at the outer edges (Figure 2.1a). A conducting material rested on top of the membrane, and the floor of the channel was also conductive such that applying an electric field between the electrodes would collapse the membrane onto the channel floor. We also contemplated attaching a post to the center of the membrane to increase the local stiffness, hoping to minimize the probability of adhesion-driven collapse of the membrane.

2.3.1.1 Model setup

We modeled the actuator as a parallel-plate capacitor with electrodes separated by a distance g, where one plate is movable, representing the deflecting membrane, and attached to a spring with spring constant k (Figure 2.1b). The parameter y represents the displacement of the membrane and the extension of the spring. First, we derived expressions for the spring constant of the membrane based on plate theory[13]. Then, we calculated the actuation potential using these spring constant expressions and force-balance equations.

2.3.1.2 Development of an expression for the spring constant or stiffness of the membrane

The expression for static stiffness of a square or circular membrane (the two contemplated geometries for the actuator) that is fixed or clamped along the outer edges under a uniformly distributed load is given by

$$k = K_{bilayer} K_{post} \frac{K_{MS}}{K_{AR}} \left(K^{1}_{shape} \frac{E_{bm} {t_m}^{3}}{{L_e}^{4}} + K^{2}_{shape} \frac{\sigma_0 t_m}{{L_e}^{2}} \right), \tag{2.1}$$

where

k static stiffness of the membrane per unit area

$K_{bilayer}$ factor to account for bilayer configuration and is given by[14]

$$K_{bilayer} = 1 + \frac{E_2 {t_2}^{3} \left(1 - {\nu_m}^{2}\right)}{E_m {t_m}^{3} \left(1 - {\nu_2}^{2}\right)} + \frac{3\left(1 - {\nu_m}^{2}\right)\left(1 + t_2/t_m\right)^2 \left(1 + E_m t_m / E_2 t_2\right)}{\left(1 + E_m t_m / E_2 t_2\right)^2 - \left(\nu_m + \nu_2 E_m t_m / E_2 t_2\right)^2} \tag{2.2}$$

E_m Young's modulus of the membrane material

ν_m Poisson's ratio of the membrane material

t_m total thickness of the membrane

E_2 Young's modulus of the material of the conducting layer

ν_2 Poisson's ratio of the material of the conducting layer

t_2 thickness of the conducting layer

K_{post} factor to account for a cylindrical support post

K_{MS} factor to account for membrane stresses and is given by[13]

$$K_{MS} = 1 + 0.488 \left(\frac{g}{t_m} \right)^2 \tag{2.3}$$

K_{AR} factor to account for aspect ratio and is given by[13]

$$K_{AR} = 1 + \frac{16}{1 - \nu_m} \left(\frac{t_m}{L_e} \right)^2 \tag{2.4}$$

L_e equivalent planar dimension of the membrane (side length or diameter)

K^1_{shape} and K^2_{shape} membrane shape factors[15-16]

E_{bm} biaxial modulus of the membrane and is given by

$$E_{bm} = \frac{E_m}{1-\nu_m^{\,2}}, \tag{2.5}$$

σ_0 residual stress in the membrane

The expression for stiffness (equation (2.1)) is designed to represent the stiffness per unit area, since the mechanical loading due to the electrostatic fields is distributed over the entire membrane. If p is the uniform lateral pressure acting on the membrane and y_{max} is the maximum lateral deflection at the center of the membrane, then $p = ky_{max}$. The factor $K_{bilayer}$ accounts for the fact that membrane properties may not be homogenous from top to bottom, *e.g.*, if an insulating or conducting layer with non-negligible stiffness is present. In the case of a homogeneous membrane, $K_{bilayer}$ is 1. The factor K_{MS} accounts for the effect of membrane stresses that develop when the deflection of the membrane exceeds half its thickness, and the factor K_{AR} accounts for non-linear effects when the thickness of the membrane is not negligible compared with the lateral dimension of the membrane. Note that the effects of bilayer membranes, membrane stresses, and aspect ratio are typically ignored in the analysis of microfluidic electrostatic microactuators, which may lead to significant differences between analytical predictions of actuation potentials and experimentally observed values. Table 2.1 lists the values of the shape factors for square and circular membranes.

Table 2.1 Shape factors for square and circular membranes[15].

Factor	Square membrane	Circular membrane
K^1_{shape}	66.23	85.33
K^2_{shape}	13.57	16

When accounting for the presence of the cylindrical support post, the membrane is modeled as an annulus clamped at the external edges, where the central portion of the membrane is rigid (non-deformable) and constrained to move only in the out-of-plane direction relative to the membrane. An adjustment factor, K_{post}, is introduced based on the expression for stiffness of an annular membrane with a guided central section, and is given as follows[14]:

$$K_{post} = \frac{1}{64 f(b/a)} \tag{2.6}$$

where

$$b = D_{post} / 2 \tag{2.7}$$

D_{post} diameter of the post

$$a = L_e / 2 \tag{2.8}$$

L_e equivalent planar dimension of the membrane (side length or diameter)

$$f\left(\frac{b}{a}\right) = \frac{C_2 L_{14}}{C_5} - L_{11} \tag{2.9}$$

$$C_2 = \frac{1}{4}\left[1 - \left(\frac{b}{a}\right)^2 \left(1 + 2\ln\left(\frac{a}{b}\right)\right)\right] \tag{2.10}$$

$$C_5 = \frac{1}{2}\left[1 - \left(\frac{b}{a}\right)^2\right] \tag{2.11}$$

$$L_{11} = \frac{1}{64}\left[1 - 4\left(\frac{b}{a}\right)^2 - 5\left(\frac{b}{a}\right)^4 - 4\left(\frac{b}{a}\right)^2 \left(2 + \left(\frac{b}{a}\right)^2 \ln\left(\frac{a}{b}\right)\right)\right] \tag{2.12}$$

$$L_{14} = \frac{1}{16}\left[1 - \left(\frac{b}{a}\right)^4 - 4\left(\frac{b}{a}\right)^2 \ln\left(\frac{a}{b}\right)\right] \tag{2.13}$$

In the expression for membrane stiffness (equation (2.1)), typically the effects of fluid viscosity can be neglected. The force required for quasi-static compression of a fluid in an open channel is negligible, but the effect of fluid viscosity may be significant in the case of dynamic operation. In order to describe the influence of fluid viscosity on dynamic motion of the membrane, we assume the membrane motion to be damped by the fluid. This type of damping is known as squeeze film damping[12], and accounts for the energy dissipation due to expansion and compression of viscous fluids between a fixed and vibrating flat plate. We can include the effect of squeeze film damping in the expression for membrane stiffness by using an approximation of the Reynolds equation in fluid film lubrication and neglecting the inertial effects of the fluid, as follows[12, 17]:

$$k = K_{bilayer} K_{post} \frac{K_{MS}}{K_{AR}} \left(K^{1}_{shape} \frac{E_{bm} {t_m}^3}{{L_e}^4} + K^{2}_{shape} \frac{\sigma_0 t_m}{{L_e}^2} \right) + k_{fluid} \tag{2.14}$$

where

$$k_{fluid} = \frac{96 \mu {L_e}^2 \omega}{\pi^4 g^3} \tag{2.15}$$

ω vibration frequency of the membrane

μ dynamic viscosity of the fluid

Equations (2.14) and (2.15) can be used to estimate the influence of fluid viscosity on the dynamic operation of actuators by comparing the relative magnitudes of k_{fluid} and k.

The expressions for stiffness of a membrane are derived based on the following assumptions, each followed by its justification.

1. The membrane is homogenous, uniformly thick, and perfectly clamped at the outer edges. We predicted that the fabrication method would impose relatively strict tolerances on material properties and dimensions, particularly membrane thickness.

2. The deformation of the membrane is elastic. PDMS exhibits elastic behavior for the range of strain values predicted in our design[18].
3. Membrane displacement due to transverse shear is negligible. This assumption holds if the aspect ratio of the membrane (*i.e.*, the ratio of the diameter (or side length) to the thickness) is greater than 5[13]. In our designs, the aspect ratio of the membrane was generally greater than 10.
4. The Poisson's ratios of the two layers making up the bilayer membrane are not significantly different. We anticipated embedding carbon nanotubes in PDMS to form the conducting layer, and with low nanoparticles loadings, we assumed that the conducting layer would have properties similar to pure PDMS.
5. The expressions for static stiffness of the membrane can also be used to estimate the stiffness of the membrane during dynamic operation of actuators. This assumption is valid as long as the operating frequencies of the actuator are lower than the natural frequency of the membrane, which implies that the inertial effects of the membrane can be neglected. Given a PDMS membrane 500 μm in diameter and 10 μm thick, the estimated natural frequency of the membrane is 5 kHz (using the expression for the natural frequency of vibration of a clamped circular diaphragm[19]). This is much higher than the typical operating frequencies (100 Hz) that have been reported for peristaltic micropumps in microchemical systems[20].
6. We assume that the membrane is clamped along the complete outer edge. However, the sections of the membrane above the entrance and exit to the actuator are not fully clamped (Figure 2.1a). Hence, the values for the shape factors listed in Table 2.1 will be different for actuators suspended over microchannels. In the extreme case, when the side length or the diameter of the membrane is the same as the channel width (*i.e.*, only half of the membrane

edge is clamped), then the membrane behaves as a doubly-clamped (fixed-fixed) wide beam and the analytical expressions for membrane stiffness overestimate the spring constant of the membrane. Specifically, the membrane stiffness predicted by equation (2.1) is approximately 2.67 times larger than the stiffness of a doubly-clamped beam[15].

2.3.1.3. Development of expressions for the actuation potential of electrostatic actuators

In the case of the deflection of a membrane (or any deformable structure) due to forces produced by an electric field, the system becomes unstable when the electrostatic forces and the restoring mechanical forces are no longer in equilibrium[11]. Beyond a certain deflection (referred to as the "critical deflection"), the membrane collapses or snaps in (a phenomenon referred to as the "pull-in instability"). Depending on the relative magnitudes of the critical deflection and the initial gap between the plates, the operation of the electrostatic actuator is either in the stable deflection regime (*i.e.*, critical deflection is never reached) or governed by the aforementioned pull-in instability (*i.e.*, the critical deflection is exceeded). Depending on the mode of operation of the actuator, the potential needed to close the actuator (hereafter referred to as the "actuation potential") is given by either

$$V_{close} = \sqrt{\frac{2kg\left(h_c \frac{\varepsilon_{fluid}}{\varepsilon_m}\right)^2}{\varepsilon_0 \varepsilon_{flluid}}};\ y_{snapin} > g\ (\text{stable deflection regime}) \tag{2.16}$$

or

$$V_{close} = \sqrt{\frac{8k\left(g + \left(h_c \frac{\varepsilon_{fluid}}{\varepsilon_m}\right)\right)^3}{27\varepsilon_0 \varepsilon_{fluid}}};\ y_{snapin} \le g\ (\text{pull-in regime}) \tag{2.17}$$

where

V_{close} actuation potential required to close the actuator

y_{snapin} critical deflection beyond which the electrostatic forces and the restoring mechanical forces are no longer in equilibrium given by

$$y_{snapin} = \frac{1}{3}\left(h_c \frac{\varepsilon_{fluid}}{\varepsilon_m} + g \right) \tag{2.18}$$

k membrane stiffness given by equation (2.1).

g initial gap between the plates when no potential is applied

h_c thickness of the insulating layer in the membrane (Figure 2.1)

ε_0 permittivity of free space

ε_{fluid} relative permittivity of the fluid

ε_m relative permittivity of the membrane

The expressions for actuation potentials (equations (2.16) and (2.17)) do not account for the flow pressure (p_{flow}). The electric field produced between the membrane and the fixed electrode will have to perform additional work against the flow pressure, which results in an increase in the actuation potentials. Using the principle of force balance, this increase in actuation potential (V_{flow}) is approximately given by

$$V_{flow} = \sqrt{\frac{2p_{flow}\left(g + h_c \frac{\varepsilon_{fluid}}{\varepsilon_m} \right)^2}{\varepsilon_0 \varepsilon_{fluid}}} \tag{2.19}$$

where p_{flow} is the flow pressure relative to the atmosphere and is assumed to be constant along the surface of the actuator membrane.

The expressions for actuation potential of an actuator (equations (2.16) and (2.17)) are derived based on the following assumptions, each followed by its justification.

1. The fringing electric fields around the edges of the plates are assumed to be negligible**.** These fringing electric fields do not significantly influence the capacitance between parallel

plates when the electrode gap (typically ~10 μm) is small compared to the planar dimensions of the plate (50 – 1,000 μm), *i.e.*, the length or diameter of the membrane[21].

2. The electric field is assumed to be constant across the membrane as the membrane is deforming. This assumption is not true when the deflection of the membrane is significant compared to the electrode gap, since the electric field will be much higher at the center of the membrane compared to the edges. Calculating the actual deflection profile of the membrane due to the non-uniform electric field would entail numerical solution of non-linear partial differential equations or multi-physics simulations using finite element analysis (FEA). Alternatively, in order to capture the influence of the non-uniform electric field, the actuation potential value can be multiplied by a constant ($K_{nonlinear}$), which can be estimated numerically or experimentally. For example, Osterberg *et al.*[12] computed $K_{nonlinear}$ as 0.7545 using FEA simulations, while Rollier *et al.*[11] assumed $K_{nonlinear}$ to be 1 and observed a maximum difference of 6 % between analytical predictions and experimental observations for actuation potentials. In this paper, we assumed $K_{nonlinear}$ to be equal to 1, realizing that this assumption could induce an overestimation of approximately 25 % or less in the analytical predictions of actuation potentials.

2.3.1.4 Prediction of adhesion-driven collapse of elastomeric membranes

An important design consideration for elastomeric, membrane-based electrostatic actuators is the collapse of the membrane onto the floor of the channel. Collapse can occur during assembly of the microfluidic chip, or the membrane may remain adhered to the floor even after the actuation potential is removed. This phenomenon of collapse is primarily governed by the interfacial adhesion between the actuator membrane and the floor of the channel. Poly(dimethylsiloxane)-based microfluidic structures are particularly susceptible to collapse in

the presence of glass substrates due to their high interfacial adhesion energies with glass (~30–300 mJ m^{-2} in air[22-23]). Although the actuators will be actuated primarily in liquids where the surface energies will be lower, the microfluidic devices will be assembled in air, and hence, the adhesion-driven collapse in air is also be an important consideration.

Analytical models for the collapse of free-standing structures due to interfacial adhesion are available for the case of micromachined silicon-based structures in MEMS[24-28]. In these models, a dimensionless parameter Ψ (also referred to as elastocapillary number) is derived to predict whether a membrane will collapse or not during actuation[27-29]. When Ψ is less than 1, the actuators will collapse due to the interfacial adhesion, whereas actuators characterized by a higher value of Ψ do not collapse. Here, we modified the equation for Ψ by integrating the effects of multilayer and high aspect ratio membranes with a cylindrical support post, so that the equation applies to the collapse of the PDMS-based microfluidic actuators discussed in this paper:

$$\Psi = \eta_1 \frac{E_{bm} t_m{}^3 g^2 K_{post} K_{bilayer}}{\gamma L_e{}^4 K_{AR}} \left[1 + \eta_2 \frac{\sigma_0}{E_{bm}} \left(\frac{L_e}{t_m} \right)^2 + \eta_3 \left(\frac{g}{t_m} \right)^2 \right] \tag{2.20}$$

where γ is the interfacial adhesion energy, and η_1, η_2, and η_3 are constants that depend on the shape of the membrane and the boundary conditions. These constants can be analytically derived for simple shapes or determined experimentally[27-28].

2.3.1.5 Critical design parameters affecting actuation potential

We used the analytical model derived in the previous sections to identify critical design parameters that influence the actuation potential. Specifically, we investigated the design of actuators with circular membranes and used the diameter, D, for the equivalent planar dimension, L_e, although the model can also be applied to design actuators with rectangular membranes.

Table 2.2 Scaling relations of various parameters in reference to the actuation potential.

Parameter	Order of dependency	
	Stable region	Snap-in
Diameter, D	-2	-2
Membrane thickness, t_m	2.5	3
Channel height, g	0.5	1.5
Relative permittivity, ε	0.5	1

Table 2.2 lists the order of dependency of the actuation potential on different parameters (*i.e.*, scaling relations), with higher order corresponding to greater influence. The actuation potential is most sensitive to changes in membrane diameter, D, membrane thickness, t_m, and channel height, g, as expected. Less intuitive is the relation between the actuation potential and the dielectric properties of the fluid; an increase in the dielectric constant of the fluid will not necessarily decrease the actuation potential. This counter-intuitive observation is due to the fact that the dielectric constant of the conducting membrane in microfluidic actuators (*e.g.*, $\varepsilon_m = 2.7$ for PDMS) is not negligible compared to the dielectric constant of the fluid (*e.g.*, $\varepsilon_m = 80$ for water), whereas normally the dielectric constant of the top conducting layer is ignored ($\varepsilon_m = \infty$ for metals).

2.3.1.6 Design parameter space

Having identified the critical design parameters, we used the model to estimate the design space for electrostatic actuators that (i) would be feasible from a fabrication perspective, (ii) would have low actuation potentials (less than 300 V), and (iii) would not fail due to adhesion-driven collapse during fabrication or operation. From our preliminary attempts at fabricating the actuators, and also based on precedents from the literature[6-7, 30-32], we approximated reasonable values of the critical design parameters that could be attained with soft-lithographic techniques.

These are listed in Table 2.3. We then used the model to exclude conditions with high actuation potentials and a high likelihood of membrane collapse.

Table 2.3 Approximate dimensions for electrostatic actuators feasible with soft-lithographic techniques.

Parameter	Values (μm)
Diameter, D	100 – 1,000
Membrane thickness, t_m	5 – 50
Channel height, g	2 – 20

When honing the design space, we used the shape constants for a fully clamped circular membrane – $\eta_1 = 40/3$, $\eta_2 = 51/160$, and $\eta_1 = 63/200$ – in equation (2.20)[27]. We assumed the bilayer membrane to be composed of (i) a 1-μm thin insulating layer made out of PDMS ($t_2 = h_c = 1$ μm), and (ii) a thicker layer of thickness t_m, also made out of PDMS. The electrode was envisioned to be negligibly thin and sandwiched between these two layers. Thin layers of PDMS (< 100 μm in thickness) are typically obtained by spin-coating, which leads to thickness-dependent Young's modulus (lower thicknesses lead to a higher modulus) due to reordering of the polymer chains during the process[33]. Since we anticipated membranes thinner than 100 μm, a thickness-dependent Young's modulus was assumed. This and other material properties of PDMS that we used are listed in Table 2.4.

Table 2.4 Material properties of PDMS assumed while constructing the design space.

Property	Value
Young's modulus, E (thickness dependent)	2-10 MPa [33]
Poisson's ratio, ν	0.5 [35]
Relative permittivity, ε	2.75 [36]
Density, ρ	0.95 g cm^{-3} [37]

We investigated actuation theoretically in three fluids: air, oil (3M^{TM} Fluorinert FC-40; a commonly used liquid in microfluidic applications involving two-phase flows[38-39] due to its immiscibility with PDMS), and water. The dielectric constant of oil ($\varepsilon_m = 2$[40]) is similar to that of air, while the interfacial adhesion properties in oil are expected to be similar to that in water. We assumed that the interfacial adhesion energy, γ, for the PDMS-glass interface in air would be 300 mJ m^{-2} [23], and would be reduced by approximately an order of magnitude in liquids (*i.e.*, γ = 30 mJ m^{-2} in oil and water[22-23]).

Figure 2.2 shows the comprehensive parameter space with respect to diameter, D, and channel height, g, for two different membrane thicknesses, t_m. Colored contour lines show the actuation potential, while black lines demark the stiction threshold where $\Psi = 1$. Conditions predicted to require more than 300 V to actuate are shaded gray, as well as conditions likely to result in unwanted collapse of the membrane (see Figure 2.2f).

Several trends are immediately apparent. As expected, the actuation potential decreases with increasing diameter, decreasing distance between the electrodes, and decreasing thickness of the membrane. The actuation potential contours are similar for air and oil because of the similar relative permittivity in the two fluids. Likewise, the stiction threshold is the same between oil and water because we assumed the same interfacial energy in both fluid systems.

The design space for actuators operating in air is significantly constricted compared to the design space for those operating in oil or water, which is due to the high probability of the membrane collapsing in the air environment. The implications are important, because as mentioned before, even for actuators that operate in liquid environments, considering adhesion-driven collapse in air is important for avoiding collapse of the membrane during fabrication. To expand the range of feasible actuator dimensions, the simplest solution is to increase the

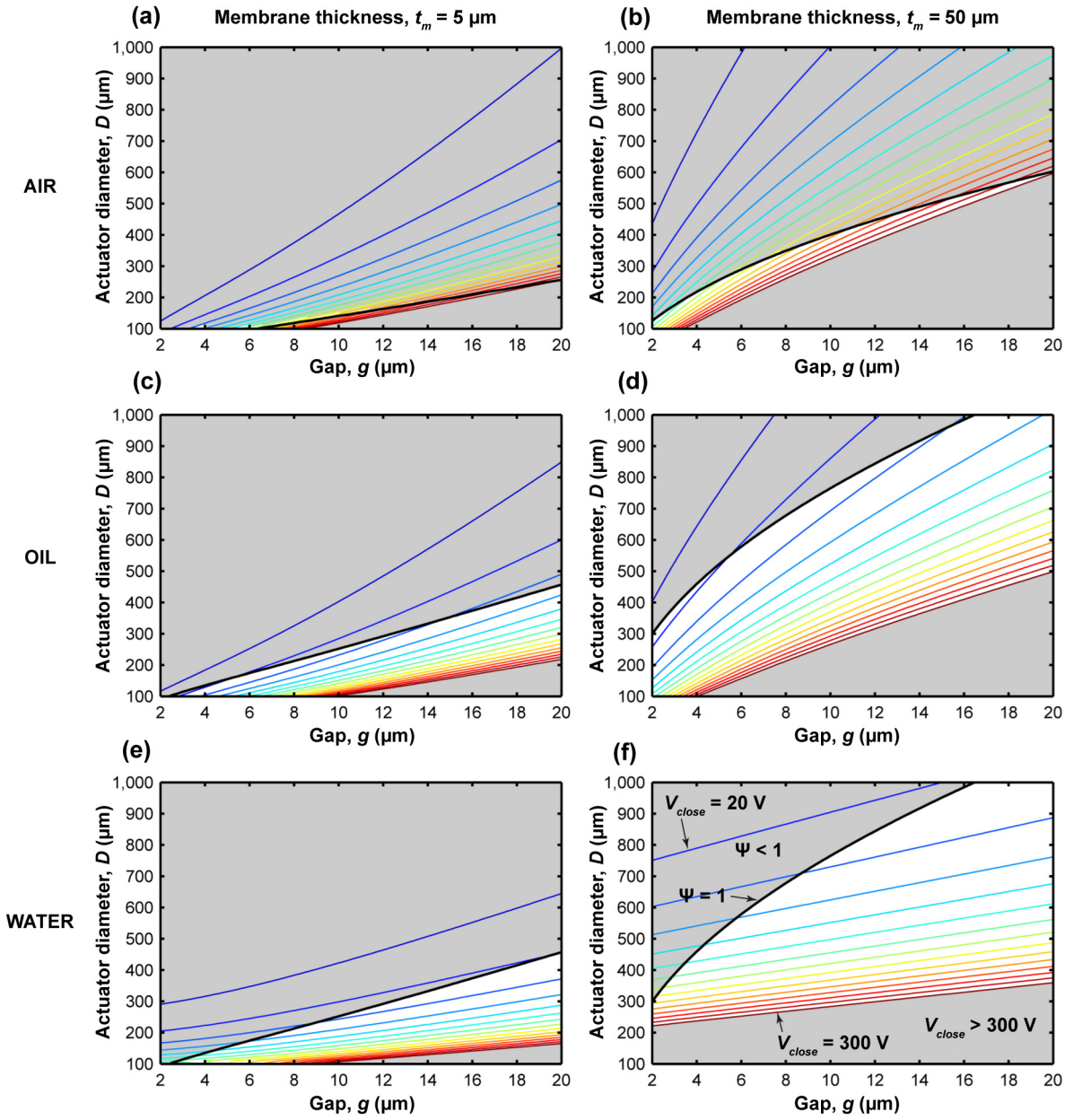

Figure 2.2 Parameter space of actuators that can be activated with potentials less than 300 V while not collapsing during operation (non-shaded regions) for a range of membrane diameters and channel heights. Two extreme values of membrane thickness are considered: t_m = 5 µm (a, c, and e), and t_m = 50 µm (b, d, and f). The design parameter space is estimated for air (a-b), oil (c-d) and water (e-f). Colored contour lines represent actuation potentials (spaced by 20 V) and black lines represent the stiction threshold (*i.e.*, where Ψ = 1).

thickness of the membrane. In the graphs, the area gained by increasing the membrane thickness (which shifts the stiction threshold upward) is greater than the area lost due to the consequential shift in the lower bound (*i.e.*, the line where V_{close} = 300 V). This holds true for actuators

operating in oil and water as well. Another way to minimize adhesion may be to apply coatings with low surface energies, such as Teflon® or monolayers with fluorinated end groups. Later, I will show how we decreased the surface energy by fabricating the lower electrode from the same materials as the membrane.

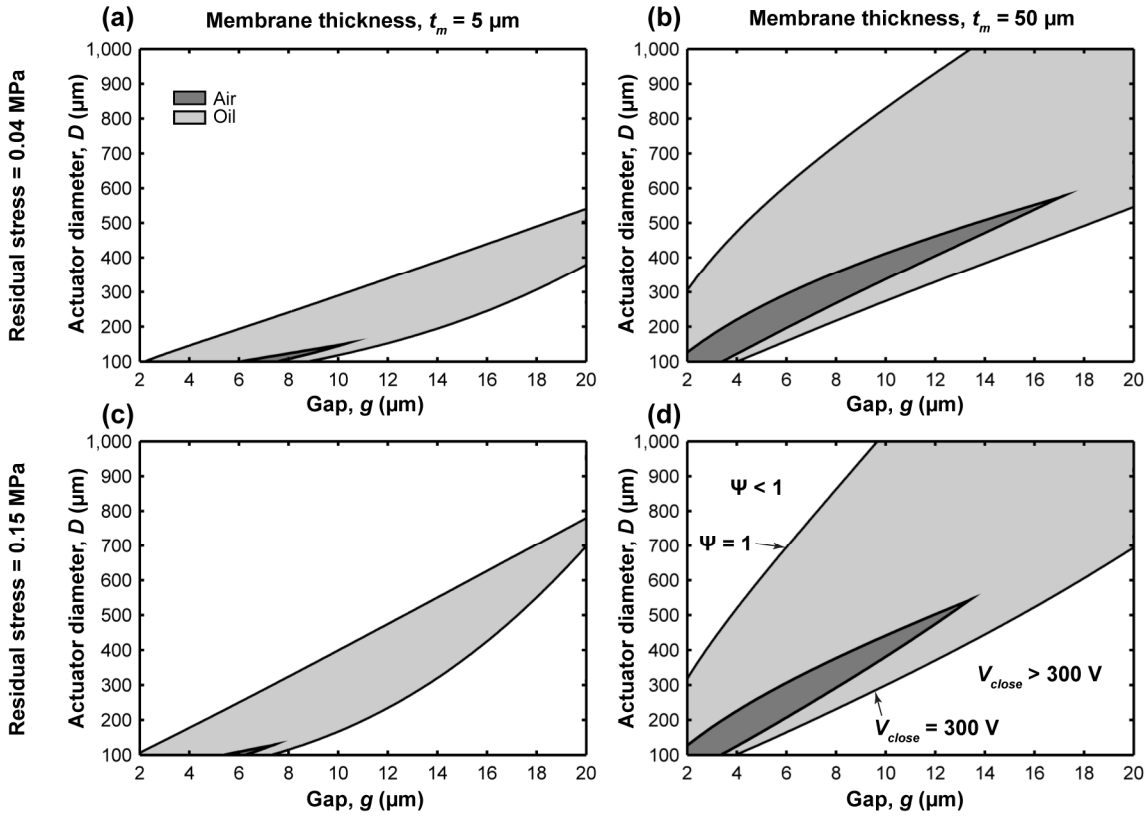

Figure 2.3 Design parameter space for microactuators for two different values of residual stresses, 0 and 0.15 MPa. The design space is estimated for two different membrane thicknesses: t_m = 5 µm (a, c) and t_m = 40 µm (b, d). The lower bounds corresponds to a potential of 300 V, and the upper bounds corresponds to the stiction threshold (*i.e.*, where Ψ = 1).

The fabrication of freestanding membranes results in residual stresses, which influences the stiffness of the membrane and consequently, the actuation potential and the elastocapillary number. Consequently, we also used the analytical model to estimate the influence of residual stresses on the design parameter space. We plot the parameter space for the actuators in Figure 2.3 similar to that in Figure 2.2, but contour lines are excluded, leaving only the stiction

threshold and the line corresponding to V_{close} = 300 V. In this case, gray areas correspond to viable conditions for fabrication and operation. Two different values of residual stresses are considered – 0.04 MPa (the lowest residual stress measured in free-standing PDMS membranes[34]) and 0.15 MPa (the maximum observed residual stresses in PDMS membranes[41]). We plot the design parameter space for air and oil only, for the sake of clarity.

Increasing the residual stress of the membrane has the most drastic effect on actuators with electrode spacing on the higher end of the spectrum. Both the stiction threshold and the line corresponding to V_{close} = 300 V shift upward. In practical terms, high residual stress will decrease the probability of collapse, but also increase the actuation potential. The effect is more pronounced for high channel heights because the membrane is required to undergo more in-plane strain while closing, and the effect of the modulus membrane stress is non-linear for high in-plane strains. For actuators with smaller electrode spacing, and consequently less in-plane strain, the shift is less significant.

If residual stresses need to be minimized to decrease the actuation potential or to accommodate actuators with smaller diameters, several strategies could be employed. Residual stresses in freestanding films are often caused by a mismatch of thermal expansion coefficients between the film and the substrate, so PDMS structures could be cured at ambient conditions rather than elevated temperatures. However, room temperature vulcanization necessitates excessively long reaction times to assure the material properties of the PDMS are able to stabilize. A pragmatic compromise might be to cure the PDMS structures at room temperature until they are sufficiently solidified to be removed from their molds. Then, after removal, the assembled device could be tempered at 200 °C for 4 hours, which has been shown to ensure that

the PDMS is completely cured, and that the mechanical properties of PDMS remain constant over time[42].

2.3.2 Fabrication and characterization of electrostatic actuators

Having identified parameter dimensions that could be implemented reasonably and that were also theoretically sound, we set out to develop a fabrication scheme that required only soft-lithographic techniques.

2.3.2.1 Electrodes compatible with soft-lithographic methods

One of the main challenges early in the project was identifying materials and procedures to easily yet effectively deposit patterned electrodes onto PDMS substrates. As mentioned previously, metal electrodes have a propensity to buckle when deposited on elastomers[43], and in certain instances, they require specially-tailored channel cross-sections to prevent them from cracking under strain[5, 44]. They also necessitate intensive fabrication procedures that may include high-vacuum deposition, photolithographic patterning, etching, and/or high-temperature annealing steps, which we wished to avoid[6-7, 31-32]. To preclude issues with buckling and cracking, very early on we decided to form electrodes from elastomers impregnated with conducting nanoparticles, hoping to confer greater flexibility to the electrodes.

The nanoparticles system we decided to focus on was that of multi-walled carbon nanotubes because of a number of desirable characteristics. Due to their high aspect ratios (ratios of length to width), carbon nanotubes form fully percolating networks at lower particle loadings than globular nanoparticles (*e.g.*, carbon black)[47]. The particle loading can be adjusted such that films of carbon nanotubes are both conductive and transparent[48]. More importantly, carbon nanotube-polymer composites have been shown to withstand high stresses without mechanical failure[45-46], and a number of solution-based methods have been reported for depositing and patterning films of carbon nanotubes[48-52]. Since carbon nanotubes are hydrophobic, they can adhere well to our

elastomer of choice, PDMS, and finally, multi-walled carbon nanotubes can be procured from commercial sources at reasonable prices. (The entirety of this study, requiring hundreds of devices, was completed with approximately 300 USD worth of MWNTs).

I investigated three methods for depositing electrodes of MWNTs onto PDMS substrates: (i) embedding MWNTs into PDMS pre-polymer and then drawing the mixture over a substrate with a razor blade[49], (ii) airbrushing a solution of MWNTs suspended in a solvent[50], and (iii) forming thin films of MWNTs by vacuum filtration[48, 51] followed by microtransfer printing[52]. The first method produced films that were relatively thick, opaque, and stiff, which would have led to unreasonable actuation potentials. Additionally, we could not identify a simple method to pattern the mixture of MWNTs and PDMS. Others have done so by first creating stencils made from photoresist, then embedding the conductive mixture into the recesses of the stencil, and dissolving away the photoresist[49], but this would have complicated our fabrication process.

Airbrushing also involved a number of challenges. The quality of the film was highly dependent on the deposition rate and the distance of the airbrush from the surface. Both parameters were difficult to control precisely. The surfactant used to suspend the MWNTs in solution essentially eliminated conductivity in the films, and again, we could not identify a straight-forward method to pattern air-brushed films.

Microtransfer printing offered the easiest route for us to deposit and pattern MWNT films in our fabrication scheme. We first suspended MWNTs in an aqueous solution with a surfactant (sodium dodecyl sulfate), followed by sonication to solubilize residual MWNT aggregates. We then filtered the solution through an alumina membrane filter, followed by a wash with ethanol to remove the surfactant. (We tested several other filter materials, including Teflon®, polycarbonate, polysulfone, and polyester, and found that MWNTs transferred most effectively

from the alumina membranes, possibly due to the hydrophilic nature of alumina membranes, as well as their rigidity. Note, however, that alumina membranes were the most expensive of the membranes tested, typically costing at least 10 USD per filter. Also, alumina membranes are not widely manufactured, which makes availability unpredictable.) After drying the MWNT film with a stream of nitrogen, we picked up select areas with a PDMS stamp. We found that MWNT films transferred more reliably to PDMS stamps that contained a deficiency in cross-linker; when we used stamps made from PDMS with a ratio of 20:1 monomer to cross-linking agent by weight, MWNT films typically transferred completely. Hence, for the entirety of the work presented here, stamps were made from PDMS with this ratio of components.

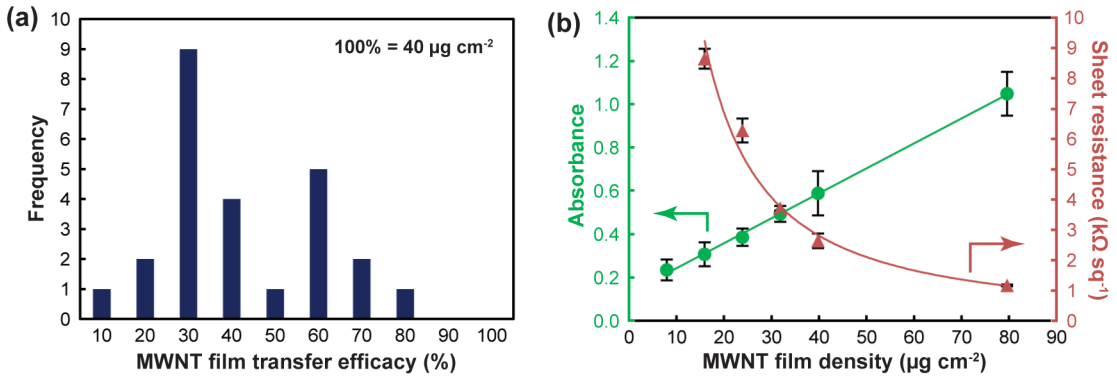

Figure 2.4 Characterization of electrodes made from multi-walled carbon nanotubes. (a) A histogram showing the extent of MWNT transfer from PDMS stamps to PDMS substrates in a sample of 25 devices, as determined by light absorbance at 400 nm. The MWNT films had an initial loading of 40 μg cm^{-2} before transfer. (b) Quantification of film transparency and sheet resistance as a function of MWNT loading.

While MWNT films usually transferred completely to PDMS stamps, they did not transfer completely from the stamp to another PDMS substrate. We found that the substrate needed to be as soft as or softer than the stamp for a reasonable transfer to occur. At the same time, PDMS structures with a low Young's modulus are more prone to unwanted collapse or adhesion. Consequently, in this work, we compromised and made the PDMS substrate from the same ratio of components as the stamp (20:1 ratio of monomer to cross-linking agent by weight). We quantified the efficacy of film transfer by measuring the optical absorbance of MWNT films

before and after stamping. Stamped films were homogeneous and 37 % ± 17 (s.d.) their original densities (Figure 2.4a). With the particle loadings we were using, this corresponded to an average absorbance of 0.3 (measured at 400 nm), and a sheet resistance of about 1.5 kΩ sq^{-1} (Figure 2.4b). Despite the wide variation in the efficacy of film transfer, I will show later that this did not appear to have a significant effect on the operation of the electrostatic actuators.

2.3.2.2 A soft-lithographic method for fabricating electrostatic actuators

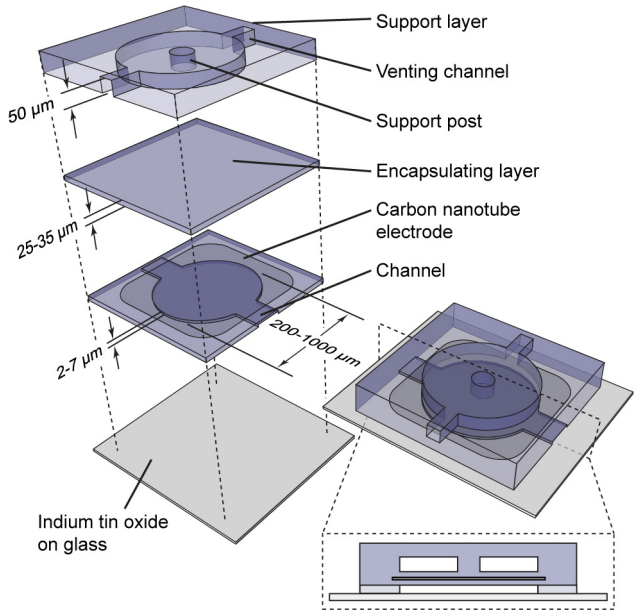

Figure 2.5 An exploded view, a perspective view, and a cross-sectional view of the preliminary design of the electrostatic actuator. Not drawn to scale.

Having identified a suitable method for depositing and patterning electrodes, we set out to fabricate a fully-operational actuator. The initial design was similar to the configuration contemplated in the model (Figure 2.1a), with slight modifications. A carbon nanotube electrode was embedded in a PDMS membrane, which was suspended over a circular microfluidic channel (Figure 2.5). A thick slab of PDMS (*i.e.*, the support layer) was attached to the top of the membrane with a cylindrical recess above the actuator chamber, and the recess contained a PDMS post attached both to the support layer and to the membrane. The diameter of the post

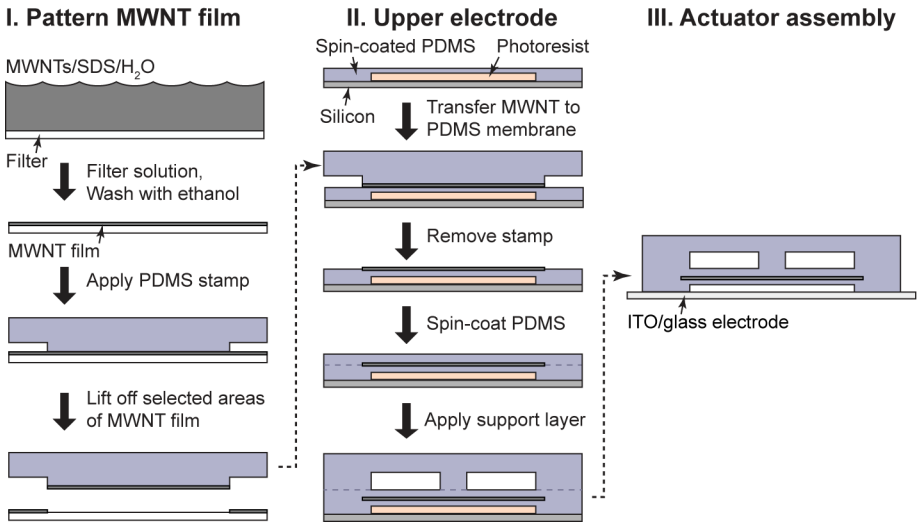

Figure 2.6 An illustration of the fabrication scheme for the initial electrostatic actuator configuration using predominantly soft lithographic techniques.

was 20 % the diameter of the membrane and was used to increase the local stiffness of the membrane to prevent premature collapse. A venting channel was also molded into the support layer so that the pressure of the air in the recess could equilibrate with atmosphere.

For the upper portion of the actuator, we utilized soft-lithographic techniques exclusively (Figure 2.6). A detailed procedure is reported above in the Materials and methods section. Briefly, the insulating layer of the membrane and the microfluidic channel were fabricated by spin-coating PDMS onto a mold of the channel, curing the PDMS, and then microtransfer printing a film of MWNTs onto the appropriate location. To enable electrical contact with a power source, a mixture of MWNTs and PDMS was deposited onto a corner of the MWNT film and cured (not shown in Figure 2.6). A second layer of PDMS was then spin-coated in order to encapsulate the electrode. This layer also provided an elastomeric surface that could be sealed to the support layer. After fully curing all the layers together, the actuator was removed from the mold and access holes were punched to the channels with a sharpened needle. For initial tests, we used a glass slide coated with a film of indium tin oxide (ITO) as the lower electrode, and we did not permanently seal the elastomeric layers to the slide. This allowed us to reuse the lower

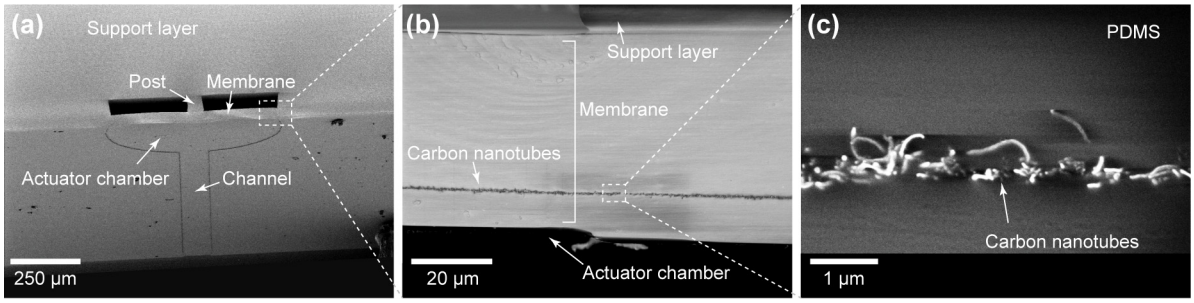

Figure 2.7 Scanning electron micrographs of an electrostatic actuator. (a) A low magnification image of a cross-section of the actuator. (b) A higher magnification image of the membrane and the embedded electrode. (c) An image of a cross-section of the electrode composed of carbon nanotubes.

electrode and to assemble the elastomeric layers onto the lower electrode in the presence of either air, water, or oil, permitting us to investigate the premature collapse of membranes with several liquid systems.

Scanning electron microscopy images of the cross-section of an electrostatic actuator are shown in Figure 2.7. The thickness of the membrane was noticeably thicker than the depth of the actuator chamber in order to prevent premature collapse of the membrane. The MWNT electrode was embedded close to the top of the actuator chamber, and at high magnification, the intermeshed morphology that lends both flexibility and conductivity to the film is visible. Most of the MWNT film was constrained to a cross-sectional region less than 1 μm high, but some carbon nanotubes protruded beyond this region.

Interestingly, we found that the thickness of the insulating layer varied depending on the height of the actuator chamber, the diameter of the actuator chamber, and the radial distance from the center of the actuator (Figure 2.8a). Near the center of the actuator, the insulating layer tended to be thicker than at the periphery, and the effect was more pronounced for taller and wider actuator chambers. I hypothesized that this was due to surface tension between the photoresist and the liquid PDMS pre-polymer. We attempted several other methods for fabricating membranes, trying to eliminate the variability in thickness (including a method where

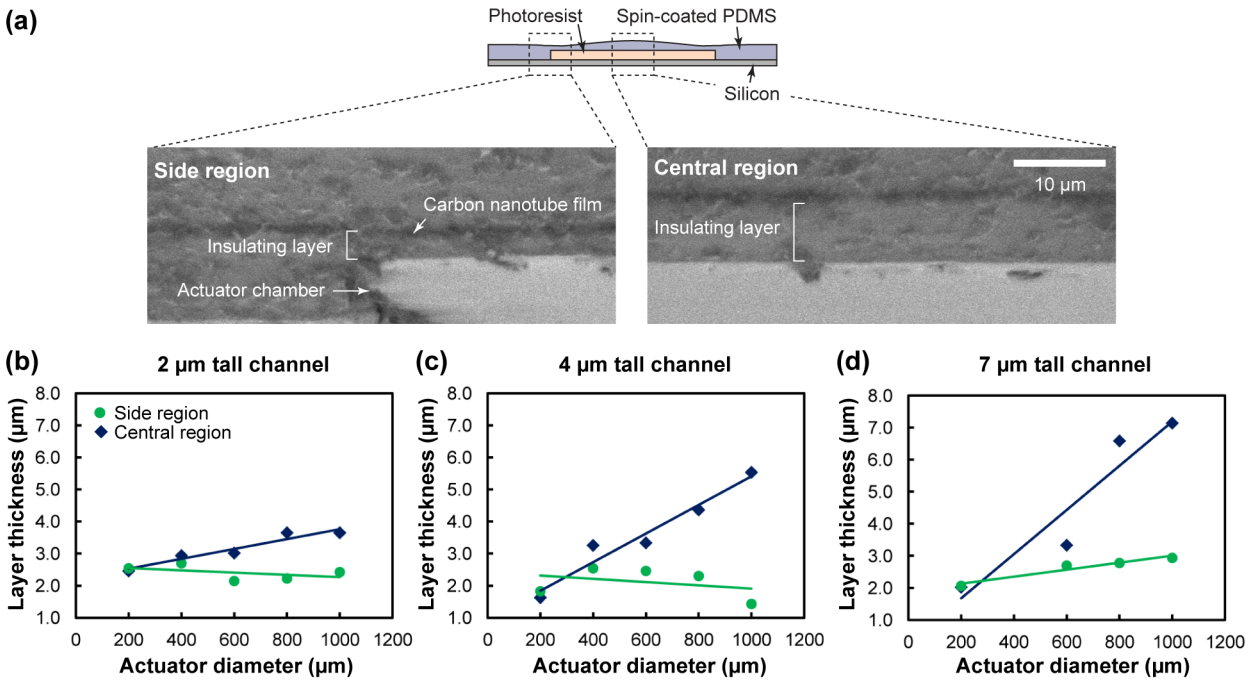

Figure 2.8 Dependence of the thickness of the insulating layer on the height of the fluid channel, the diameter of the actuator, and distance from the center of the membrane for channel heights of (a) 2 μm, (b) 4 μm, and (c) 7 μm.

liquid PDMS was sandwiched between the mold and a flat silicon wafer), but none were as easy and reliable as spin-coating. Hence, when comparing theory with experiment, we used an average value for the thickness of the insulating layer. Figure 2.8b-d shows a calibration that we performed that allowed us to predict the thickness.

2.3.2.3 Comparison of experimental results with the analytical model

We tested arrays of circular actuators with three different channel heights, g, (2, 4 and 7 μm),

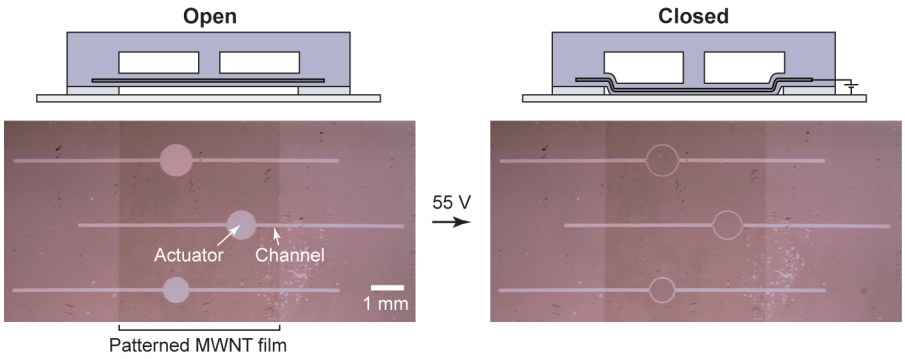

Figure 2.9 Illustrations (side view) and micrographs (top view) of electrostatic actuators in the open and closed states. The actuators shown were tested with air in the actuator chamber.

two different membrane thicknesses, t_m, (25 ± 6 μm (s.d) and 35 ± 6 μm (s.d.)), and eight different diameters, D, (200 – 900 μm) to compare experimental results with our model's predictions. To interface the actuators with a power source, a lead with an alligator clip was attached to the ITO film, and a second lead with a clip was attached to a metal wire, which was then inserted into the conducting mixture of PDMS in contact with the embedded electrode. We slowly increased the potential until we observed the membrane come into contact with the lower electrode (Figure 2.9), and documented the potential where actuation occurred.

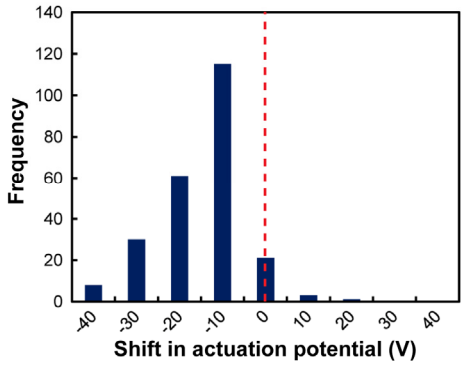

Figure 2.10 A graph illustrating the drift in actuation potential after three actuation attempts for actuators with three different channel heights.

In preliminary experiments, we noticed that the actuation potential drifted downward when the actuator was activated multiple times. Over the course of three actuations (with several minutes elapsing between actuation events), the potential shifted an average of -10 ± 10 V (s.d.) (Figure 2.10). After several more iterations, the membranes adhered to the lower electrode and would not release without an outside force. I hypothesized that this phenomenon might be due to the triboelectric effect; *i.e.*, peeling the elastomeric membrane off the oxide surface was redistributing electrons and causing charge accumulation on the surface of the membrane. Others have shown that charged surface groups migrate back into the bulk over time[53], so I heated the actuators between actuation attempts in an attempt to accelerate this process. The heat treatment effectively eliminated the potential drift. More detailed studies are needed to

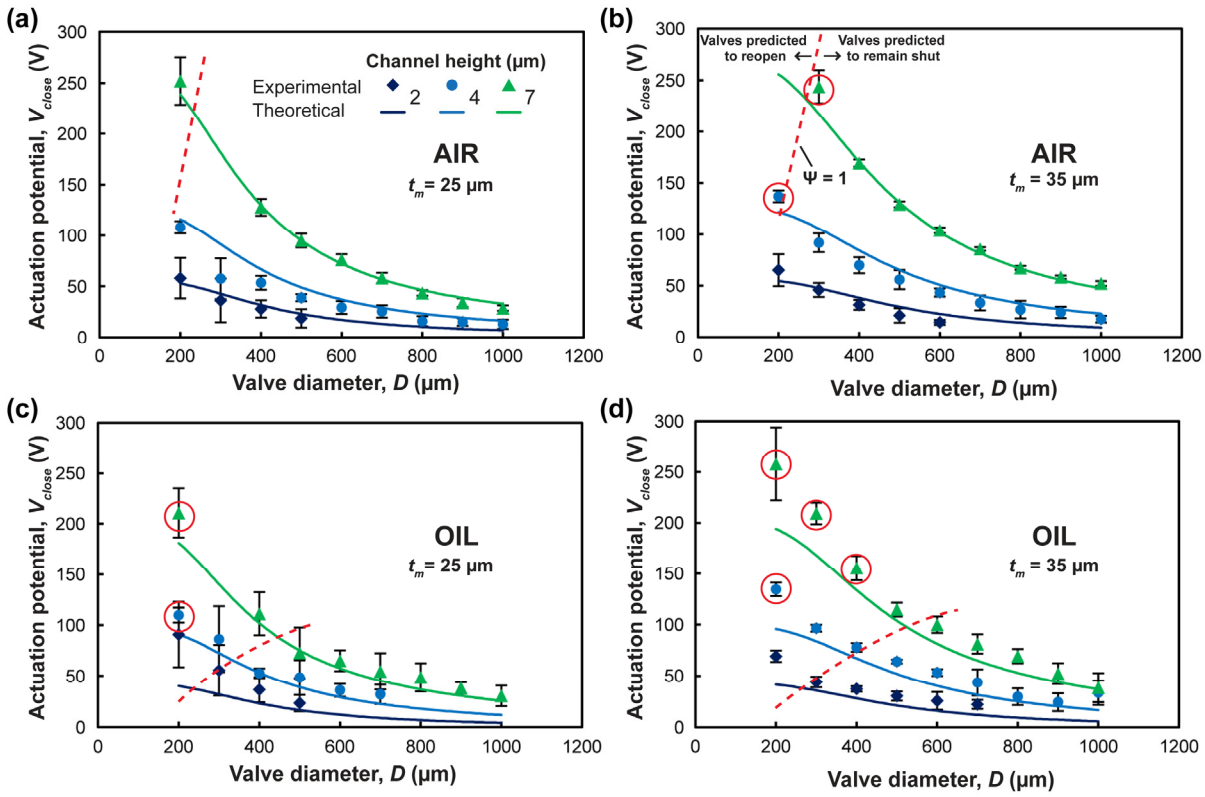

Figure 2.11 Comparison between actuation potentials predicted with the analytical model (lines) and those determined experimentally (points) for electrostatic actuators of different diameters with three different channel heights (2, 4 and 7 μm), two different membrane thicknesses (25 and 35 μm), and two different fluids between the electrodes (air and fluorinated oil). The conditions were (a) t_m = 25 μm in air, (b) t_m = 35 μm in air, (c) t_m = 25 μm in air, and (d) t_m = 35 μm in oil. The points above the red dashed lines indicated conditions where the actuator was analytically predicted to reopen after the actuation potential was removed, while the points below the red dashed lines indicated conditions where the actuator was predicted to remain closed. Red circles indicate which conditions led to actuators that reopened experimentally. Each actuator was tested five times. Error bars indicate one standard deviation.

definitively prove the mechanism behind the potential drift, however. Other factors could be contributing, including ionization due to high electric fields or the formation of insulated islands of nanoparticles, which could trap charges.

Figure 2.11 shows a comparison of our analytical predictions with the experimental outcomes, taking the variable thickness of the insulating layer into account and assuming a low residual stress in the membrane. Every data point indicates the average actuation potential obtained from three actuators, each activated five times (and heated at 70 °C for at least 30 min.

between actuation events). Error bars show the standard deviation of all the data collected for each set of conditions.

For all the conditions tested, we observed the actuators snapping into contact with the channel floor beyond a certain threshold potential, indicative of a pull-in instability, which was predicted by the model. We also observed good agreement between experimentally observed values of actuation potentials and analytically predicted values, with the deviation being between 7 % and 30 %. Some of the observed deviation can be attributed to the assumptions used while deriving the expressions for actuation potentials, and more likely, the values used for material properties (*e.g.*, Young's modulus), which were taken from literature. We observed that the membranes tended to sag slightly once released from their molds, which could have affected the actuation potential, and the stiffness of the carbon nanotube electrodes could have also been a factor. Finally, the variability in the density of the carbon nanotube films could have contributed, but the distribution of the data suggests that if the density of the films was a factor, it did not substantially shift the potential one way or the other.

The lowest observed actuation potential was 15 V (with a diameter of 600 μm, membrane thickness of 35 μm, and a channel height of 2 μm in the presence of air) (Figure 2.11c). However, under these conditions, the actuator was incapable of re-opening after the electric potential was released. For conditions where the actuator was able to re-open, the lowest observed actuation potential was 110 V (with a diameter of 200 μm, membrane thickness of 25 μm, and a channel height of 4 μm in the presence of oil) (Figure 2.11b). While the potentials needed to activate our actuators were lower than those of many of the precedents of polymer-based electrostatic actuators, they were still relatively high to be easily implemented with rapidly

oscillating fields (which are necessary for the actuators to operate with ionic solutes passing between the electrodes).

The model predicted that conditions above the red dashed lines would not collapse during fabrication and operation (*i.e.*, $\Psi > 1$). Every data point corresponds to a condition where the membrane did not collapse during fabrication (for at least 5 attempts), and a circle around a data point indicates a condition where the actuator reopened after the membrane was actuated. The accuracy with which the model could predict stiction was highly reliant on the value of the surface energy between the membrane and the channel floor. As we did not have the means to measure the value directly, we relied on values reported in literature, which varied widely, by as much as an order of magnitude[22-23]. Evaluating the accuracy of the model with regards to stiction will necessitate more accurate methods for measuring surface energy.

2.4 Conclusions

In summary, the analytical model we developed was capable of accurately predicting the potentials needed to close polymer-based electrostatic actuators. It was also capable of predicting which configurations of parameters led to unwanted adhesion of the membrane to the channel floor. The model guided the development of a fabrication procedure that consisted of mainly soft-lithographic techniques, which we believe will help make electrostatic actuators more widely accessible to researchers.

Due to the potentials required to operate the actuators, utilizing rapidly oscillating electric fields proved impractical. The equipment required to generate such fields would be excessive for portable applications, and the power requirements would be prohibitive as well. Hence, the design presented in this chapter was not capable of interacting *directly* with aqueous solutions.

The initial design could still be useful in a couple of different situations without modification, however. Firstly, in scenarios where all the reagents are non-polar, the actuators would still be operable. However, PDMS also swells in the presence of many non-polar solvents[54], so the actuator's materials would likely have to be adjusted. Secondly, the actuators might be useful for droplet-based systems where aqueous solutions are separated by a non-polar carrier phase (*e.g.*, fluorinated oil) or air. In this case, the actuators would be capable of actuating while oil or air slugs pass between the electrodes. However, since a plethora of lab-on-a-chip applications deal solely with aqueous phase reagents, the remainder of my dissertation discusses strategies that we implemented to avoid direct interaction between aqueous solutes and the electric fields produced by the actuators.

2.5 References

1. E.A. Costner, M.W. Lin, W.-L. Jen and C.G. Willson, "Nanoimprint lithography materials development for semiconductor device fabrication" *Annual Review of Materials Research,* 2009, 39, 155-180.

2. L.J. Guo, "Recent progress in nanoimprint technology and its applications" *Journal of Physics D: Applied Physics,* 2004, 37, R123.

3. H. Schift, "Nanoimprint lithography: An old story in modern times? A review" *Journal of Vacuum Science & Technology B: Microelectronics and Nanometer Structures,* 2008, 26, 458-480.

4. B.S. Driggs, M.M. Enzelberger and S.R. Quake, "Electrostatic valves for microfluidic devices" U.S. Patent 7232109, 2002.

5. D. Juncker, M. Nannini and V. Logiudice, "Electrical microvalve and method of manufacturing thereof" U.S. Patent 12513381, 2007.

6. T. Bansal, M.-P. Chang and M.M. Maharbiz, "A class of low voltage, elastomer-metal 'wet' actuators for use in high-density microfluidics" *Lab on a Chip,* 2007, 7, 164-166.

7. M.-P. Chang and M.M. Maharbiz, "Electrostatically-driven elastomer components for user-reconfigurable high density microfluidics" *Lab on a Chip,* 2009, 9, 1274-1281.

8. G. Flores, G. Mercado, J.A. Pelesko and N. Smyth, "Analysis of the dynamics and touchdown in a model of electrostatic MEMS" *SIAM Journal on Applied Mathematics,* 2007, 67, 434-446.

9. N.C. Goulbourne, M.I. Frecker and E. Mockensturm, In *Electro-elastic modeling of a dielectric elastomer diaphragm for a prosthetic blood pump*, Smart Structures and Materials 2004: Electroactive Polymer Actuators and Devices (EAPAD), San Diego, CA, USA, SPIE: San Diego, CA, USA, 2004; pp 122-133.

10. C. Wang, W. Guo and Q. Feng, "Deflection and stability of membrane structures under electrostatic and Casimir forces in microelectromechanical systems" *Acta Mechanica,* 2005, 180, 49-60.

11. A.S. Rollier, B. Legrand, D. Collard and L. Buchaillot, "The stability and pull-in voltage of electrostatic parallel-plate actuators in liquid solutions" *Journal of Micromechanics and Microengineering,* 2006, 16, 794-801.

12. P.M. Osterberg and S.D. Senturia, "M-TEST: A test chip for MEMS material property measurement using electrostatically actuated test structures" *Journal of Microelectromechanical Systems,* 1997, 6, 107-118.

13. S. Timoshenko and S. Woinowsky-Krieger, *Theory of plates and shells*. 2nd ed.; McGraw-Hill Book Company: New York, 1959.

14. W.C. Young, *Roark's formulas for stress and strain* 7th ed.; McGraw-Hill: New York, 2002.

15. M.D. Giovanni, *Flat and corrugated diaphgram design handbook*. Marcel Dekker Inc.: New York, 1982.

16. M.K. Small and W.D. Nix, "Analysis of the accuracy of the bulge test in determining the mechanical properties of thin films" *Journal of Materials Research,* 1992, 7, 3242 - 3249.

17. R.B. Darling, C. Hivick and J. Xu, "Compact analytical modeling of squeeze film damping with arbitrary venting conditions using a Green's function approach" *Sensors and Actuators A: Physical,* 1998, 70, 32-41.

18. J. Paul, S. Sindhu, M.H. Nurmawati and S. Valiyaveettil, "Mechanics of prestressed polydimethylsiloxane-carbon nanotube composite" *Applied Physics Letters,* 2006, 89, 184101-3.

19. A.R. Atwell, R.S. Okojie, K.T. Kornegay, S.L. Roberson and A. Beliveau, "Simulation, fabrication and testing of bulk micromachined 6H-SiC high-g piezoresistive accelerometers" *Sensors and Actuators A: Physical,* 2003, 104, 11-18.

20. J. Xie, J. Shih, Q. Lin, B. Yang and Y.-C. Tai, "Surface micromachined electrostatically actuated micro peristaltic pump" *Lab on a Chip,* 2004, 4, 495-501.

21. M. Hosseini, G. Zhu and Y.-A. Peter, "A new formulation of fringing capacitance and its application to the control of parallel-plate electrostatic micro actuators" *Analog Integrated Circuits and Signal Processing,* 2007, 53, 119-128.

22. K.J. Hsia, Y. Huang, E. Menard, J.U. Park, W. Zhou, J. Rogers and J.M. Fulton, "Collapse of stamps for soft lithography due to interfacial adhesion" *Applied Physics Letters,* 2005, 86, 154106-3.

23. K.G. Sharp, G.S. Blackman, N.J. Glassmaker, A. Jagota and C.-Y. Hui, "Effect of Stamp Deformation on the Quality of Microcontact Printing: Theory and Experiment" *Langmuir,* 2004, 20, 6430-6438.

24. M.P. de Boer and T.A. Michalske, "Accurate method for determining adhesion of cantilever beams" *Journal of Applied Physics,* 1999, 86, 817-827.

25. R. Maboudian and R.T. Howe, "Critical Review: Adhesion in surface micromechanical structures" *Journal of Vacuum Science & Technology B: Microelectronics and Nanometer Structures,* 1997, 15, 1-20.

26. E.E. Parker, W.R. Ashurst, C. Carraro and R. Maboudian, "Adhesion characteristics of MEMS in microfluidic environments" *Journal of Microelectromechanical Systems,* 2005, 14, 947-953.

27. C.H. Mastrangelo and C.H. Hsu, "Mechanical stability and adhesion of microstructures under capillary forces - Part II: Experiments" *Journal of Microelectromechanical Systems,* 1993, 2, 44-55.

28. C.H. Mastrangelo and C.H. Hsu, "Mechanical stability and adhesion of microstructures under capillary forces - Part I: Basic theory" *Journal of Microelectromechanical Systems,* 1993, 2, 33-43.

29. Z. Yapu, "Stiction and anti-stiction in MEMS and NEMS" *Acta Mechanica Sinica,* 2003, 19, 1-10.

30. V. Studer, G. Hang, A. Pandolfi, M. Ortiz, W.F. Anderson and S.R. Quake, "Scaling properties of a low-actuation pressure microfluidic valve" *Journal of Applied Physics,* 2004, 95, 393-398.

31. E. Yıldırım, M.A.S. Arıkan and H. Külah, "A normally-closed electrostatic parylene microvalve for micro total analysis systems" *Sensors and Actuators A: Physical*.

32. E. Yıldırım and H. Külah, "Analysis and characterization of an electrostatically actuated in-plane parylene microvalve" *Journal of Micromechanics and Microengineering,* 2011, 21, 105009.

33. M. Liu, J. Sun, Y. Sun, C. Bock and Q. Chen, "Thickness-dependent mechanical properties of polydimethylsiloxane membranes" *Journal of Micromechanics and Microengineering,* 2009, 19, 035028.

34. A. Thangawng, R. Ruoff, M. Swartz and M. Glucksberg, "An ultra-thin PDMS membrane as a bio/micro–nano interface: fabrication and characterization" *Biomedical Microdevices,* 2007, 9, 587-595.

35. D. Armani, C. Liu and N. Aluru In *Re-configurable fluid circuits by PDMS elastomer micromachining*, Twelfth IEEE International Conference on Micro Electro Mechanical Systems, MEMS '99., C. Liu, Ed. 1999; pp 222-227.

36. Sylgard 184 silicone elastomer data sheet. Dow Corning, 2008.

37. J.E. Mark, *Polymer Data Handbook*. Oxford Unversity Press: New York, 1999.

38. H. Song, J.D. Tice and R.F. Ismagilov, "A microfluidic system for controlling reaction networks in time" *Angewandte Chemie International Edition,* 2003, 42, 768-772.

39. D. Chatterjee, B. Hetayothin, A.R. Wheeler, D.J. King and R.L. Garrell, "Droplet-based microfluidics with nonaqueous solvents and solutions" *Lab on a Chip,* 2006, 6, 199-206.

40. 3M™ Fluorinert™ Electronic Liquid FC-40 Product information. Dow Corning, 2010.

41. M. Maghribi, J. Hamilton, D. Polla, K. Rose, T. Wilson and P. Krulevitch In *Stretchable micro-electrode array for retinal prosthesis*, 2nd Annual International IEEE-EMB Special Topic Conference on Microtechnologies in Medicine & Biology 2002; pp 80-83.

42. F. Schneider, T. Fellner, J. Wilde and U. Wallrabe, "Mechanical properties of silicones for MEMS" *Journal of Micromechanics and Microengineering,* 2008, 18, 065008.

43. N. Bowden, S. Brittain, A.G. Evans, J.W. Hutchinson and G.M. Whitesides, "Spontaneous formation of ordered structures in thin films of metals supported on an elastomeric polymer" *Nature,* 1998, 393, 146-149.

44. N. Pekas, Q. Zhang, M. Nannini and D. Juncker, "Wet-etching of structures with straight facets and adjustable taper into glass substrates" *Lab on a Chip,* 2010, 10, 494-498.

45. R. Andrews and M.C. Weisenberger, "Carbon nanotube polymer composites" *Current Opinion in Solid State and Materials Science,* 2004, 8, 31-37.

46. J.N. Coleman, U. Khan, W.J. Blau and Y.K. Gun'ko, "Small but strong: A review of the mechanical properties of carbon nanotube–polymer composites" *Carbon,* 2006, 44, 1624-1652.

47. J. Engel, J. Chen, C. Nannan, S. Pandya and L. Chang In *Multi-walled carbon nanotube filled conductive elastomers: Materials and application to micro transducers*, Micro Electro Mechanical Systems, 2006. MEMS 2006 Istanbul. 19th IEEE International Conference on, 2006; 2006; pp 246-249.

48. Z. Wu, Z. Chen, X. Du, J.M. Logan, J. Sippel, M. Nikolou, K. Kamaras, J.R. Reynolds, D.B. Tanner, A.F. Hebard and A.G. Rinzler, "Transparent, conductive carbon nanotube films" *Science,* 2004, 305, 1273-1276.

49. C. Liu, "Recent developments in polymer MEMS" *Advanced Materials,* 2007, 19, 3783-3790.

50. M. Kaempgen, G.S. Duesberg and S. Roth, "Transparent carbon nanotube coatings" *Applied Surface Science,* 2005, 252, 425-429.

51. L. Hu, D.S. Hecht and G. Grüner, "Percolation in transparent and conducting carbon nanotube networks" *Nano Letters,* 2004, 4, 2513-2517.

52. Y. Zhou, L. Hu and G. Gruner, "A method of printing carbon nanotube thin films" *Applied Physics Letters,* 2006, 88, 123109-3.

53. M.J. Owen and P.J. Smith, "Plasma treatment of polydimethylsiloxane" *Journal of Adhesion Science and Technology,* 1994, 8, 1063-1075.

54. J.N. Lee, C. Park and G.M. Whitesides, "Solvent compatibility of poly(dimethylsiloxane)-based microfluidic devices" *Analytical Chemistry,* 2003, 75, 6544-6554.

Chapter 3

Instructing pneumatic microsystems with integrated electrostatic actuators*

3.1 Introduction

Since the initial design of the electrostatic actuator was not capable of interacting directly with aqueous solutions, I investigated ways of indirectly controlling fluid flow with the actuators. Considering the versatility, robustness, and ubiquity of pneumatic microvalves, I chose to interface the electrostatic actuators with pneumatic microsystems. The electrostatic components were responsible for converting electrical signals into mechanical forces, and the pneumatic microvalves interacted with aqueous solutions. The strategies I adopted were largely informed by several precedents for controlling pneumatic microsystems with portable ancillaries, alluded to in Chapter 1. Generally speaking, these methods can be placed into one of two categories: (i) processes that generate pressure-pulses by compressing a fluid chamber on-chip, and (ii) schemes that use arrays of actuators to direct pressure from an external source to the appropriate pneumatic control channel. In the former, researchers have used solenoid valves[1], Braille pins[2], and screws[3] to compress the chamber. However, all of these actuators occupy a significant footprint on the chip, Braille pins and solenoid valves consume significant power, and screws are not automated. I saw an opportunity for the electrostatic actuators to improve on these shortcomings while being integrated monolithically with the rest of the microfluidic system.

*Part of the work presented in this chapter has been published previously: J.D. Tice, A.V. Desai, T.A. Bassett, C.A. Apblett, and P.J.A. Kenis, "Electrostatic microvalves for integrated microchemical systems" *The 15th International Conference on Miniaturized Systems for Chemistry and Life Sciences*, October 2-6, 2011, Seattle, WA. Reproduced with permission from The Chemical and Biological Microsystems Society.

I was also confident that our electrostatic actuators could improve on previously reported methods for directing pressure from an external source to the chip. Currently, the most common way of directing pressure is through an array of external solenoid valves, which is both too power intensive and bulky for portable applications. Bruce *et al*. have reported external array of electrostatic actuators that consume less power (see Figure 1.6f)[4], but their electrostatic actuators suffer from drift in actuation potentials, which eventually renders the actuators ineffective. In this chapter, I address the issue of potential drift and show that our actuators can be integrated with pneumatic microsystems. I then show how the actuators can be used to regulate pneumatic control channels pressurized up to ~100 kPa.

3.2 Materials and methods

3.2.1 Fabrication of electrostatic actuators with elastomer-based lower electrodes

Molds for channels and actuator chambers were made by patterning SU-8 5 photoresist (Microchem Corp.) onto silicon wafers using standard photolithographic techniques in accordance with the manufacturer's specifications. For channels 2 μm tall, the photoresist was spun at 7,200 rpm for 30 seconds, and for channels 7 μm tall, the photoresist was spun at 1,700 rpm for 30 seconds. Molds for the stamps were fabricated using SU-8 50 spun at 2,000 rpm for 30 seconds. To reduce adhesion between poly(dimethlysiloxane) (PDMS) and the molds, a surface treatment was performed by placing the molds in a vacuum desiccator along with several drops of (tridecafluoro-1,1,2,2-tetrahydrooctyl)trichlorosilane (Gelest, Inc.), and then applying vacuum overnight.

To construct the upper layers of the actuator, a thin layer of PDMS (20:1 ratio of monomer to cross-linking agent by weight; General Electric RTV 615, Hisco, Inc.) was first spin-coated onto

the mold at 10,000 rpm for 300 seconds (for 2 μm tall channels) or 50 seconds (for 7 μm tall channels) such that a thin film covered the channel features. The PDMS film was cured in an oven at 70 °C for 1 hour and then allowed to cool to room temperature. To form the electrode, an aqueous suspension of multi-walled carbon nanotubes (MWNTs) (20-30 nm outer diameter, 10-30 μm length, > 95 wt% purity, ash < 1.5 wt%; Cheaptubes, Inc.) with a ratio of 1 g MWNTs : 10 g sodium dodecyl sulfate : 1 mL deionized water was prepared and sonicated (Vibra-Cell VCX130PB, Sonics & Materials, Inc.) for approximately 30 minutes to solubilize the MWNTs. A 0.1 mL sample was diluted into approximately 20-30 mL deionized water and stirred briefly. The dilute suspension was filtered through an alumina membrane (Whatman Anodisc™ inorganic membrane, 0.1 or 0.2 μm pore size, 47 mm diameter) that had been wet with ethanol. After the aqueous suspension had fully passed through the membrane, the MWNTs that remained on the membrane were washed with ethanol until the filtrate was free of bubbles. A PDMS stamp (20:1 ratio of monomer to cross-linking agent by weight, cured overnight at 70 °C) was brought into contact with the MWNT film. Areas in contact with the stamp were lifted off the membrane filter and then applied to the PDMS film formed previously. Pressure was applied by hand, and after lifting off the PDMS stamp, a fraction of the MWNT film transferred to the PDMS film. Electrical contacts were made from a mixture of PDMS (5:1 ratio of monomer to cross-linking agent by weight) and 10 wt% MWNTs, which was applied on the designated area of the MWNT electrode and subsequently cured for 15 minutes in an oven at 70 °C. To encapsulate the MWNT electrode, a second layer of PDMS (20:1 ratio of monomer to cross-linking agent by weight) was spin-coated on top of the electrode at 2,400 rpm for 30 seconds and allowed to cure until tacky in an oven at 70 °C for 20-30 minutes. The PDMS support layer (5:1 ratio of monomer to cross-linking agent by weight; cured at 70 °C for 1 hour) was aligned onto

the membrane. The support layer contained cylindrical posts centered in the recesses over the actuator chambers that were 20 % the diameter of the underlying chambers. After aligning the support layer, uncovered regions of the spin-coated PDMS layers were filled with liquid PDMS (5:1 ratio of monomer to cross-linking agent by weight) and the whole assembly was cured overnight in an oven at 70 °C. Afterward, the upper layers of the actuator were removed from the mold and holes were punched to the inlets of the microchannels using a sharpened 20 gauge steel needle.

To fabricate the lower electrode for the actuator, a featureless silicon wafer was treated with silane vapor as described previously, and a thin layer of PDMS (20:1 ratio of monomer to cross-linking agent by weight), diluted in hexanes (10:1 ratio of hexanes to PDMS by weight) was spin-coated onto the wafer at 10,000 rpm for 120 seconds. The thin PDMS layer was cured in an oven at 70 °C for 1 hour, and then a MWNT film was applied as described above. Electrical contacts were also applied, and the wafer was then covered with a layer of PDMS (5:1 ratio of monomer to cross-linking agent by weight) several millimeters thick. The PDMS was cured overnight at 70 °C.

To seal the upper layers of the actuator to the lower electrode, both surfaces participating in the seal were exposed to oxygen plasma generated with an atmospheric plasma system (Atomflo™ 400L system equipped with an AH-250L head, Surfx Technologies). The system was configured to 100 W RF power, with an oxygen flow rate of 0.03 L min^{-1} and a helium flow rate of 15.0 L min^{-1}. Two situations were investigated. In the first, the lower electrode was passed under the plasma repeatedly for a duration of ~1 minute. The upper layers were passed under three times for about one second each pass. In the second situation, both surfaces were passed three times under the plasma for about one second each pass. For both cases,

immediately after exposure to plasma, the separate layers were aligned and brought into contact. To complete the seal, devices was heated at 70 °C for at least 1 hour.

3.2.2 Characterizing drift in actuation potentials

The actuator chambers were filled with fluorinated oil (3M™ Fluorinert™ FC-40), wires were inserted into the electrical contacts on the device, and the wires were attached to electrical leads connected to a DC power supply (Hewlett Packard model 6209B). The upper electrode was negatively polarized. The potential was increased slowly (~10 V s^{-1}) until the membrane came into contact with the floor of the actuator chamber. Afterward, the potential was released, and the process was repeated immediately afterward. At select instances, 5 minutes were allowed to elapse between actuation attempts. The actuator was viewed under an inverted microscope (Leica, DMI4000) equipped with a 1600 × 1200 pixel charge-coupled device camera (QImaging, Retiga-2000R) and phase contrast optics to clearly visualize contact of the membrane with the floor of the actuator chamber.

3.2.3 Fabrication of electrostatic actuators for generating pressure pulses

The fabrication was accomplished as described in Section 3.2.1, with the following modifications. To fabricate the lower electrode along with an integrated pneumatic microvalve, a featureless silicon wafer was treated with silane vapor, and a thin layer of PDMS (20:1 ratio of monomer to cross-linking agent by weight), diluted in hexanes (10:1 ratio of hexanes to PDMS by weight) was spin-coated onto the wafer at 10,000 rpm for 120 seconds. The thin PDMS layer was cured in an oven at 70 °C for 1 hour, and then a MWNT film was applied as described previously. Electrical contacts were also applied and cured at 70 °C for 15 minutes. I then spin-coated a second layer of PDMS (20:1 ratio of monomer to cross-linking agent by weight) at 6,000 rpm for 30 seconds. The PDMS was cured at 70 °C for 20-30 minutes until slightly tacky,

and then another layer of PDMS (5:1 ratio of monomer to cross-linking agent by weight; cured at 70 °C for at least 1 hour) with a rounded microchannel was aligned and placed on top. Uncovered regions of the spin-coated PDMS layers were filled with liquid PDMS (5:1 ratio of monomer to cross-linking agent by weight) and the whole assembly was cured overnight at 70 °C. The mold for the rounded channel was made by spin-coating Microposit™ SPR220™-7 photoresist at 1500 rpm for 60 seconds. The remainder of the photoresist processing was done according to the manufacturer's specifications. Following development, the mold was heated at 150 °C for 30 minutes to heat the photoresist above its glass transition temperature and allow it to reflow, and then the mold was silanized.

3.2.4 Testing electrostatic actuators for generating pressure pulses

The upper layers of the electrostatic actuator were not sealed permanently to the lower electrode. Rather, after filling the fluid channel of the pneumatic microvalve with food coloring diluted with water, I placed several drops of fluorinated oil (3M™ Fluorinert™ FC-40) onto the lower electrode and then placed the upper layers on top. Pressure was applied by hand to remove residual oil from between the layers such that a reversible bond could form. Leads from a DC power supply (Hewlett Packard model 6209B) were attached to wires which were inserted into the electrical contacts made of PDMS and MWNTs, with the upper electrode negatively polarized. A potential of 300 V was applied between the electrodes, and images were captured through a stereoscope (Leica M025 C).

3.2.5 Fabrication of electrostatic gates for instructing pneumatic control lines

The fabrication was accomplished as described in Section 3.2.1, with the following modifications. To fabricate the lower electrode along with an integrated pneumatic microvalve, a featureless silicon wafer was treated with silane vapor, and a thin layer of PDMS (20:1 ratio of

monomer to cross-linking agent by weight), diluted in hexanes (10:1 ratio of hexanes to PDMS by weight) was spin-coated onto the wafer at 10,000 rpm for 120 seconds. The thin PDMS layer was cured in an oven at 70 °C for 1 hour, and then a MWNT film was applied as described previously. Electrical contacts were also applied and cured at 70 °C for 15 minutes. We then spin-coated a second layer of PDMS (20:1 ratio of monomer to cross-linking agent by weight) at 6,000 rpm for 30 seconds. The PDMS was cured at 70 °C for 20-30 minutes until slightly tacky, and then another layer of PDMS (5:1 ratio of monomer to cross-linking agent by weight; cured at 70 °C for at least 1 hour) with a rounded microchannel was aligned and placed on top. Uncovered regions of the spin-coated PDMS layers were filled with liquid PDMS (5:1 ratio of monomer to cross-linking agent by weight) and the whole assembly was cured overnight at 70 °C. The mold for the rounded channel was made by spin-coating Microposit™ SPR220™-7 photoresist at 1500 rpm for 60 seconds. The remainder of the photoresist processing was done according to the manufacturer's specifications. Following development, the mold was heated at 150 °C for 30 minutes to heat the photoresist above its glass transition temperature and allow it to reflow, and then the mold was silanized.

To seal the upper layers of the actuator to the lower electrode, both surfaces participating in the seal were exposed to oxygen plasma generated with an atmospheric plasma system (Atomflo™ 400L system equipped with an AH-250L head, Surfx Technologies). The system was configured to 100 W RF power, with an oxygen flow rate of 0.03 L $min.^{-1}$ and a helium flow rate of 15.0 L $min.^{-1}$. Both surfaces were passed three times under the plasma for about one second each pass. For both cases, immediately after exposure to plasma, the separate layers were aligned and brought into contact. To complete the seal, devices was heated at 70 °C for at least 1 hour.

3.2.6 Characterizing the pressures accommodated by electrostatic gates

The actuator chambers were filled with fluorinated oil (3M™ Fluorinert™ FC-40). Wires were inserted into the electrical contacts on the device, and the wires were attached to electrical leads connected to a DC power supply (Hewlett Packard model 6209B) with the upper electrode negatively polarized. The inlet of the control channel was attached to a source of pressurized nitrogen *via* a pressure controller (Cole Parmer, model 68027-780). The outlet was shut with a piece of Teflon® tubing that was filled with cured PDMS. A potential was applied across the electrodes to close the gate, and then the pressure in the gate chamber was increased slowly (~0.1 kPa s^{-1}) until the membrane released from the floor of the microchannel. Afterward, the pressure was decreased at the same rate until the membrane snapped back into contact with the channel floor. This process was undertaken at least three times per gate.

3.2.7 Testing electrostatic gates coupled to a pneumatic microvalve

The actuator chambers were filled with fluorinated oil (3M™ Fluorinert™ FC-40). Wires were inserted into the electrical contacts on the device, and the wires were attached to electrical leads connected to a DC power supply (Hewlett Packard model 6209B) with the upper electrode negatively polarized. The inlet of the control channel was attached to a vial filled with fluorinated oil and attached to a source of pressurized nitrogen *via* a pressure controller (Cole Parmer, model 68027-780). The inlet pressure was adjusted to 8 kPa, and the outlet was vented to atmosphere. The reagent channel was filled with a mixture of blue food coloring with 50 % ethanol by volume. To shut the pneumatic microvalve, a potential of 300 V was applied to the gate downstream of the pneumatic microvalve. To open the pneumatic microvalve, the same potential was applied to the upstream gate, and then the potential applied to the downstream gate was released. Images were captured through a stereoscope (Leica M025 C).

3.2.8 Fabrication of electrostatic gates with pressure-balancing channels

Molds for channels and actuator chambers were made by patterning SU-8 5 photoresist (Microchem Corp.) onto silicon wafers using standard photolithographic techniques in accordance with the manufacturer's specifications. For channels 2 μm tall, the photoresist was spun at 7,200 rpm for 30 seconds, and for channels 7 μm tall, the photoresist was spun at 1,700 rpm for 30 seconds. In some cases, posts were patterned onto the molds to enable the formation of through-holes during the fabrication of the gates. To pattern the posts, SU-8 photoresist was spin-coated on top of the previously developed SU-8 structures at 2,000 rpm for 30 seconds and processed according to the maufacturer's specifications. The posts were 100-200 μm in diameter. Molds for the support layer were either made with SU-8 50, spin-coated at 2,000 rpm for 30 seconds, or SU-8 5, spin-coated at 3,000 rpm for 30 seconds. Molds for the stamps were fabricated using SU-8 50 spun at 2,000 rpm for 30 seconds. To reduce adhesion between poly(dimethlysiloxane) (PDMS) and the molds, a surface treatment was performed by placing the molds in a vacuum desiccator along with several drops of (tridecafluoro-1,1,2,2-tetrahydrooctyl)trichlorosilane (Gelest, Inc.), and then applying vacuum overnight.

To construct the upper layers of the actuator, a thin layer of PDMS (20:1 ratio of monomer to cross-linking agent by weight) was first spin-coated onto the mold at 10,000 rpm for 300 seconds (for 2 μm tall channels) or 50 seconds (for 7 μm tall channels) such that a thin film covered the channel features. Posts, however, protruded through this film. The PDMS film was cured in an oven at 70 °C for 1 hour and then allowed to cool to room temperature. To form the electrode, an aqueous suspension of multi-walled carbon nanotubes (MWNTs) (20-30 nm outer diameter, 10-30 μm length, > 95 wt% purity, ash < 1.5 wt%; Cheaptubes, Inc.) with a ratio of 1 g MWNTs : 10 g sodium dodecyl sulfate : 1 mL deionized water was prepared and sonicated (Vibra-Cell

VCX130PB, Sonics & Materials, Inc.) for approximately 30 minutes to solubilize the MWNTs. A 0.1 mL sample was diluted into approximately 20-30 mL deionized water and stirred briefly. The dilute suspension was filtered through an alumina membrane (Whatman Anodisc™ inorganic membrane, 0.1 or 0.2 μm pore size, 47 mm diameter) that had been wet with ethanol. After the aqueous suspension had fully passed through the membrane, the MWNTs that remained on the membrane were washed with ethanol until the filtrate was free of bubbles. A PDMS stamp (20:1 ratio of monomer to cross-linking agent by weight, cured overnight at 70 °C) was brought into contact with the MWNT film. Areas in contact with the stamp were lifted off the membrane filter and then applied to the PDMS film formed previously. Pressure was applied by hand, and after lifting off the PDMS stamp, a fraction of the MWNT film transferred to the PDMS film. Electrical contacts were made from a mixture of PDMS (5:1 ratio of monomer to cross-linking agent by weight) and 10 wt% MWNTs, which was applied on the designated area of the MWNT electrode and subsequently cured for 15 minutes in an oven at 70 °C. To encapsulate the MWNT electrode, a second layer of PDMS (20:1 ratio of monomer to cross-linking agent by weight) was spin-coated on top of the electrode at 3,000 rpm for 30 seconds and allowed to cure until tacky in an oven at 70 °C for 20-30 minutes. The PDMS support layer (5:1 ratio of monomer to cross-linking agent by weight; cured at 70 °C for 1 hour) was aligned onto the membrane, and after, uncovered regions of the spin-coated PDMS layers were filled with liquid PDMS (5:1 ratio of monomer to cross-linking agent by weight). The whole assembly was cured overnight in an oven at 70 °C. Afterward, the upper layers of the gate were removed from the mold and holes were punched to the inlets of the microchannels using a sharpened 20 gauge steel needle. If SU-8 posts were patterned onto the molds for the channels, then through-holes would naturally form after releasing the PDMS layers from the mold. If not, a scalpel was used

to cut a triangular hole in the designated area to allow fluidic communication between the control channel and the pressure-balancing channel.

To fabricate the lower electrode for the gate, a featureless silicon wafer was treated with silane vapor as described previously, and a thin layer of PDMS (20:1 ratio of monomer to cross-linking agent by weight), diluted in hexanes (10:1 ratio of hexanes to PDMS by weight) was spin-coated onto the wafer at 10,000 rpm for 120 seconds. The thin PDMS layer was cured in an oven at 70 °C for 1 hour, and then a MWNT film was applied as described above. Electrical contacts were also applied, and the wafer was then covered with a layer of PDMS (5:1 ratio of monomer to cross-linking agent by weight) several millimeters thick. The PDMS was cured overnight at 70 °C.

To seal the upper layers of the gate to the lower electrode, both surfaces participating in the seal were exposed to oxygen plasma generated with an atmospheric plasma system (Atomflo™ 400L system equipped with an AH-250L head, Surfx Technologies). The system was configured to 100 W RF power, with an oxygen flow rate of 0.03 L min^{-1} and a helium flow rate of 15.0 L min^{-1}. Both surfaces were passed three times under the plasma for about one second each pass. For devices with ~2 μm tall gate chambers, the membrane was pushed up into the pressure-balancing chamber such that an irreversible bond formed between the membrane and the top of the cavity, which prevented the membrane from collapsing when the separate layers were aligned and brought into contact. To complete the seal, devices was heated at 70 °C for at least 1 hour.

3.2.9 Characterizing the pressures accommodated by pressure-balanced electrostatic gates

The gate chambers were filled with fluorinated oil (3M™ Fluorinert™ FC-40). Wires were inserted into the electrical contacts on the device, and the wires were attached to electrical leads connected to a DC power supply (Hewlett Packard model 6209B) with the upper electrode

negatively polarized. The inlet of the control channel was attached to a vial filled with fluorinated oil and attached to a source of pressurized nitrogen *via* a pressure controller (Cole Parmer, model 68027-780). The outlet was shut with a piece of Teflon® tubing that was filled with cured PDMS. To test the potentials needed to close the gates at a given pressure, the pressure was held constant and the potential was increased slowly (~1 V s^{-1}) until the membrane touched the floor of the channel. After, the potential was increased further in intervals of 20 V and micrographs were taken at each setting through a stereoscope. To quantify the area of the membrane in contact with the floor of the channel, the pixels corresponding to the collapsed area were counted with Adobe Photoshop. To test the pressures needed to re-open the gates at a given potential, the potential was held constant and the pressure was increased slowly (~0.1 kPa s^{-1}) until the membrane released from the floor of the microchannel. As the pressure was increased, micrographs were taken through a stereoscope in intervals of ~6 kPa. Again, pixels were counted to characterize the area of the membrane in contact with the floor of the channel.

3.2.10 Fabrication of microfluidic pressure amplifier circuits

Microfluidic pressure amplifier circuits with integrated pressure-balanced electrostatic gates were fabricated as in Section 3.2.8 with the following modifications. The molds for the channels were made from a mixture of SU-8 2005 and cyclopentanone in a 2:1 volume ratio. The mixture was spin-coated onto a silicon wafer at 2,000 rpm for 30 seconds and then developed according to the manufacturer's specifications for undiluted SU-8 2005, yielding features ~2 μm tall. The molds for the support layer were made from SU-8 2005, spin-coated at 5,000 rpm for 30 seconds, yielding features ~3 μm tall. In certain instances, the support layer contained a cavity not only above the membrane of the gate, but also above the channel leading to the gate. If a membrane-based pressure sensor was integrated into the circuit, a ~2 mm diameter hole was punched in the

support layer in the area directly above the sensor. Through-holes connecting the gate chamber with the pressure-balancing channel were cut with a scalpel.

To integrate a pneumatic microvalve into the circuit, the lower electrode was made by spin-coating a thin layer of PDMS (20:1 ratio of monomer to cross-linking agent by weight), diluted in hexanes (10:1 ratio of hexanes to PDMS by weight) onto a featureless wafer at 10,000 rpm for 120 seconds. The thin PDMS layer was cured in an oven at 70 °C for 1 hour, and then a MWNT film was applied as described above. Electrical contacts were also deposited, and then a second layer of PDMS (20:1 ratio of monomer to cross-linking agent by weight) was spin-coated on top at 2,400 rpm for 30 seconds. The PDMS was allowed to cure until tacky in an oven at 70 °C for 20-30 minutes. Afterward, a slab of PDMS (5:1 ratio of monomer to cross-linking agent by weight; cured at 70 °C for at least 1 hour) containing a rounded microchannel was aligned and placed on top. The mold for the rounded channel was made as described in Section 3.2.3. Uncovered regions of the spin-coated PDMS layers were filled with liquid PDMS (5:1 ratio of monomer to cross-linking agent by weight) and the whole assembly was cured overnight at 70 °C.

To seal the upper layers of the circuit to the lower electrode, both surfaces participating in the seal were exposed to oxygen plasma generated with an atmospheric plasma system (Atomflo™ 400L system equipped with an AH-250L head, Surfx Technologies). The system was configured to 100 W RF power, with an oxygen flow rate of 0.03 L min^{-1} and a helium flow rate of 15.0 L min^{-1}. Both surfaces were passed three times under the plasma for about one second each pass. Any suspended membrane was pushed up into the cavities in the support layer such that an irreversible bond formed between the membrane and the top of the cavity, which helped prevent the membrane from collapsing when the separate layers were aligned and brought into contact.

In some instances, 20-30 minutes were allowed to elapse after plasma exposure before aligning and bringing the surfaces into contact. To complete the seal, devices was heated at 70 °C for at least 1 hour.

3.2.11 Characterizing pressures generated by microfluidic pressure amplifier circuits

The control channels and gate chambers were filled with fluorinated oil (3M™ Fluorinert™ FC-40). Wires were inserted into the electrical contacts on the device, and the wires were attached to electrical leads connected to a DC power supply (Hewlett Packard model 6209B) with the upper electrode negatively polarized. The inlet of the control channel was attached to a vial filled with fluorinated oil and attached to a source of pressurized nitrogen *via* a pressure controller (Cole Parmer, model 68027-780). Initially, the outlet was shut with a piece of Teflon® tubing that was filled with cured PDMS. The pressure was increased in increments of 5 kPa, and images of the pressure sensor were taken through a stereoscope. The images were later used to calibrate the sensor. Two different pressure sensors were used. In one case, the pressure sensor consisted of a membrane suspended above a microfluidic chamber in fluidic communication with the control channel. In the other case, the pressure sensor consisted of a piece of glass capillary, with one end melted shut with a flame. This capillary, filled only with air, was inserted into a piece of Teflon® tubing, which was filled with fluorinated oil and in fluidic communication with the control channel.

To characterize the pressures that could be generated by use of the electrostatic gate, the outlet was opened, and the electrostatic gate was actuated at a given potential. An image of the pressure sensor was again collected and compared with the calibration curve to extract a reading.

3.2.12 Characterizing pressure amplifier circuits coupled with pneumatic microvalves

The gate chambers were filled with fluorinated oil (3M™ Fluorinert™ FC-40). Wires were inserted into the electrical contacts on the device, and the wires were attached to electrical leads connected to a custom-designed electrical circuit that produced a square-wave signal with a peak-to-peak voltage of 250 V. The upper electrode was negatively polarized. The inlet of the control channel was attached to a vial filled with fluorinated oil and attached to a source of pressurized nitrogen *via* a pressure controller (Cole Parmer, model 68027-780). The reagent channel was filled with a mixture of food coloring water. A gate with a chamber height of 2 μm and a diameter of 400 μm was cycled at 0.2 Hz while applying a pressure of 40-60 kPa.

3.2.13 Determination of actuator dimensions

To determine critical valve dimensions, valves were cut in half to expose the cross-sections and then observed with a scanning electron microscope (JEOL 6060LV SEM). Channel depths were measured with a profilometer (Dektak 3030).

3.3 Results and discussion

3.3.1 Monolithic construction of electrostatic actuators

The actuators reported in the previous chapter were primarily composed of PDMS and MWNTs, with the lower electrode consisting of an indium tin oxide (ITO) film deposited on glass. For the purpose of corroborating our mathematical model, this construction of the lower electrode was adequate. However, to implement the actuators in meaningful applications, two challenges needed to be addressed. Firstly, the fabrication of the ITO electrodes deviated from the philosophy of simplicity I was trying to achieve. The ITO films were thermally evaporated onto glass, patterned with either lift-off or chemical etching methods, and then thermally

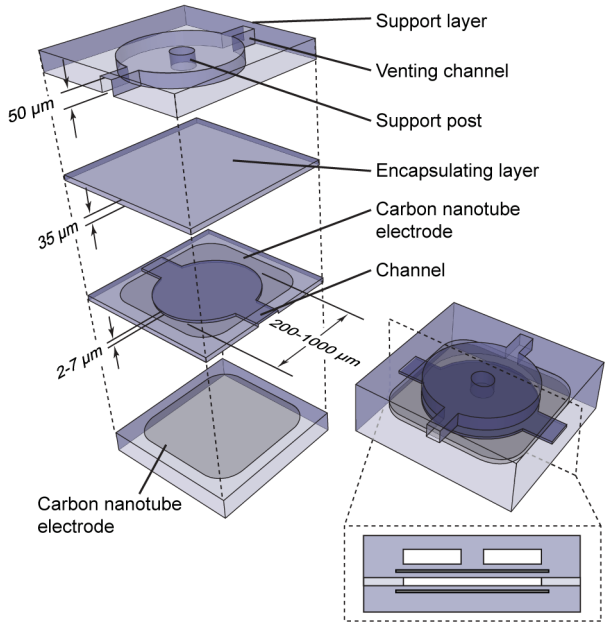

Figure 3.1 An exploded view, a perspective view, and a cross-sectional view of a monolithic design for the electrostatic actuator. Not drawn to scale.

annealed – intensive procedures compared with soft-lithography. Secondly, the actuation potential drifted substantially when the actuators were operated with an ITO lower electrode, a phenomenon I attributed to contact electrification.

To address both issues, I investigated several soft-lithographic methods to fabricate the lower electrode from PDMS and MWNTs. Switching to a completely monolithic architecture (Figure 3.1) allowed me to simplify the fabrication process. In addition, I reasoned that material symmetry between the membrane and the lower electrode would eliminate the accumulation of surface charges due to the triboelectric effect, and consequently, eliminate drift in the actuation potential. Similarly, others have shown that coating both electrodes of an electrostatic actuator with the same "non-stick" surface treatment can prevent stiction[5-7].

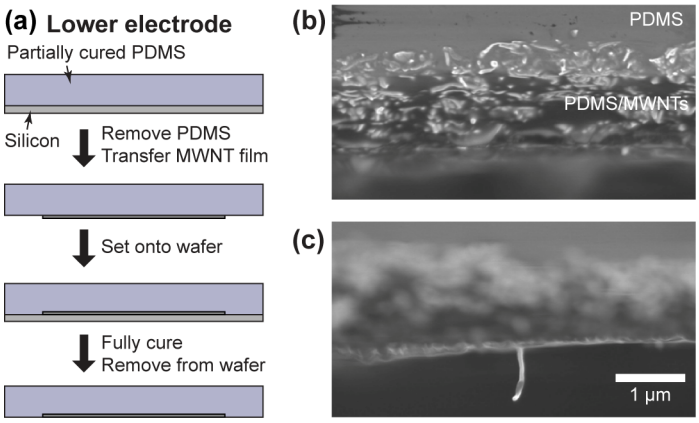

Figure 3.2 (a) Illustration of a method for fabricating electrodes by reflowing PDMS around a film of MWNTs. (b) An SEM micrograph of a MWNT film after the reflow process. (c) A micrograph of a MWNT protruding beyond the surface of the PDMS matrix.

In my initial approach (Figure 3.2a), I poured a layer of PDMS (20:1 ratio of monomer to cross-linking agent by weight) several millimeters thick onto a featureless silicon wafer and then removed the PDMS before it was fully cured. I then transferred a film of MWNTs to the PDMS and set the surface with the MWNTs back into contact with the silicon wafer. After the PDMS fully cured, images collected with scanning electron microscopy revealed that the PDMS percolated through the MWNT network (Figure 3.2b). This approach minimized the proximity of the MWNT electrode to the channel. However, handling partially-cured PDMS was challenging. The PDMS tended to distort while being reapplied onto the silicon wafer. Also, some of the MWNTs protruded beyond the PDMS matrix (Figure 3.2c), which could have resulted in high local electric fields, increasing the probability of electrical breakdown in the upper insulating layer or electrolysis in the working fluid. Finally, the Young's modulus of the lower electrode was low, increasing the probability of channels collapsing.

One interesting aspect of this approach, however, was the ability of the PDMS to mold itself around photoresist features if they were added to the silicon wafer. Both the PDMS and the

MWNT electrode retained their shapes after being removed from the mold. Hence, this approach could be an effective means of fabricating three-dimensional, conformal electrodes in PDMS.

In a separate approach, I spin-coated PDMS onto a silicon wafer, deposited a film of MWNTs with microcontact printing, and then encapsulated the MWNT film with a thicker layer of PDMS. Even with spin-rates up to 10,000 rpm, however, the insulating layer of PDMS remained several microns thick. The model predicted a large increase in the actuation potential if the insulating layer remained this thick. Therefore, to minimize the thickness of the insulating layer, I diluted the PDMS with hexanes (1:9 ratio of PDMS to hexanes, by weight), and then spin-coated the solution at the maximum spin-rate allowable with our equipment (10,000 rpm). The resulting film of PDMS was less than one micron thick[8]. (Note that I used a container made from high density polyethylene or glass to mix the PDMS with hexanes. Certain polymers, such as polystyrene, leach into hexanes. If this was allowed to happen, then the thin film of PDMS would typically peel off during the stamping process.)

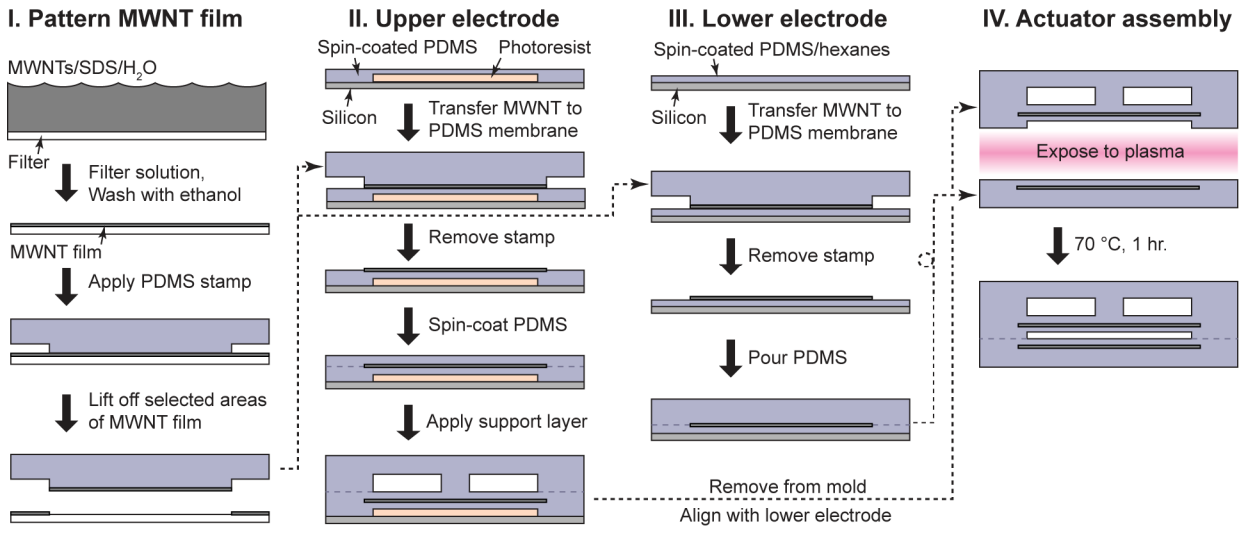

Figure 3.3 An illustration of the fabrication scheme for monolithic electrostatic actuators using soft-lithographic techniques exclusively.

I integrated the above approach into the full fabrication scheme for the actuators, shown in Figure 3.3. The upper layers of the actuator were fabricated as described previously. After

fabricating the lower electrode from PDMS and MWNTs, both sides were exposed to oxygen plasma, brought into contact, and then heated to make the seal permanent.

Applying a sufficient potential across the electrodes brought the membrane into contact with the lower electrode (Figure 3.4). Although a thorough characterization similar to Figure 2.11 was never performed, data from other experiments consistently showed that the monolithic actuator design required lower potentials to actuate than the design with the ITO lower electrode. Actuators with channel heights of 7 μm, membrane thicknesses of 35 ± 6 μm (range), and diameters of 200 μm actuated at 233 ± 19 V (s.d); actuators with diameters of 400 μm actuated at 157 ± 18 V (s.d.); and actuators with diameters of 600 μm actuated at 113 ± 20 V (s.d.). Membranes in the monolithic design were also less likely to collapse during assembly and less prone to stiction during operation.

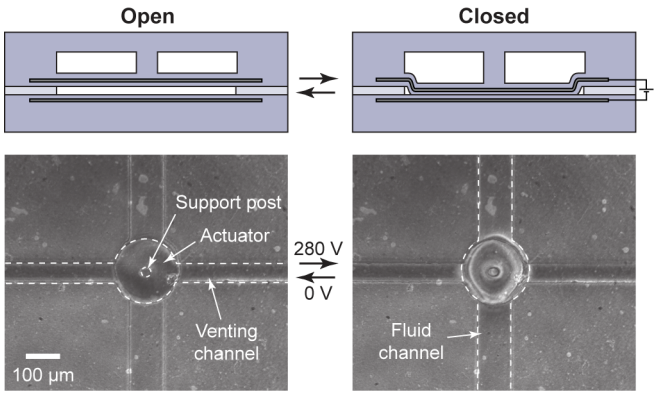

Figure 3.4 Illustrations (side view) and micrographs (top view) of monolithic electrostatic actuators in the open and closed states. The actuators shown were tested with oil (3M™ Fluorinert™ FC-40) in the actuator chamber.

Having found a method to fabricate the actuators *exclusively* with soft-lithographic techniques, I explored whether the PDMS/MWNT lower electrodes would address the problem of potential drift inherent with ITO lower electrodes. I first assembled an actuator without exposing any surface to oxygen plasma. While only allowing a temporary seal, this method assured that the material compositions of both the membrane and the lower electrode were

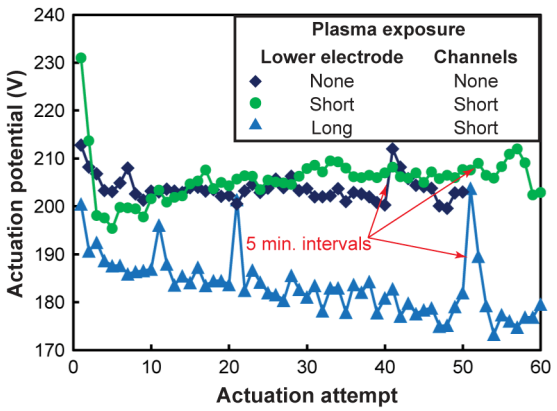

Figure 3.5 Graph of actuation potentials over the course of at least 50 actuation attempts for actuators sealed with three different conditions.

symmetric. I activated the actuator 50 times, waiting several seconds between actuation attempts. After a small drop in potential occurring over the first several actuation events, the actuation potential stabilized (Figure 3.5).

Next, I exposed both sides equally to plasma (3 seconds each) in order to create a permanent bond while still maintaining material symmetry. I activated the completed actuator 60 times, again waiting several seconds between actuation attempts. The potential dropped over the course of the first several actuation attempts, then increased until reaching a plateau and stabilizing. The transient increase in potential may have been due to slightly different plasma exposure levels prior to forming the seal, as I controlled the exposure duration by hand.

Finally, to further support my hypothesis, I postulated it should be possible to create potential drift by treating the two halves of the actuator unequally with plasma. In this scenario, I treated the upper layer briefly as before, but the lower electrode was exposed to plasma for approximately one minute. Studies by others have shown that this level of plasma exposure creates an oxidized material distinct from the native PDMS, essentially "glassifying" the surface[9]. When I activated this actuator 60 times, the potential dropped over the entirety of the trial.

At one point in each of the trials, I paused for 5 minutes between actuation attempts to observe any effects due to the frequency of activation. Interestingly, for the case where neither side was treated with plasma and the case where the two sides were treated asymmetrically, the actuation potential recovered its initial value after the 5 minute pause. Upon resuming actuation at a higher frequency, it dropped again to the value prior to the delay, showing that the system is capable of "remembering" potential drift. Several mechanisms could be present. Repetitive strains on the membrane could cause a rearrangement of the polymer network and MWNTs, which might electrically isolate areas of the electrode, causing charge accumulation. Surface charges might accumulate and drop the potential until adequate time is allowed for the charges to migrate into the bulk of the PDMS. Charge injection could be occurring, or finally, high frequencies could result in resistive heating that might either alter the material properties of the actuator or reconfigure the MWNT network, leading to a drop in actuation potential.

Thus far, the data are consistent with the presence of contact electrification in asymmetric material systems. Actuation potential drift can be eliminated by fabricating both the membrane and the lower electrode from the same material. However, further characterization is needed to definitively elucidate the mechanism behind the drift as well as the mechanism responsible for the sensitivity of actuation potential to actuation frequency.

3.3.2 Pressurizing pneumatic control channels with electrostatic actuators

The monolithic design of the electrostatic actuator permitted simple integration of the actuators with pneumatic microsystems. To instruct pneumatic microvalves with the electrostatic actuators, I first attempted connecting the actuator chambers with the control lines of pneumatic microvalves. The actuator chamber served as a fluid reservoir, such that when the actuator closed, the fluid reservoir compressed and the control line pressurized (Figure 3.6).

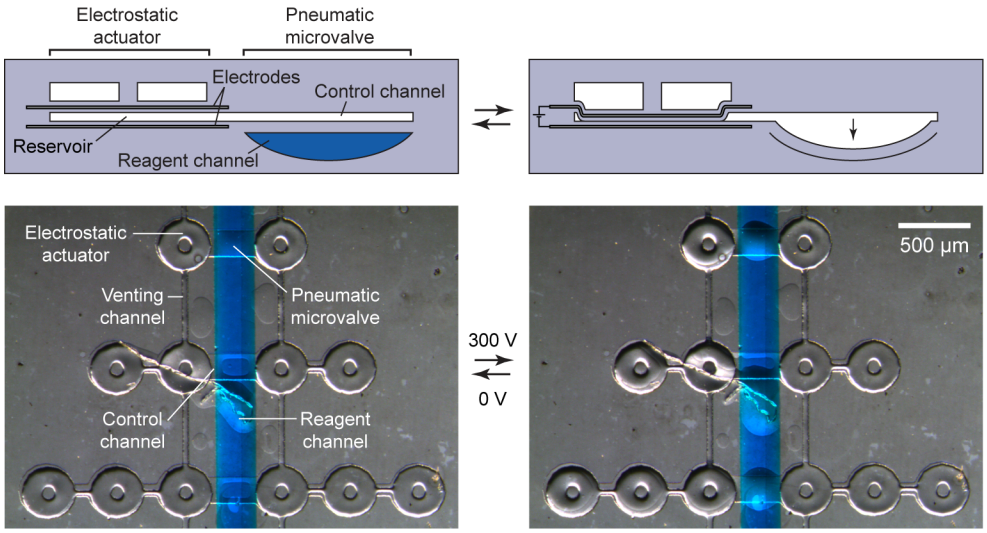

Figure 3.6 Illustrations and micrographs of electrostatic actuators used to compress fluid control lines, which in turn activated pneumatic microvalves.

Early on, several difficult challenges emerged. Firstly, the hydraulic fluid that I used in the control channel (3M™ Fluorinert™ FC-40) was prone to evaporation. Others have used ionic fluids as the hydraulic fluid in analogous actuation schemes[2], since ionic fluids generally have low volatility and are less prone to evaporation. However, ionic fluids would interfere with the electric fields generated by the electrostatic actuator in our system. To gather preliminary results, I assembled the device without sealing the upper layers of the device with the lower layers. I placed several drops of oil between the layers and allowed them to seal reversibly before testing the device (see Materials and methods). While this approach allowed me to reuse the device and refill the control channels, the peripheral areas of the membrane of the pneumatic microvalve tended to delaminate during actuation (see micrographs in Figure 3.6).

Secondly, the size of the fluid reservoir could not accommodate competing requirements for the electrostatic actuators and the pneumatic microvalves. Small reservoirs favored operation of the electrostatic actuators, since small diameters averted stiction of the membrane and small electrode spacing increased the strength of the electric field. On the other hand, large reservoirs favored operation of the pneumatic microvalves, since larger volume displacements generated

higher pressures. In the initial trial, the electrostatic actuators were unable to completely shut pneumatic microvalves, partly due to the volume restriction of the fluid reservoirs. Even with multiple electrostatic actuators operating in a concerted manner on one pneumatic microvalve, the microvalve did not shut. Other factors likely contributed as well. Again, the peripheral area surrounding the pneumatic microvalves delaminated. Also, it appeared that half of the electrostatic actuators did not activate. This may have been due to pressurization of the control line, which pushed the membranes upward and increased the actuation potential. It could also be due to a flaw in the electrical components on the device.

Thirdly, scaling this approach to devices with high numbers of pneumatic microvalves would not be efficient. The actuators were not large enough to create volume displacements capable of actuating multiple pneumatic microvalves at once. Consequently, devices using this approach would need at least one electrostatic actuator per microvalve.

3.3.3 Switches for pneumatic control channels using electrostatic gates

Due to the limitations of the previous strategy, I investigated a second approach for transmitting pressure pulses to pneumatic microvalves *via* electrostatic actuators. I integrated two electrostatic actuators into the control channel for a pneumatic microvalve – one upstream and another downstream (Figure 3.7). The inlet of the control channel was attached to an external pressure source, in this case a cylinder of compressed nitrogen. The outlet of the control channel was vented to atmosphere. Initially, the upstream electrostatic actuator was activated while the downstream actuator was held open, which vented the control channel to atmosphere (Figure 3.7a,c). Under this configuration, the pneumatic microvalve remained open. By activating the downstream actuator and releasing the upstream actuator, pressurized fluid was allowed to fill the control channel (Figure 3.7b,d). While the downstream actuator did not form a hermetic seal, the local fluidic resistance was increased substantially, thereby allowing pressure

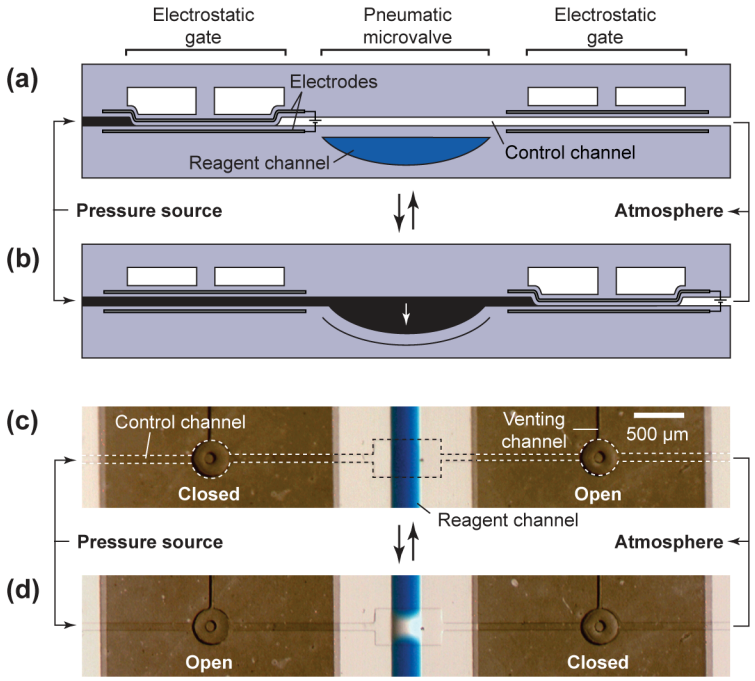

Figure 3.7 (a-b) Illustrations and (c-d) micrographs of a pneumatic microvalve controlled with two electrostatic gates. In the control channel, black-colored regions denote high pressure, while white-colored regions denote low pressure.

to build up in the pneumatic microvalve. Under this configuration, the pneumatic microvalve closed. Because the actuators served to block fluid flow and switch between pressurization states, I commonly refer to the actuators as "gates".

While the above circuit was capable of generating low amplitude pressure pulses, increasing the pressure easily overwhelmed the electrostatic actuators. The operating pressure that an electrostatic gate could accommodate was limited by one of two thresholds: (i) the maximum pressure that could be applied to the fluidic control channel while still permitting the electrostatic gate to close, or (ii) the maximum pressure that the electrostatic gate could isolate in the closed state before being forced open.

I quantified both these thresholds, varying the diameter of the gates from 200-600 μm (Figure 3.8). For each gate, the total thickness of the membrane was between 29 and 41 μm; the channel was 7 μm high; and the support post was 20% of the diameter of the membrane. The

width and height of the venting channel in the support layer were both 50 µm. Fluid channels leading to the gate were 100 µm wide and 7 µm tall. The thickness of the MWNT electrodes was approximately 1 µm. With the pressure high enough to keep the gate opened, I applied a constant potential and then slowly decreased the pressure until the gate snapped shut (solid symbols in Figure 3.8). Then, I increased the pressure until the gate re-opened (open symbols in Figure 3.8).

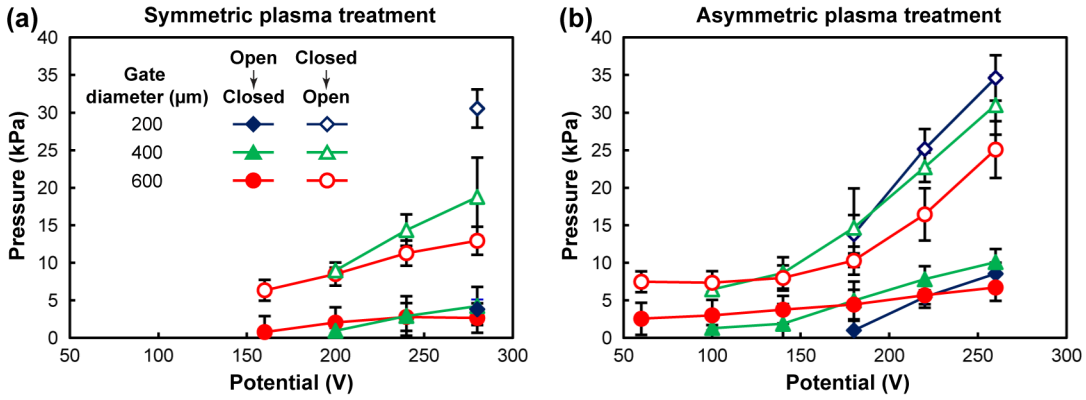

Figure 3.8 Graphs of the potentials needed to close electrostatic gates at specified pressures (solid symbols) and the pressures needed to re-open the gates at fixed potentials (open symbols). Two scenarios are shown: (a) for gates that were sealed with a symmetric plasma treatment, and (b) those sealed with an asymmetric treatment. Error bars represent one standard deviation. A minimum of three gates were tested for each data point, each gate being actuated at least three times.

In the scenario where gates were initially open, the pressure that could be applied while still permitting actuation increased linearly with electric potential. The maximum pressure measured at closure was 4 kPa, using a gate with a diameter of 400 µm and an actuation potential of 280 V (Figure 3.8a). The maximum pressures for gates of different diameters were similar, however.

When the gates were initially shut, gates with smaller diameters were more effective at isolating pressure in the fluidic control line before re-opening. The pressures that could be isolated also appeared to increase linearly with electric potential. The highest pressure isolated was 30 kPa, using a gate with a diameter of 200 µm and an applied potential of 280 V (Figure 3.8a).

For the data shown in Figure 3.8a, the electrostatic gates were assembled by treating both halves with the same plasma exposure during fabrication. By increasing the plasma exposure to the lower electrode during fabrication (thereby creating a material asymmetry), I increased the operating pressures of the gates (Figure 3.8b). Before quantifying the threshold pressures, I conditioned the gates by actuating them at least 50 times each. Then, I cycled the gates between the open and closed states as before.

With the asymmetric plasma treatment, the highest pressure that could be applied to the fluid channel while still allowing the gate to actuate was 10 kPa. The maximum pressure isolated by a gate initially in the closed state was 35 kPa. Trends between operation pressure and electrical potential appeared to be linear above 160 V. (Note that in this study, I limited potentials to 260 V as opposed to 280 V with devices that were treated symmetrically with plasma. I did this to reduce the probability of electrical breakdown between electrodes.)

In summary, the results show that controlling pneumatic actuators with the electrostatic gates will be limited by the maximum pressure that the gates can actuate under when initially in the open state. Currently the threshold is 4 kPa for gates that have been treated symmetrically with plasma, and 10 kPa for those that have been treated asymmetrically. Others have reported that pressures of this magnitude are adequate to operate pneumatic valves with a wide range of parameters[10]. However, in our experience, pneumatic microvalves with actuation pressures this low tend to become stuck in the closed position. Consequently, I sought to make the gates compatible with higher pressures.

3.3.4 An electrostatic gate for regulating highly-pressurized microfluidic channels

The main issue with the initial design of the electrostatic gate was that the membrane easily deflected upward when the control channel was pressurized. To counteract this deflection, I

attempted to balance the pressure on the top and the bottom of the membrane. Previously, researchers in the field of Microelectromechanical Systems used the same approach to activate electrostatic actuators with potentials less than 120 V while applying pressures up to 50 kPa[11-12]. Using our monolithic design, I applied a pressure of 10 kPa to both the channel below the membrane and the cavity above. However, even with potentials up to 300 V, the actuator did not close. (Without applying pressure, the actuator normally closed at ~150 V). Consequently, I studied the effects of pressurization on structure deformation with a finite element analysis package, COMSOL Multiphysics®, utilizing the solid mechanics module (Figure 3.9).

I assigned PDMS the following material properties listed below in Table 3.1:

Table 3.1 Values of PDMS properties assumed in the simulations of the electrostatic gates.

Property	Value
Young's modulus, membrane	4.0 MPa
Young's modulus, bulk	1.5 MPa
Poisson's ratio	0.49
Density	965 kg m^{-3}

The PDMS was treated as an incompressible, linear elastic material, and I ignored the effect of embedded carbon nanotubes on material stiffening. Others have shown that the Young's modulus of PDMS is affected by the ratio of base polymer to cross-linking agent[13] as well as the thickness of the PDMS layer[13-14]. Hence, different moduli were used for the PDMS in the membrane and the PDMS in the support layer and lower layer of the device (bulk).

First, I simulated the effect of applying pressure only to the microfluidic channel below the membrane. As predicted, the membrane deflected upward, although the post suppressed the deflection slightly in the center (Figure 3.9a). Without the post, the membrane deflected about twice as far for a given pressure (Figure 3.9b). In both cases, the deflection was drastic enough

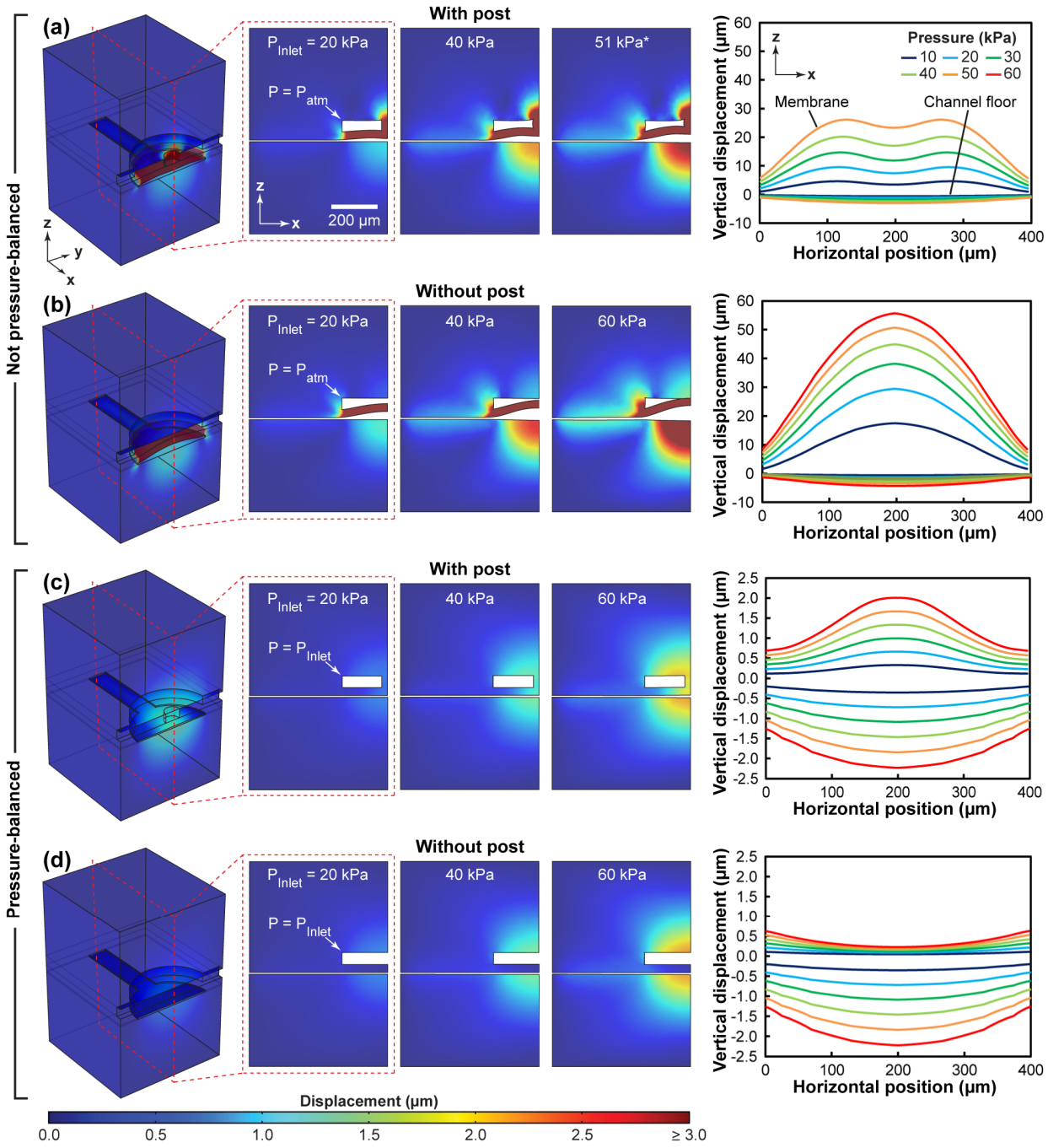

Figure 3.9 Simulations of the effect of pressurization on different actuator configurations using a finite element method. (a-b) Simulation results for actuators where pressure was applied only in the main channel. (c-d) Simulation results for actuators where pressure was applied both in the main channel and in the venting channel. The actuators contained posts in the recess above the membrane for (a) and (c). The posts were omitted in (b) and (d). The graphs shown on the right depict the deflection of the membrane and the floor of the channel in the x-z plane that passes through the center of the actuator. Note that the scale of the y-axis differs between the graphs in (a-b) and the graphs in (c-d). (*The solution for an actuator with an applied pressure of 60 kPa and with a post above the membrane did not converge. Possibly, the solver was unable to manage the large compressive strain. Hence, I show the solution with the highest possible value for pressure that also converged.)

to require actuation potentials of over a kilovolt with pressures greater than 50 kPa (according to the previously discussed model in Chapter 2).

Next, I simulated the effect of applying pressure to both the main microfluidic channel and the cavity above the membrane (Figure 3.9c). In the case with a post centered above the membrane, deflection was significantly diminished, by about a factor of 15. However, closer inspection showed that the membrane still deflected upward in the middle. This deformation appeared to be a consequence of the cavity above the membrane bulging, thereby pulling the post upward and the membrane with it. Also, the post likely needed to compress slightly to supply a sufficient normal force to offset the pressure in the channel.

When the post was removed and pressure applied to both channels, the deflection of the membrane was minimized (Figure 3.9d). As in previous cases, the edges of the membrane deflected slightly due to bulging of the microfluidic channel that led to the actuator chamber. However, the simulation predicted that the center of the membrane would move less than half a micron. Deflection of the floor of the main microfluidic channel was the main contributor to increased separation between the electrodes.

Having determined the conditions that would minimize the deflection of the structures in the actuator, I developed a design that could perform pressure-balancing above and below the membrane. Note that in Figure 3.7, the downstream electrostatic actuator experienced different pressures in the control channel depending on the state of the upstream actuator. Hence, I wanted to incorporate an element that could dynamically adjust the pressure of the cavity above the membrane to match that of the main channel. I also wanted avoid the use of external actuators or other equipment in order to maintain operational simplicity.

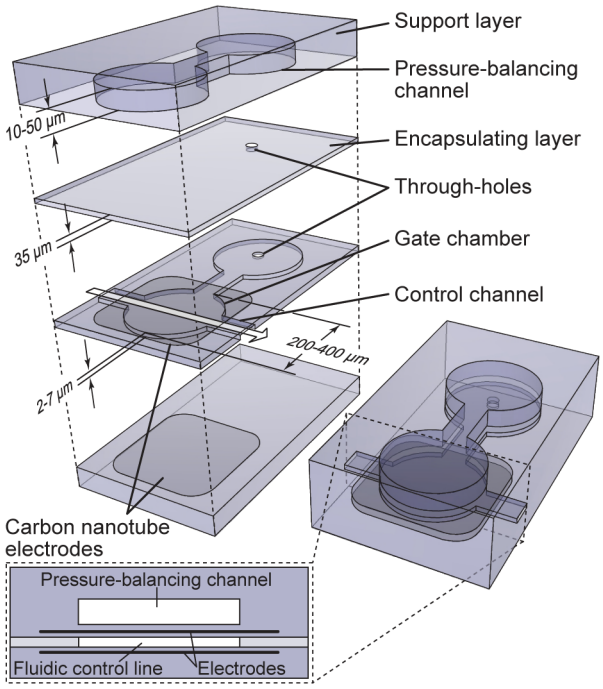

Figure 3.10 An illustration of a pressure-balanced electrostatic gate. Typical dimensions for height of the pressure-balancing channel, encapsulating layer, gate chamber, and diameter of the gate chamber are given. Not drawn to scale.

The design solution we arrived at is shown in Figure 3.10. We incorporated a periphery microchannel that led from the gate chamber to a through-hole and then to the cavity above the gate's membrane, allowing the pressure of the hydraulic fluid on both sides of the membrane to equalize passively. Simulations predicted minor deflections of the membrane, slightly greater than those shown in Figure 3.9d, since expansion of the peripheral channel added additional displacement to the edge of the membrane (Figure 3.11).

To fabricate the pressure-balanced electrostatic gate, I followed the procedure presented earlier in Figure 3.3, with several modifications (Figure 3.12). To form a through-hole between the control channel and the pressure-balancing channel, I incorporated a post into the mold for the control channel[15]. When PDMS was spin-coated onto the mold, the post protruded beyond the PDMS film, thus forming a hole when the PDMS was cured. Several difficulties arose with this approach, however. To properly break through the PDMS film, the post needed to be

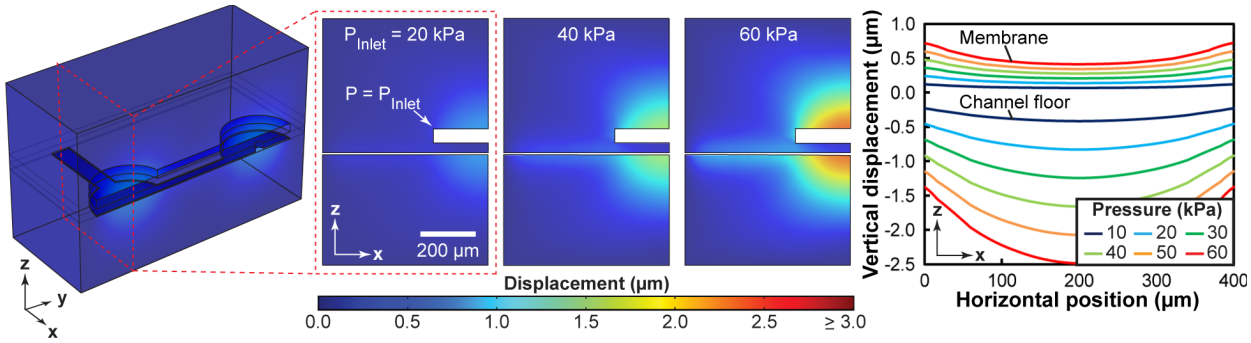

Figure 3.11 Simulation of the effect of pressurization on the design of a pressure-balanced electrostatic gate. The graph shown on the right depicts the deflection of the membrane and the floor of the channel in the x-z plane that passes through the center of the actuator.

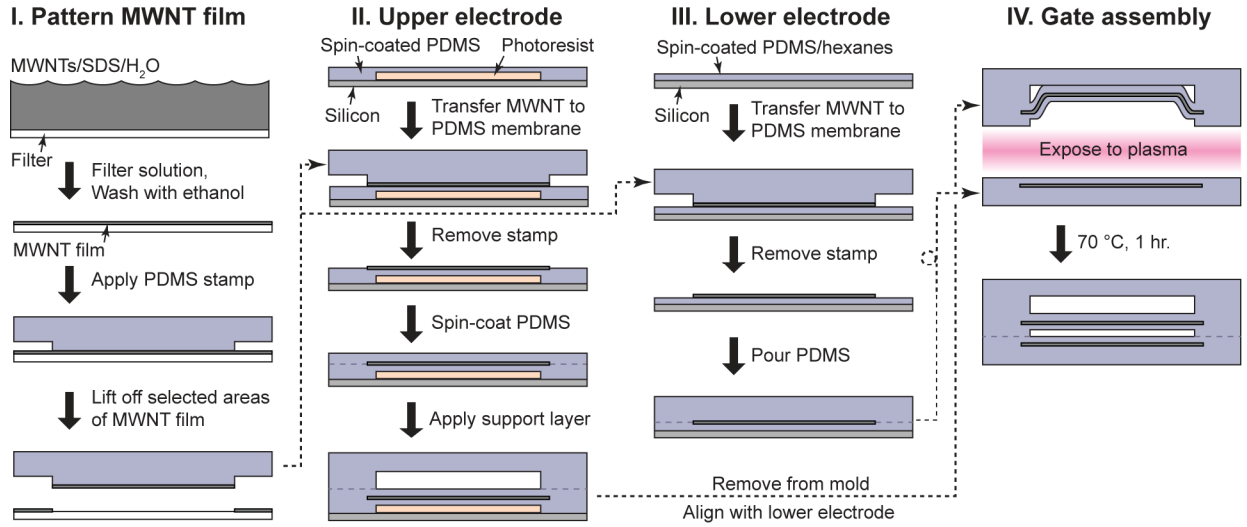

Figure 3.12 An illustration of the fabrication scheme for pressure-balanced electrostatic gates, including a method to prevent collapse of the membrane during the final sealing process.

fabricated with a high aspect ratio. Due to limitations with our UV-exposure tool and photomasks, posts with high aspect ratios tended to be tapered, with the thin end attached to the silicon substrate and the thick end oriented upward. The shape of the posts made them susceptible to separation from the substrate when the PDMS film was removed. Consequently, I resorted to cutting the through-holes manually with a scalpel for the majority of the results presented here. As another option, others have shown that through-holes can be formed in a high-throughput, automated manner *via* laser ablation[16].

We also observed that membranes suspended above shallow actuator chambers tended to collapse during fabrication and seal permanently to the channel floor. To prevent this, the pressure-balancing channel was designed to be shallow for gates with 2 μm tall chambers so that the membranes could reversibly adhere to the top of the pressure-balancing channels during fabrication and released later by filling the channels with oil. Membranes did not collapse as readily for gates with 7 μm heights, so the pressure-balancing channels could be designed taller.

Finally, shallow control channels also had a propensity to collapse during fabrication. We found that allowing ~20 minutes to elapse after exposing the PDMS layers to plasma decreased the chances of collapse when the layers were brought into contact.

To test the effectiveness of the pressure-balancing scheme, I created a series of gates and characterized the actuation potential (*i.e.*, the minimum electric potential needed to close the gate) as a function of the diameter of the gate, the distance between the membrane and the channel floor (which I refer to as the "gap"), and the pneumatic pressure applied to the control channel. For simplicity, I refer to the gate as "open" when the membrane was not in contact with the channel floor and "closed" when the membrane was in contact (Figure 3.13a). The actuation potential increased linearly with applied pressure over the range tested, and also increased with gap size (Figure 3.13c,f; solid symbols). The actuation potential decreased with increasing diameter. With the largest tested diameter of 400 μm and the shallowest gap of 2 μm, the gates actuated with applied pressures up to 62 kPa using an actuation potential of 302 V ± 18 (s.d.). This was more than twelve times the pressure that could be accommodated by a gate with similar dimensions, but without a pressure-balancing scheme (Figure 3.8a).

After a gate was closed, I gradually increased the pressure of the fluidic control line to determine the maximum pressure that could be applied without reopening the gate (Path 3→4 in

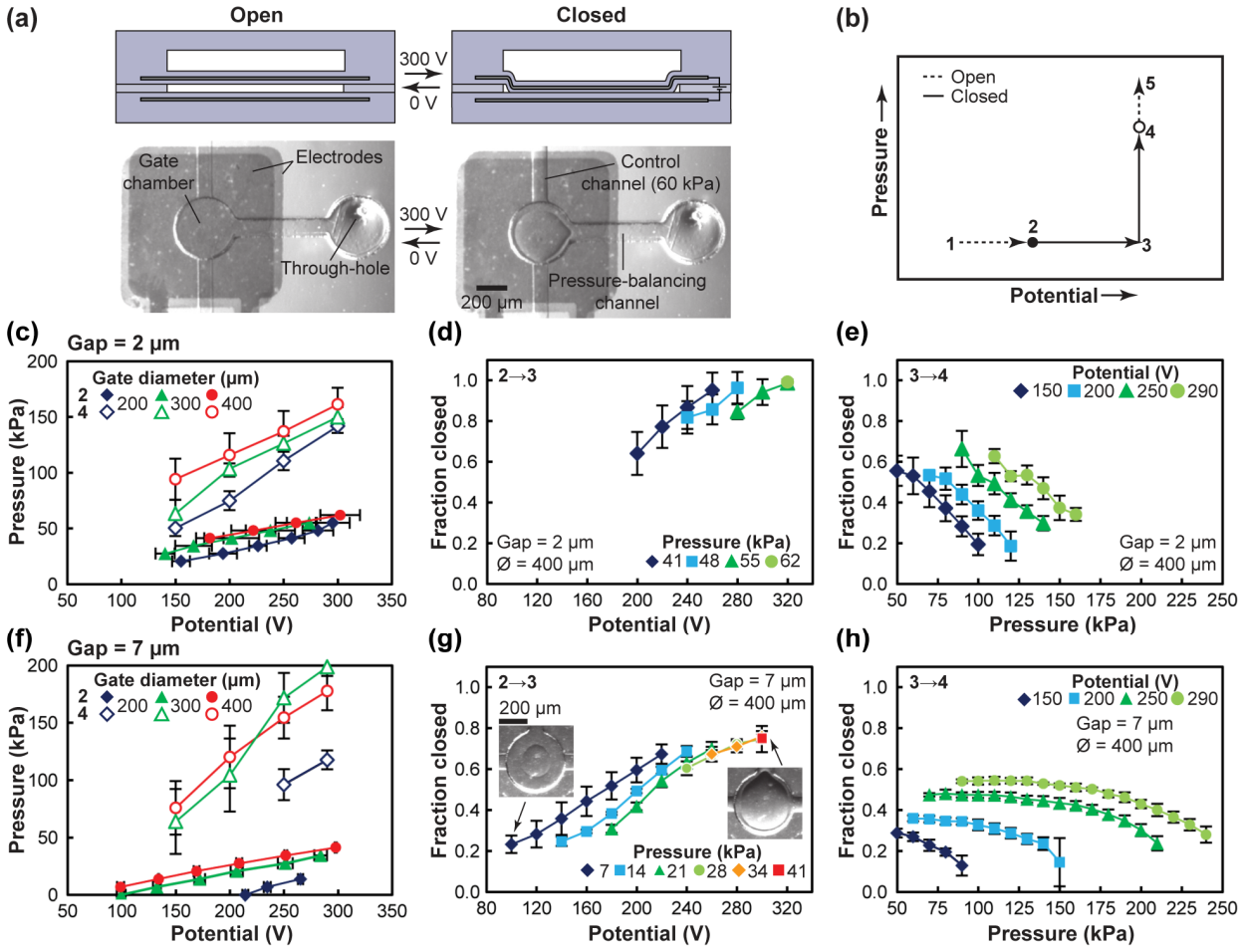

Figure 3.13 The effects of pressurization and electric potential on the operation of pressure-balanced gates. (a) Illustrations (side view, not to scale) and micrographs (top view) of an electrostatic gate in the open and closed states. An electric potential of 300 V was used to actuate the gate with an applied pressure of 60 kPa in the control line. The gate had a diameter of 400 µm and a gap of 7 µm between the membrane and the channel floor. (b) A graphic representation of a test cycle. (c) A graph of the threshold potentials needed to close (*i.e.* establish initial contact between the membrane and the channel floor) electrostatic gates at fixed pressures (solid symbols; point 2 in (b)), and the threshold pressures needed to re-open the gates at fixed potentials (open symbols; point 4 in (b)). The initial gap between the membrane and the channel floor was 2 µm. (d) A graph showing the fraction of a gate's membrane in contact with the channel floor as a function of electric potential when the pressure was held constant (path 2→3 in (b)). The initial gap was 2 µm. (e) A graph showing the fraction of a gate's membrane in contact with the channel floor as a function of pressure when the potential was held constant (path 3→4 in (b)). The initial gap was 2 µm. (f-g) Same as (c-e), respectively, only the initial gap between the membrane and the channel floor was 7 µm. Error bars indicate one standard deviation. Ø = diameter.

Figure 3.13b). I found that the pressure-balancing scheme also improved this aspect of gate operation (Figure 3.13f), as gates with shallow gaps of 2 µm, 400 µm diameter and 300 V applied potential could hold off 150 kPa, a ten-fold improvement over previous designs without pressure-balancing (Figure 3.8a). Since larger diameters improved the amount of pressure that

the gate could accommodate, I decided to focus on gates with a diameter of 400 μm for the remainder of the study.

Due to the rectangular cross-section of the gate chamber, the gate chamber could never be completely obstructed by actuating the membrane. When the gate was closed, a narrow fluidic path formed along the periphery of the gate chamber (Figure 3.13a). The ensuing leakage was beneficial for the system, as it allowed pressurized fluid to access to the pressure-balancing chamber at all times during operation. However, to successfully regulate control channels, the gates needed to increase the local fluidic resistance as much as possible in the closed state. Hence, with the gates closed, I characterized the area of the membrane in contact with the channel floor as a function of electric potential, pressure, and gap size.

First, while keeping the pressure constant, I varied the electric potential (Path 2→3 in Figure 3.13b; see also micrographs in Figure 3.13g). When the fluidic control line was 2μm tall, we were able to bring the membrane into nearly full contact with the channel floor with an applied potential of 300 V (Figure 3.13d). Gates with fluidic control lines that were 7 μm deep were able to close up to approximately 75% at 300 V (Figure 3.12g). I also varied the pressure while keeping the potential constant. (Path 3→4 in Figure 3.13b; Figure 3.13e,h). Gates with shallow channels were more sensitive to changes in pressure, but at pressures lower than 100 kPa, they had more of the membrane in contact with the channel floor. Hence, I used gates with gates with 2 μm gaps to create a microfluidic pneumatic control circuit (Figure 3.14).

The circuit was designed similarly to that presented in Figure 3.7. One gate was placed upstream of a pneumatic microvalve while a second gate was placed downstream. The gap between the membrane and the channel floor was 2 μm, and the diameter of the gate was 400 μm. Initially, the upstream gate was shut with the downstream gate closed, which vented the control

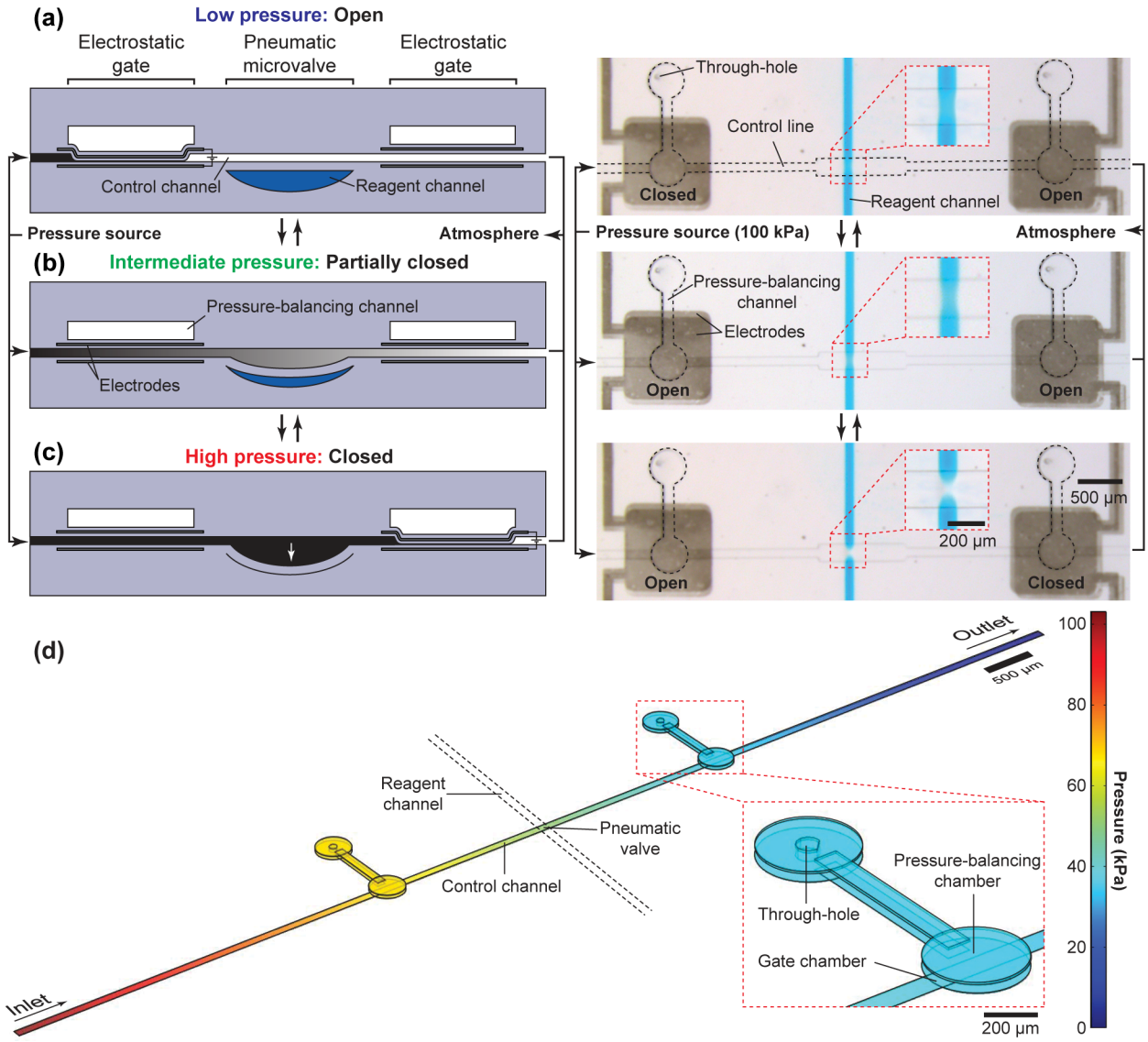

Figure 3.14 Demonstration of a pneumatic microvalve controlled with two pressure-balanced electrostatic gates. Illustrations and micrographs are shown corresponding to (a) the open state for the pneumatic microvalve, (b) an intermediate state where both electrostatic gates are open, resulting in a pressure gradient in the fluidic control line that partially closes the pneumatic microvalve, and (c) the closed state for the pneumatic microvalve. (d) A simulation of the pressure drop in the microfluidic circuit with both electrostatic gates open. The simulation comprised a finite element method, where PDMS was approximated as a rigid material for computational simplicity.

channel and kept the pneumatic microvalve in the open position (Figure 3.14a). The downstream gate was then shut and the upstream gate opened such that the control channel pressurized, allowing the pneumatic microvalve to close (Figure 3.14c). According to the characterization I performed previously (Figure 3.13c), in this state, it was not possible to re-close the upstream gate with pressures above ~60 kPa. However, if both electrostatic gates were opened,

uninhibited fluid flow was permitted through the control channel, which caused a pressure gradient to develop in the control channel (Figure 3.14b). The circuit was designed such that when both gates were opened and the inlet was supplied with a pressure of 100 kPa, the pressure experienced by the upstream gate would be ~60 kPa (Figure 3.14d). Under these conditions, the upstream gate could again close, returning the circuit to its original configuration. By taking advantage of the pressure drop in the intermediate state, the circuit was capable of actuating pneumatic microvalves with pressures up to ~100 kPa.

3.3.5 Microfluidic pressure-amplifier circuits with integrated electrostatic gates

Initially, two electrostatic gates were used to control a single pneumatic line. However, I was also able to modify the circuit to operate with only a single gate. Figure 3.14 shows that only the downstream gate was necessary to switch the pneumatic valve from the partially closed state (which is also a partially open state) to the fully closed state. I omitted the upstream gate, and I moved the downstream gate and the pneumatic microvalve as close to the outlet as possible (Figure 3.15a). With the gate open, a pressure gradient developed in the fluidic control line such that the pressure in the pneumatic valve portion of the fluidic control line was inadequate to completely obstruct the reagent channel. By shifting the location of the actuators, I minimized the pressure experienced by the pneumatic microvalve when the electrostatic gate was open (Figure 3.15b). As before, closing the gate increased the fluidic resistance downstream of the pneumatic microvalve and subsequently increased the local pressure experienced by the valve.

In the above configuration, the electrostatic gate operated analogously to a junction field-effect transistor (JFET) in a simple single-stage common-source amplifier circuit (Figure 3.15c). Fluid flow was equated with the conventional current, and pressure was equated with voltage. I represent the electrostatic gate as a p-channel JFET, since we applied positive potentials to

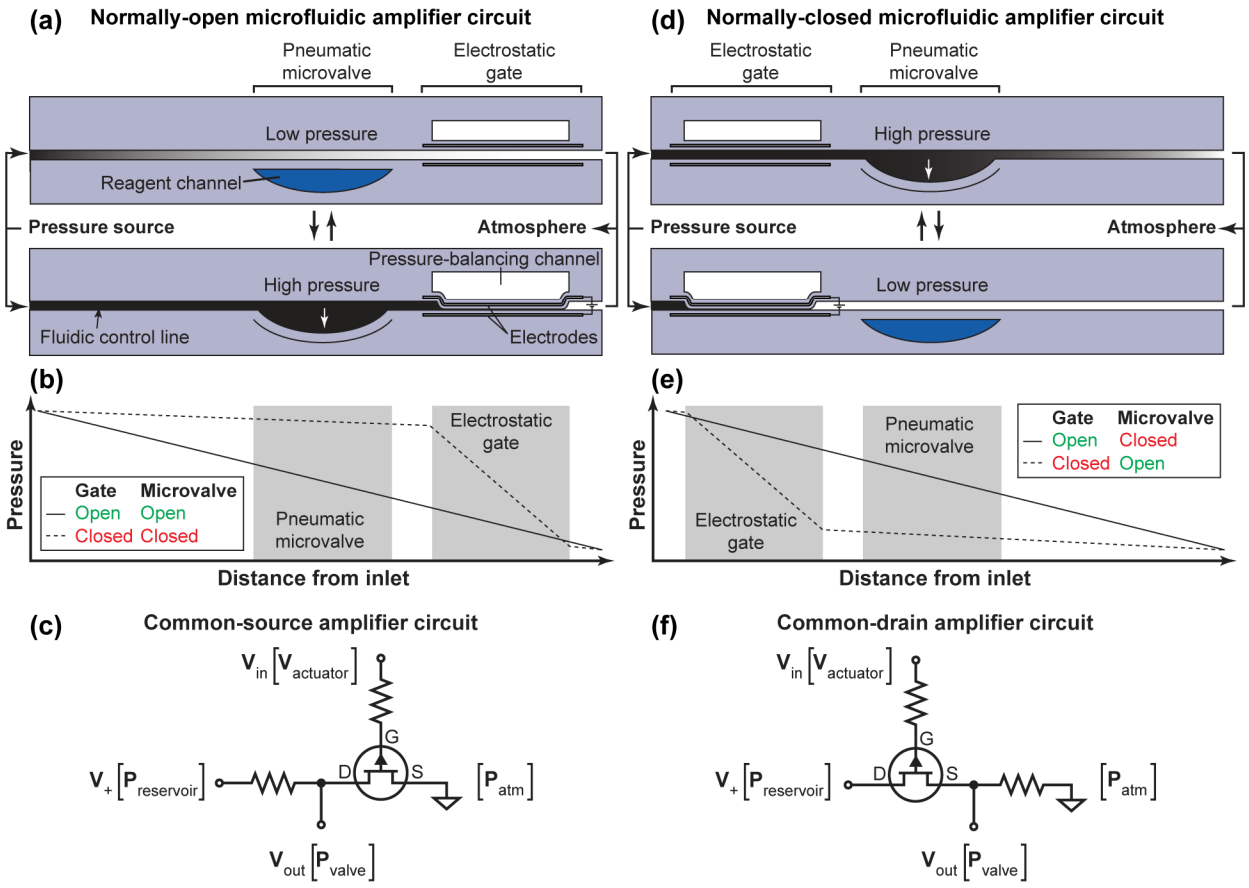

Figure 3.15 Microfluidic amplifier circuits with integrated pressure-balanced electrostatic gates. (a) A diagram of a normally-open microfluidic amplifier where the gate is downstream of the pneumatic microvalve and both are located near the outlet of the control channel. (b) A qualitative graph of the pressure drops in a normally-open microfluidic circuit with the gate open or closed. (c) A circuit diagram of an electrical single-stage field-effect transistor amplifier in the common-source configuration (D denotes drain; G denotes gate, and S denotes source; standard abbreviations for the electrical terminals are shown, with the microfluidic circuit equivalents shown in brackets). (d) A diagram of a normally-closed microfluidic amplifier where the gate is upstream of the pneumatic microvalve and both are located near the inlet of the control channel. (b) A qualitative graph of the pressure drops in a normally-closed microfluidic circuit with the gate open or closed. (c) A circuit diagram of an electrical single-stage field-effect transistor amplifier in the common-drain configuration.

actuate the gate. Due to the topological similarity, and also because the pneumatic microvalve was open in the rest state, I refer to this assemblage of microfluidic components as a "normally-open microfluidic pressure amplifier circuit".

By reversing the inlet and outlet, the fluid circuit can be switched to a topology analogous to a common-drain amplifier, as illustrated in Figure 3.15d-f. I refer to this configuration as a normally-closed microfluidic pressure amplifier circuit. The pressure gradient closes the

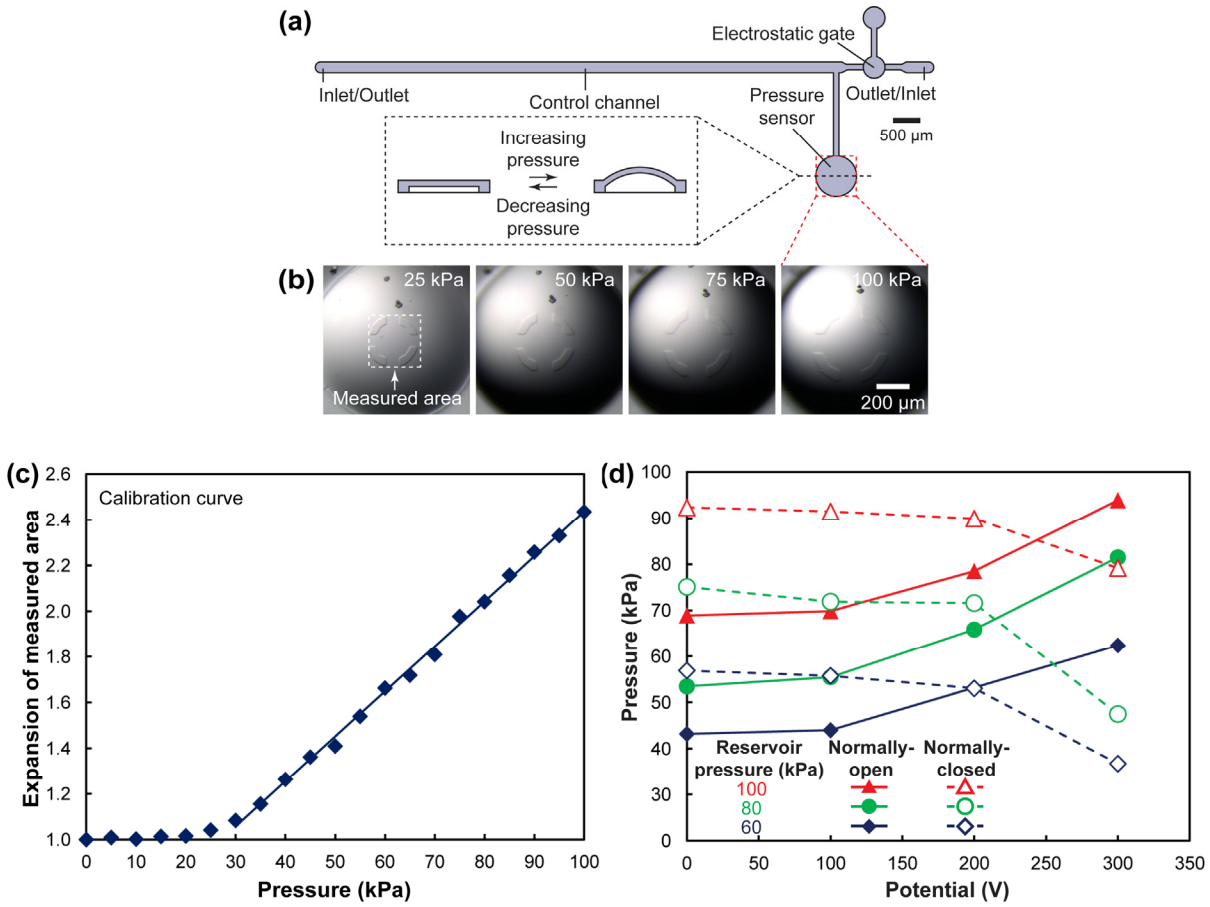

Figure 3.16 Measuring the pressure output of microfluidic pressure amplifier circuits. (a) A schematic diagram of a test device with an integrated membrane-based pressure sensor. The top-down view is drawn to scale. (b) Micrographs of the pressure sensor's response to several pressures. (c) A calibration curve showing the expansion of the measured area in response to applied pressures. (d) A graph illustrating the pressure output of both normally-open and normally-closed microfluidic pressure amplifier circuits for several values of potential and input pressure.

pneumatic microvalve when the electrostatic gate is open, and closing the gate lowers the downstream pressure, allowing the pneumatic microvalve to open.

To measure the pressures generated by the microfluidic amplifier circuits (P_{valve} in Figure 3.15c,f), a microfluidic pressure sensor was designed comprising a circular fluidic chamber attached to the fluidic control line (Figure 3.16a). A membrane was suspended above the fluidic chamber of the pressure sensor such that pressurization of the chamber caused the membrane to flex (Figure 3.16b). Reference marks were patterned into the membrane, allowing the amount of flexing to be quantified and calibrated (Figure 3.16c). Pressure sensors were integrated into both

normally-open and normally-closed microfluidic pressure amplifier circuits where pneumatic valves would generally be located. The pressures at these locations were then measured as a function of the pressure at the inlet ($P_{reservoir}$ in Figure 3.15c,f) and the electric potential applied to the electrostatic gates ($V_{actuator}$ in Figure 3.15c,f). In the normally-open microfluidic amplifier circuit, increasing the electric potential from 0 V to 300 V caused the pressure measured by the sensor to increase by approximately 20 kPa for all inlet pressures tested (60, 80, and 100 kPa) (Figure 3.16d). In the normally-closed microfluidic amplifier circuit, increasing the electric potential from 0V to 300 V caused the pressure measured by the sensor to decrease between 10-20 kPa. The highest pressures accommodated by these circuits were nearly 20 times larger than the pressures used in the initial design of the pneumatic switch (Figure 3.7).

Interestingly, I observed that even near the outlet of an unobstructed control channel, the pressure sensors registered pressure drops of only ~30 % relative to the inlet pressure. This suggests that the ratio of the fluidic resistance upstream of the pressure sensor relative to the fluidic resistance downstream was not as high as anticipated. I investigated several possible explanations. The outlet of the control channel was originally a hole punched with a 20 gauge steel needle, resulting in a diameter of ~0.5 mm. Back pressures due to surface tension were assumed negligible because the contact angles at Fluorinert™/PDMS/air interfaces were generally low. Using the inlet pressures indicated above, the flow rate of hydraulic fluid through the circuit was on the order of microliters per week; hence the pressure drop due to flow through the outlet port was assumed negligible. The height of the outlet port was typically ~5 mm tall, which theoretically could generate back-pressures of up to ~100 Pa – also negligible compared to the measured values. Furthermore, I measured the pressure with the outlet port completely cleaved from the device such that the control channel vented directly out the side of the device.

Only a small change in pressure (approximately -5 kPa) at the sensor's position was observed. Head loss due to sudden expansions (such as the transition from the control channel to the outlet port) generally would not be expected to be significant[17]. To validate this assumption, I performed a simple two-dimensional simulation of the transition area between the control channel and the outlet port using a finite element method. However, no significant fluid resistance was suggested. Any unanticipated fluid resistance due to the small contractions and expansions in the channel were also ruled out by simulations such as those shown in Figure 3.14d.

Finally, one other explanation might lie in the expansion of PDMS microchannels while pressurized. Perry *et al.* modeled the effect of elastic modulus on the pressure drop through a simple, slit-type microchannel[18]. For highly elastic channels, high pressures caused drastic expansion of the cross-section of the microvalve. Hence, areas with high pressure also experienced low fluidic resistance. The model predicts aberrations within the same order of magnitude as the pressures I measured.

Regardless of the effects of elasticity, the pressure amplifier circuits were still highly effective at switching pneumatic microvalves between a partially-open state and the fully closed state (Figure 3.17). I first tested the pneumatic microvalve with an external pressure sensor to identify the actuation pressure needed to fully close the microvalve. I then applied a pressure ~5-15 kPa lower than the actuation pressure in the case of the normally-open microfluidic pressure amplifier circuit, or ~5-15 kPa higher than the actuation pressure in the case of the normally-closed circuit. The electrostatic gate was then used to activate the pneumatic microvalve with a potential of 300 V.

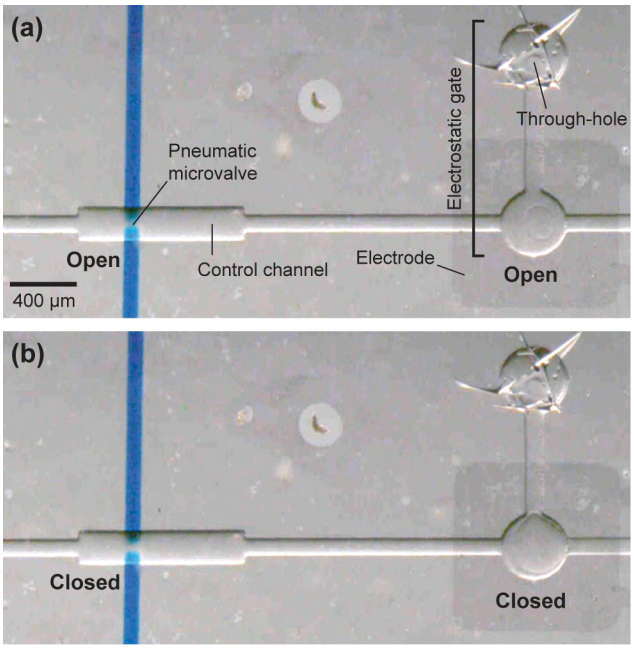

Figure 3.17 Micrographs of a normally-open microfluidic pressure amplifier circuit where the pneumatic microvalve is (a) partially-open and (b) fully closed.

As mentioned previously, touch-mode electrostatic actuators commonly face the issue of drift in actuation potential due to a build-up of charge on the surfaces of electrodes. Either actuation potentials become prohibitively high, or the elements of the actuator fuse together, precluding further operation. I cycled the electrostatic gate continuously more than 2000 times without observing these common failure modes, which I believe is due to the material symmetry between the membrane and the lower electrode. Instead, actuation was eventually inhibited by a loss of conductivity between the electrical controls and the electrical circuits in the device. Once the connection was reset, the gate was able to actuate more than 2000 times again before the same failure mechanism reemerged. I hypothesize that the small cross-sectional area of contact between electrical controls and the microfluidic device induced high current fluxes at the interface, which gradually burned out the connection. Failure rates could be decreased simply by using connections with larger cross-sectional interfaces, perhaps in conjunction with liquid metals to mediate contact between the conductive polymers and electrical wiring[19].

3.4 Conclusions

3.4.1 Summary

In summary, by developing a monolithic design for the electrostatic actuator, the fabrication process was significantly simplified, and previously observed drift in the actuation potential was virtually eliminated. The PDMS/MWNT construction also allowed the electrostatic actuators to be easily integrated with other microfluidic components, thereby increasing the actuators' utility. By coupling the electrostatic actuators with pneumatic microvalves, the issue with ions interacting with electric fields was circumvented. I attempted two different approaches to instruct pneumatic microsystems with the actuators. By compressing a fluid reservoir with an actuator, I was able to pressurize the control channel of a microfluidic valve. Currently, however, the pressures are not adequate to completely close pneumatic microvalves. I also used the electrostatic actuators to regulate the pressure from external source and control where pressurized fluid was directed on-chip. Simulations with a finite element method informed several design changes, including a pressure-balancing element for the membrane. Once implemented, the modifications enabled the electrostatic actuators to pressurize pneumatic valves up to ~100 kPa using potentials less than or equal to 300 V.

3.4.2 Future directions

Several opportunities are available for future work, mainly to do with the microfluidic pressure amplifier circuits. Firstly, simulations predicted that with the pressure-balanced design of the electrostatic gate, the deflection of the lower electrode was the main contributor to increased separation between the electrodes (Figure 3.11). Deflection could be reduced if the stiffness of the lower electrode was increased (*e.g.*, by fabricating the electrode from an indium tin oxide film deposited on glass and then covering the oxide with a thin insulating layer of

PDMS, or by using a thermopolymer-supported electrode). The support layer of the gate would also benefit from stiffer materials, because if the channels were prevented from bulging, then the membrane would also deflect less at the periphery. With these changes in place, the electrostatic gate could potentially withstand higher pressures.

Secondly, the design of the microfluidic pressure amplifier circuits could be adjusted to increase the difference in pressure generated by the activated state versus the inactivated state. Currently, the maximum difference is ~20 kPa (Figure 3.16d). Consider the normally-open microfluidic pressure amplifier circuit, analogous to a common-source electrical single stage amplifier (Figure 3.15a-c). Another equivalent electrical circuit diagram is shown in Figure 3.18.

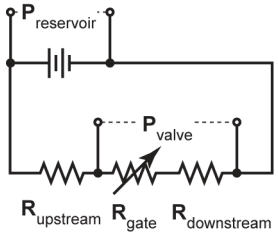

Figure 3.18 An equivalent circuit diagram of a normally-open microfluidic pressure amplifier circuit.

The pressure experienced by the pneumatic microvalve, P_{valve}, will be

$$P_{valve} = P_{reservoir}\left[\frac{R_{gate} + R_{downstream}}{R_{upstream} + R_{gate} + R_{downstream}}\right], \tag{3.1}$$

where

$P_{reservoir}$ pressure of the compressed gas cylinder

$R_{upstream}$ fluid resistance of the microfluidic channel upstream of the electrostatic gate

R_{gate} adjustable fluid resistance of the electrostatic gate

$R_{downstream}$ fluid resistance of the microfluidic channel downstream of the electrostatic gate

P_{atm} atmospheric pressure

When the gate is open (*i.e.*, $R_{gate} \rightarrow 0$), the pressure experienced by the valve in the open state is minimized for $R_{upstream} >> R_{downstream}$. Assuming this condition is met, the pressure experienced by the valve in the closed sate is then maximized when $R_{gate} >> (R_{upstream} + R_{downstream})$. Already in the design presented in Figure 3.16a, I made the upstream length of channel much longer than the downstream length to strive toward the first condition. However, by lengthening the upstream region, the overall channel resistance, $(R_{upstream} + R_{downstream})$, also increased. One way to decrease the total fluid resistance, while keeping $R_{upstream}$ much higher than $R_{downstream}$, would be to add additional height to both the upstream and downstream channel segments. This could be done by performing multi-layer photolithography for the channel mold, for instance.

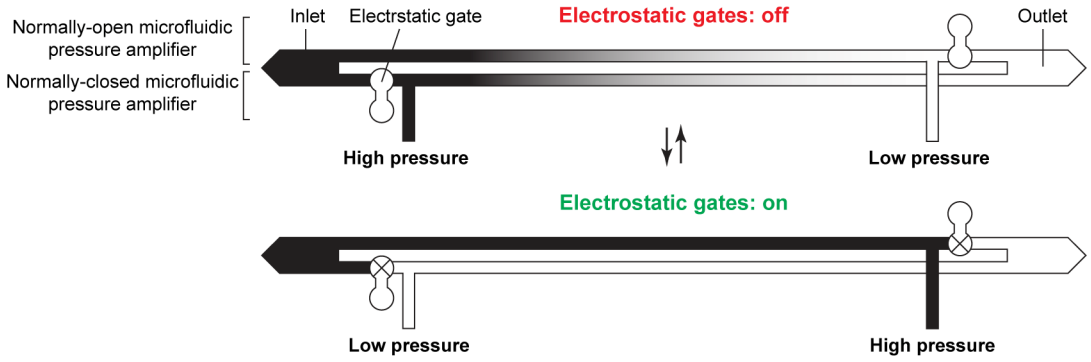

Figure 3.19 Illustration of a contemplated pneumatic switch where one electrical input controls two pneumatic outputs.

Finally, a number of interesting microfluidic system components could be constructed by combining multiple microfluidic pressure amplifier circuits together. Among them is a contemplated pneumatic switch where two amplifier circuits are united to alternately apply high pressure to one of two pneumatic control channels (Figure 3.19). Combining several of these switches together could produce a binary-tree multiplexer for pneumatic microsystems, such as those reported previously[20]. In the precedent, which was controlled with external solenoid valves (Figure 1.2a), N fluid channels required $2 \log_2 N$ separately instructed pneumatic lines. In

addition to the chip, the system comprised one pressure source, 2 $\log_2 N$ individually instructed solenoid valves, and 2 $\log_2 N$ pneumatic ports on the chip. In my scheme with the amplifier circuits, only one electrical input would be needed to control two electrostatic gates and the corresponding pneumatic outputs. Overall, N fluid channels could be instructed with one pneumatic input and $\log_2 N$ electrical inputs.

3.4.3 Implications

Compared to the precedents of portable ancillaries for instructing pneumatic microsystems (see Section 1.2.2), the microfluidic pressure amplifier circuits presented here offer advantages in terms of size, integration, fabrication, and scalability. They are also compatible with many of the strategies reported for decreasing the number of pneumatic control lines in pneumatic microsystems, including serial instruction methods[21]. Because of their monolithic construction in PDMS, the amplifier circuits could be easily incorporated into the plethora of pneumatic microsystems already reported, bringing the added advantage of portability. In sum, the potential for these actuators to bring sophisticated fluid manipulation to point-of-care devices is highly promising.

3.5 References

1. K.A. Addae-Mensah, Y.K. Cheung, V. Fekete, M.S. Rendely and S.K. Sia, "Actuation of elastomeric microvalves in point-of-care settings using handheld, battery-powered instrumentation" *Lab on a Chip,* 2010, 10, 1618-1622.

2. W. Gu, H. Chen, Y.-C. Tung, J.-C. Meiners and S. Takayama, "Multiplexed hydraulic valve actuation using ionic liquid filled soft channels and Braille displays" *Applied Physics Letters,* 2007, 90, 033505-3.

3. D.B. Weibel, M. Kruithof, S. Potenta, S.K. Sia, A. Lee and G.M. Whitesides, "Torque-actuated valves for microfluidics" *Analytical Chemistry,* 2005, 77, 4726-4733.

4. A. Douglas, A.L. Gregory and K.G. Bruce, "An electrostatic microvalve for pneumatic control of microfluidic systems" *Journal of Micromechanics and Microengineering,* 2012, 22, 025019.

5. B. Byunghoon, H. Jeahyeong, R.I. Masel and M.A. Shannon, "A bidirectional electrostatic microvalve with microsecond switching performance" *Journal of Microelectromechanical Systems,* 2007, 16, 1461-1471.

6. E.E. Parker, W.R. Ashurst, C. Carraro and R. Maboudian, "Adhesion characteristics of MEMS in microfluidic environments" *Journal of Microelectromechanical Systems,* 2005, 14, 947-953.

7. Z. Yapu, "Stiction and anti-stiction in MEMS and NEMS" *Acta Mechanica Sinica,* 2003, 19, 1-10.

8. A. Thangawng, R. Ruoff, M. Swartz and M. Glucksberg, "An ultra-thin PDMS membrane as a bio/micro–nano interface: fabrication and characterization" *Biomedical Microdevices,* 2007, 9, 587-595.

9. M.J. Owen and P.J. Smith, "Plasma treatment of polydimethylsiloxane" *Journal of Adhesion Science and Technology,* 1994, 8, 1063-1075.

10. V. Studer, G. Hang, A. Pandolfi, M. Ortiz, W.F. Anderson and S.R. Quake, "Scaling properties of a low-actuation pressure microfluidic valve" *Journal of Applied Physics,* 2004, 95, 393-398.

11. W. van der Wijngaart, H. Ask, P. Enoksson and G. Stemme, "A high-stroke, high-pressure electrostatic actuator for valve applications" *Sensors and Actuators A: Physical,* 2002, 100, 264-271.

12. K. Yoshida, S. Tanaka, Y. Hagihara, S. Tomonari and M. Esashi, "Normally closed electrostatic microvalve with pressure balance mechanism for portable fuel cell application" *Sensors and Actuators A: Physical,* 2010, 157, 290-298.

13. M. Liu and Q. Chen, "Characterization study of bonded and unbonded polydimethylsiloxane aimed for bio-micro-electromechanical systems-related applications" *Journal of Micro/Nanolithography, MEMS and MOEMS,* 2007, 6, 023008.

14. M. Liu, J. Sun, Y. Sun, C. Bock and Q. Chen, "Thickness-dependent mechanical properties of polydimethylsiloxane membranes" *Journal of Micromechanics and Microengineering,* 2009, 19, 035028.

15. E.P. Kartalov, C. Walker, C.R. Taylor, W.F. Anderson and A. Scherer, "Microfluidic vias enable nested bioarrays and autoregulatory devices in Newtonian fluids" *Proceedings of the National Academy of Sciences,* 2006, 103, 12280-12284.

16. J. Huft, D.J. Da Costa, D. Walker and C.L. Hansen, "Three-dimensional large-scale microfluidic integration by laser ablation of interlayer connections" *Lab on a Chip,* 2010, 10, 2358-2365.

17. R.W. Fox, P.J. Pritchard and A.T. McDonald, *Fox and McDonald's introduction to fluid mechanics*. John Wiley & Sons, Inc.: Hoboken, NJ, 2011.

18. S.L. Perry, J.J.L. Higdon and P.J.A. Kenis, "Design rules for pumping and metering of highly viscous fluids in microfluidics" *Lab on a Chip,* 2010, 10, 3112-3124.

19. H. Huan and L. Chang In *Characterizations and optimization of electrical contact between nanocomposite elastomer and metal*, Solid-State Sensors, Actuators and Microsystems Conference, 2009. TRANSDUCERS 2009. International, 21-25 June 2009; 2009; pp 1103-1105.

20. T. Thorsen, S.J. Maerkl and S.R. Quake, "Microfluidic large-scale integration" *Science,* 2002, 298, 580-584.

21. J.A. Weaver, J. Melin, D. Stark, S.R. Quake and M.A. Horowitz, "Static control logic for microfluidic devices using pressure-gain valves" *Nature Physics,* 2010, 6, 218-223.

Chapter 4
Normally-closed electrostatic microvalves

4.1 Introduction

In the previous chapter, I implemented an *indirect* approach to prevent interaction between the electric fields of electrostatic actuators and ions in aqueous solutions. An electrostatic actuator translated an electrical signal into a mechanical force, which was then further translated into a pneumatic force. Pneumatic microvalves, rather than the electrostatic actuators, interacted directly with reagents. This approach had the advantage of generating pressures up to ~100 kPa. However, in applications where high pressures are not required, the added bulk of a pressure source might be disadvantageous. In an effort to further minimize the ancillaries needed to operate portable valve-based microfluidic systems, I investigated ways to adapt electrostatic actuators for interacting *directly* with aqueous reagents.

I implemented two approaches, both informed by precedents in the literature (see Section 1.2.4). In the first, I sought to adapt a method reported by Maharbiz *et al.*, where high frequency oscillating electric fields were used to avoid electrode screening in normally-open microvalves[1-2]. A cursory exploration of this strategy, however, revealed several significant challenges. After reviewing these, I will discuss a second approach, where I minimized interaction between the electric field and solutes by adopting a normally-closed architecture[3].

4.2 Materials and methods

4.2.1 Fabrication of normally-closed electrostatic microvalves

Molds for venting channels and microvalve chambers were made by patterning SU-8 5 photoresist (Microchem Corp.) onto silicon wafers using standard photolithographic techniques in accordance with the manufacturer's specifications. The photoresist was spun at 1,700 rpm for 30 seconds. Molds for the stamps were fabricated using SU-8 50 spun at 2,000 rpm for 30 seconds. The molds for the reagent channels were spin-coated at 2,000 rpm for 30 seconds. To reduce adhesion between PDMS and the molds, a surface treatment was performed by placing the molds in a vacuum desiccator along with several drops of (tridecafluoro-1,1,2,2-tetrahydrooctyl)trichlorosilane (Gelest, Inc.), and then applying vacuum overnight.

To construct the layer of the microvalve containing the upper electrode, a thin layer of PDMS (20:1 ratio of monomer to cross-linking agent by weight; General Electric RTV 615, Hisco, Inc.) was first spin-coated onto the mold at 10,000 rpm for 50 seconds such that a thin film covered the channel features. The PDMS film was cured in an oven at 70 °C for 1 hour and then allowed to cool to room temperature. To form the electrode, an aqueous suspension of multi-walled carbon nanotubes (MWNTs) (20-30 nm outer diameter, 10-30 μm length, > 95 wt% purity, ash < 1.5 wt%; Cheaptubes, Inc.) with a ratio of 1 g MWNTs : 10 g sodium dodecyl sulfate : 1 mL deionized water was prepared and sonicated (Vibra-Cell VCX130PB, Sonics & Materials, Inc.) for approximately 30 minutes to solubilize the MWNTs. A 0.1 mL sample was diluted into approximately 20-30 mL deionized water and stirred briefly. The dilute suspension was filtered through an alumina membrane (Whatman Anodisc™ inorganic membrane, 0.1 or 0.2 μm pore size, 47 mm diameter) that had been wet with ethanol. After the aqueous suspension had fully passed through the membrane, the MWNTs that remained on the membrane were washed with

ethanol until the filtrate was free of bubbles. A PDMS stamp (20:1 ratio of monomer to cross-linking agent by weight, cured overnight at 70 °C) was vulcanized on a mold with lateral dimensions scaled to be 2.8% larger than required, in order to account for shrinkage after removal from the mold. The stamp was ~5 mm thick. After curing, the stamp was brought into contact with the MWNT film. Areas in contact with the stamp were lifted off the membrane filter and then applied to the PDMS film formed previously. Pressure was applied by hand, and after lifting off the PDMS stamp, a fraction of the MWNT film transferred to the PDMS film. Electrical contacts were made from a mixture of PDMS (5:1 ratio of monomer to cross-linking agent by weight) with 10 wt% MWNTs, which was applied on the designated area of the MWNT electrode and subsequently cured for 15 minutes in an oven at 70 °C. To encapsulate the MWNT electrode, a layer of PDMS (5:1 ratio of monomer to cross-linking agent by weight) was poured over the electrode, several millimeters thick. The PDMS was cured overnight at 70 °C. Access holes for the microchannels were punched using a sharpened 20 gauge steel needle.

To form the membrane of the microvalve, a featureless silicon wafer was treated with silane vapor as described previously, and a thin layer of PDMS (20:1 ratio of monomer to cross-linking agent by weight), diluted in hexanes (10:1 ratio of hexanes to PDMS by weight) was spin-coated onto the wafer at 10,000 rpm for 120 seconds. The thin PDMS layer was cured in an oven at 70 °C for 1 hour, and then a MWNT film was applied as described above. In this case, the PDMS stamp was vulcanized on a mold with lateral dimensions scaled to be 2.4% larger than required. Electrical contacts were also applied and cured. A second layer of PDMS (20:1 ratio of monomer to cross-linking agent by weight) was spin-coated on top of the electrode at 2,400 rpm for 30 seconds. While the PDMS was still in liquid form, a ring of cured PDMS (10:1 ratio of

monomer to cross-linking agent by weight) was placed around the periphery, and then the membrane was cured overnight at 70 °C.

To seal the upper layer of the microvalve to the membrane, all the PDMS components were first removed from their respective molds. When removing the membrane, a section of the support ring was first delaminated, and then the receding edge between the PDMS and the silicon was wet with ethanol to aid the release of the membrane. Care was taken when removing the portions of the membrane that contained electrical contacts. Often, the contacts were agitated from side to side with a pair of forceps to aid release. Once removed, the membrane was flipped and placed onto a flat slab of cured PDMS (20:1 ratio of monomer to cross-linking agent by weight), resting on a frosted glass slide. The glass slide was frosted to avoid adhesion, albeit reversible, between the PDMS and the glass. Usually, one edge of the membrane was brought into contact with the PDMS slab, and then the remainder of the membrane was slowly brought into contact, allowing the sealing edge to propagate from one side to the other. Care was taken to avoid entraining air pockets between the membrane and the PDMS slab.

The frosted glass slide with the PDMS membrane was affixed to the bottom of a custom-made aligner. Essentially, the aligner consisted of a dual axis x-y translation stage (Edmund optics) with a tip-tilt stage suspended above. The lower stage was equipped with a 3 inch wafer chuck with a vacuum port, while the upper stage held a transparent glass slide. The upper layer of the microvalve was reversible adhered to a separate glass slide, which was then taped to the upper stage. Both surfaces participating in the seal were exposed to oxygen plasma generated with an atmospheric plasma system (Atomflo™ 400L system equipped with an AH-250L head, Surfx Technologies). The system was configured to 100 W RF power, with an oxygen flow rate of 0.03 L min^{-1} and a helium flow rate of 15.0 L min^{-1}. The surfaces were passed three times

under the plasma for about one second each pass. After aligning, the PDMS layers were brought into contact, and then the aligner was flipped upside down so that the entirety of the PDMS membrane could came into contact with the upper layer of PDMS. Note that up to 20 minutes could elapse between the plasma treatment and bringing the PDMS surfaces into contact, and a permanent seal would still form. The glass slide supporting the upper layer of PDMS was released from the upper stage, and then the glass and PDMS layers were placed in an oven set at 70 °C overnight. After the heat treatment, the support ring affixed to the membrane was trimmed away from the remainder of the device, and then the slab beneath the membrane was removed.

The reagent channels were molded in PDMS with a 10:1 ratio of monomer to cross-linking agent by weight. Lateral dimensions of the mold were designed to be 1% larger than required to account for shrinkage. Access holes for the microchannels were punched using a sharpened 20 gauge steel needle. The channels were then reversibly sealed to a glass slide, and the slide was taped to the upper stage of the aligner. The previously assembled layers of the microvalve containing the electrodes were suspended above a featureless silicon wafer in order to properly visualize the features while aligning. Tape was used as a spacer to keep the PDMS from adhering to the silicon. Both surfaces participating in the seal were exposed to oxygen plasma as before, aligned, and brought into contact. Immediately after, the aligner was then flipped upside down, releasing the reagent channels from the spacers and the silicon wafer. A slight vacuum was repetitively applied to the venting channel by tethering a syringe to the inlet of the channel with a piece of tubing, and then withdrawing and reinserting the plunger of the syringe twenty times. This peeled the membrane off the valve seat, which prevented the two components from sealing together permanently. A syringe was tethered to the inlet of the venting channels with a piece of tubing, and then the plunger was withdrawn and reinserted into the barrel twenty times.

Without removing the PDMS components from the glass slide, the device was placed in an oven set at 70 °C overnight to complete the seal. After the heat treatment, the device was removed from the glass.

4.2.2 Characterization of actuation potentials

To characterize the actuation potentials of the microvalves, the venting channel and actuator chambers were filled with fluorinated oil (3M™ Fluorinert™ FC-40). The reagent channels were filled with blue food coloring (Durkee® food coloring; ACH Food Companies, Inc.) Wires were plunged into the electrical contacts for both electrodes, and an electrical potential was applied with a DC power supply (Hewlett Packard model 6209B). The potential was gradually increased (~10 V s^{-1}) until the membrane released from the valve seat and came into contact with the roof of the actuator chamber. The process was repeated at least three times per valve. Four valves with a symmetrically-placed valve seat were tested, and four valves with an asymmetrically-placed valve seat were tested.

4.2.3 Controlling microvalves with portable electrical ancillaries

A custom-designed electrical system was fabricated to control the valves (See Appendix ???). Gold electrical probes were affixed to a chassis for interfacing the elastomer chip. Each probe was aligned with its corresponding PDMS/MWNT electrical contact in the device and then plunged into the polymer. A brass plate was used to clamp the device onto the probes. The device was illuminated with an array of white light emitting diodes suspended between the rows of electrical probes. Channels were filled as described above and the electrical controls were programmed to supply 300 V of potential across the desired probes.

4.3 Results and discussion

4.3.1 Limitations of normally-open electrostatic microvalves

The original design of our actuator employed a normally-open architecture; *i.e.*, the fluid channel was unobstructed without applying an electric potential. Electrodes were embedded both in the membrane and the floor of the microchannel, and if aqueous solutions were flowed through the actuator, they passed through the electric field. Maharbiz *et al.* have reported a design that is similar with respect to the placement of the electrodes (see Figure 1.8c)[1-2]. However, Maharbiz's materials and fabrication methods differ significantly from ours. By incorporating stiff, photo-curable PDMS and thin oxide layers, the researchers were able to minimize the spacing between their electrodes, which in turn reduced the actuation potential of their microvalve to ~15 V. To prevent ions from migrating to the electrode surfaces and screening the electric field, the polarity of the field was switched rapidly.

The electrostatic actuators reported here were simpler to fabricate due to our soft-lithographic approach. However, the actuation potentials required by our system were prohibitively high to interact with aqueous solutions. Potentials greater than 100 V combined with frequencies on the order of 1-10 MHz[4] would necessitate sophisticated electronics. Furthermore, the resulting power and energy storage requirements would adversely affect the portability of the system.

In Chapter 2, I showed that both membrane thickness and valve diameter affect actuation potential more strongly than the Young's modulus of the membrane. By increasing the stiffness of the membrane, I hoped to allow for thinner membranes and wider actuator diameters, which would reduce the actuation potential of the microvalves. I tested two different materials as replacements for the conventional PDMS we used (General Electric RTV 615; Bulk Young's modulus of ~1-10 MPa). The first was the same photocurable PDMS used by Maharbiz *et al.*

(Dow Corning® WL-5150 photodefinable spin-on silicone; bulk Young's modulus of 160 MPa). Second was a photocurable, thiolene-based optical adhesive (Norland optical adhesive; bulk Young's modulus of 930 MPa).

Because the photocurable PDMS was provided in a solvent (mesitylene), it could not be layered. If the liquid precursor were cast onto a cured layer, then the solvent in the precursor would swell the cured layer. Consequently, I used the photocurable PDMS as the initial layer of the membrane, deposited the MWNT electrode, and then encapsulated the electrode with GE RTV 615. However, when I tried to release the upper layers of the actuator from the mold, the membrane consistently tore, most likely due to the brittleness of the photocurable PDMS layer. I attempted to coat the mold with a different surface treatment to aid in the release of the membrane, but molds treated with CYTOP produced the same results.

Thiolene-based elastomers[5] have recently drawn attention in the field of microfluidics for their ability to resist swelling in the presence of solvents that are notoriously incompatible with PDMS[6]. However, I found that a commercially available thiolene material (Norland optical adhesive 60) could not be properly spin-coated onto our molds. The optical adhesive did not adequately wet the silicon substrate, so the polymer precursor either spun off the mold or formed a thin film that eventually beaded up into droplets. Although a number of fabrication strategies have emerged for thiolene-based elastomers[7-9], none of them incorporate spin-coating. Thin layers are most often formed by clamping thiolene precursors between two flat surfaces, which would be difficult to achieve for layers less than 1 μm in thickness. Another difficulty in fabrication often arises from oxygen-quenching of radicals during the photopolymerization process. In summary, no adequate replacement for PDMS was identified.

In parallel with my attempt to address the issue of high actuation potentials, I also sought to address a separate challenge regarding the electrical circuits of our devices. Maharbiz *et al.* incorporated gold films into their microvalve[1-2], which typically have sheet resistances on the order of 1 Ω sq^{-1}. The sheet resistances of our MWNT films were on the order of 1,000 Ω sq^{-1} – too high to accommodate high frequency alternating currents, as explained below.

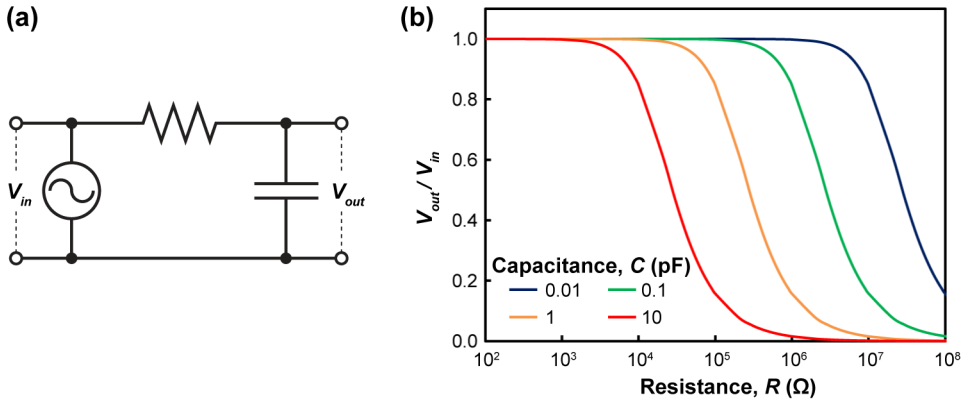

Figure 4.1 (a) An electrical circuit model of the electrostatic actuator (capacitor) driven by an alternating current source. (b) A prediction of the effect of resistance on the potential experienced by the actuator relative to the potential applied by the power source.

Consider an electrical circuit model of the electrostatic actuator illustrated in Figure 4.1. The capacitor represents the electrostatic microvalve. The ratio of the potential across the microvalve, V_{out}, relative to the potential applied by the source, V_{in}, will be as follows:

$$\frac{V_{out}}{V_{in}} = \frac{1/fC}{\sqrt{R^2 + (1/fC)^2}}, \tag{4.1}$$

where f is the frequency of the electric field, C is the capacitance of the electrostatic actuator, and R is the resistance of the circuit leading from the source to the actuator. I approximated the actuator as a simple parallel plate capacitor with capacitance,

$$C = \frac{\pi \varepsilon_{fluid} \varepsilon_0 D^2}{4g}, \tag{4.2}$$

where ε_{fluid} is the relative permittivity of the fluid between the electrodes, D is the diameter of the actuator and g is the distance between the electrodes. Then, using the extreme values of D and g identified from our model presented in Chapter 2 (see Section 2.3.1.6) and the relative permittivity of the oil mentioned previously (3M^{TM} Fluorinert FC-40 oil), I determined that the range of values for the capacitance of the electrostatic actuator would lie between 0.01 – 10 pF. Work by Zavadil *et al.* predicted that in our situation, the minimum frequency of an electric field needed to avoid electrode screening would be 1 MHz (See Section 1.2.4 and Figure 1.9)[4]. Using this value in combination with the range of capacitances identified above, I plotted V_{out}/V_{in} over a range of values for resistance (Figure 4.1b). The plot suggests that for circuits with resistances above 1 MΩ, the potential experienced by the actuator will decrease significantly compared to the potential applied by a source. Even though the charge capacity of the actuator is low, high resistance will prevent charges from saturating the electrodes before they are evacuated by a change in polarity. The resistances of test circuits composed of MWNTs were on average 1 MΩ, showing that we would need different materials to form electrodes.

We investigated several metallic nanoparticles systems as potential replacements for MWNTs. Firstly, we synthesized spherical gold nanoparticles with 10-20 nm diameters. The synthesis was well-established in the literature and easily scaled up[10]. Also, the nanoparticles dispersed fully in aqueous media, so we were able to form thin films of the nanoparticles by vacuum filtration, as we did with MWNTs. However, the films required high particle loadings to achieve conductivity, and more detrimentally, we were unable to transfer films of the nanoparticles to PDMS stamps.

Secondly, we attempted synthesizing gold nanoparticles that had plate-like morphologies. We were able to successfully create hexagonal gold nanocrystals according to a synthetic route

previously reported[11], and unlike the spherical nanoparticles, the hexagonal nanocrystals transferred to PDMS stamps, though not as reliably as MWNT films. A disadvantage of this approach was that reagents were used in low concentrations to favor crystal growth over nucleation. Consequently, the amount of product per batch was lower than with spherical nanoparticles. Also, the hexagonal nanoparticles did not disperse fully into aqueous solutions, making them difficult to process into films.

Finally, we attempted to synthesize gold nanobelts[12], envisioning that the greater surface area compared with spherical nanoparticles would encourage transfer of the nanobelts to PDMS stamps, and also predicting that the large length to width ratio of the nanobelts would enable full percolation at low particle loadings. However, we were unable to achieve high yields of the nanobelts.

4.3.2 Design, fabrication, and characterization of a normally-closed microvalve

Given the difficulty associated with both lowering actuation potentials and decreasing the resistance of the electrodes, I abandoned the normally-open microvalve design. Instead, I opted to develop a normally-closed microvalve, similar in concept to the microvalve reported by Yildirim *et al.* (see Figure 1.8d)[3]. In my design, one electrode was embedded in the membrane as before, but the second was placed on the ceiling of a cavity above the membrane, instead of on the bottom of the microchannel (Figure 4.2). Beneath the membrane, an obstruction was designed into the valve seat such that fluid flow was blocked until the membrane was actuated. By reorienting the electrodes, aqueous fluids were prevented from flowing through the electric field, thereby eliminating the possibility of electrode screening.

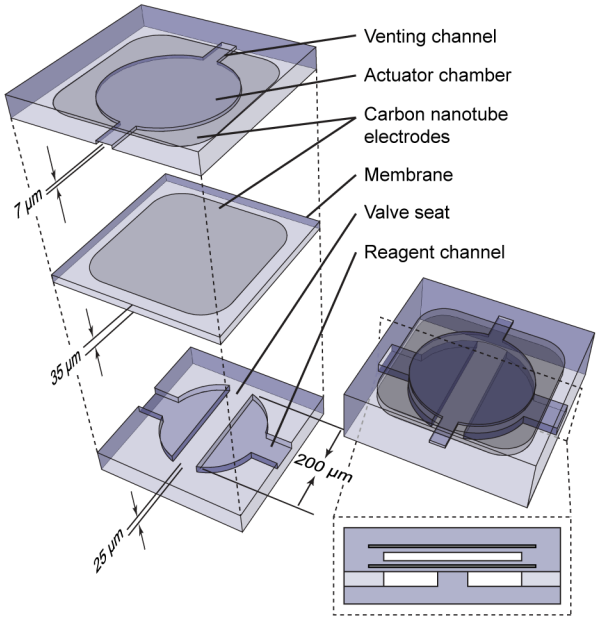

Figure 4.2 An exploded view, a perspective view, and a cross-sectional view of a normally-closed electrostatic microvalve fabricated exclusively with soft-lithographic techniques. Not drawn to scale.

Whereas Yildirim *et al.* constructed their valve from parylene, metal, and oxides using standard microfabrication techniques, I strove to maintain a monolithic architecture composed only of PDMS and MWNTs. I also used soft-lithographic techniques exclusively to accomplish the fabrication.

The fabrication procedure is depicted in Figure 4.3 and is described in detail in the Materials and methods. Briefly, the top electrode was fabricated by spin-coating PDMS over a mold for the actuator chamber. After curing the PDMS, a MWNT electrode was deposited *via* microtransfer printing, and then encapsulated with another layer of PDMS.

The membrane was constructed by spin-coating a mixture of PDMS and hexanes onto a featureless silicon wafer to create a film less than 1 µm thick[13]. A MWNT electrode was then deposited, and the electrode was encapsulated by spin-coating a second layer of PDMS on top. I wanted to orient the thin layer of PDMS in the membrane toward the upper electrode, as this would provide the minimal distance between the electrodes and minimize the actuation potential.

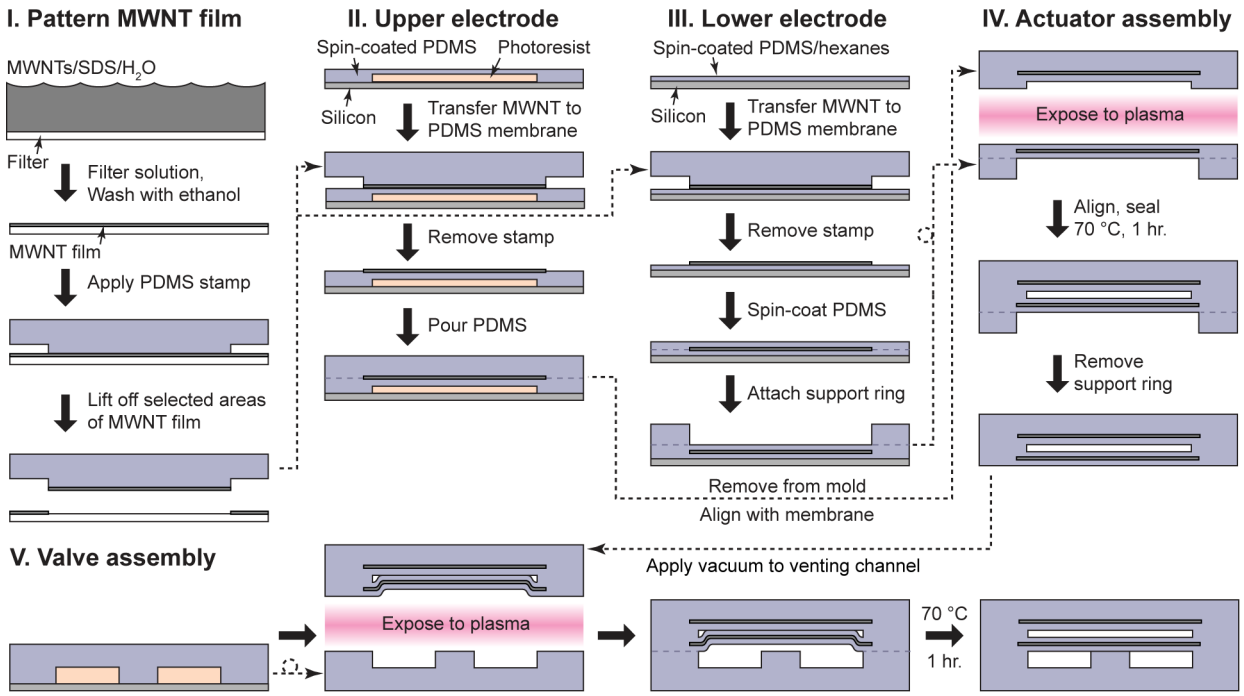

Figure 4.3 An illustration of the fabrication scheme for monolithic, normally-closed electrostatic microvalves using soft-lithographic techniques exclusively.

Because the thin layer was resting directly on the silicon substrate, I attached a ring of PDMS around the periphery of the membrane. Once the membrane was fully cured, I used the ring to help remove the membrane from the silicon and keep it taught. I then placed the membrane on a separate slab of PDMS for further support, making sure not to entrain pockets of air between the membrane and the PDMS slab. I was then able to expose both the upper electrode and the membrane to oxygen plasma, align them, and seal them together.

The reagent channel was molded in PDMS. This layer was ~5 mm thick; the microchannels were ~25 μm deep, and the lateral dimensions were initially designed to be 1.4% larger than intended. When the PDMS was removed from the mold, the layer would shrink slightly due to the thermal expansion coefficient of PDMS. Both this layer and the membrane were exposed to oxygen plasma and then brought into contact. Normally, the membrane also came into contact with the valve seat during this step. This would cause the membrane to seal permanently, thus

rendering the valve useless. To prevent the membrane from sealing, I applied vacuum to the venting channel before bringing the oxidized surfaces into contact so that the membrane would not touch the valve seat. I kept the vacuum applied until the final heat treatment was complete.

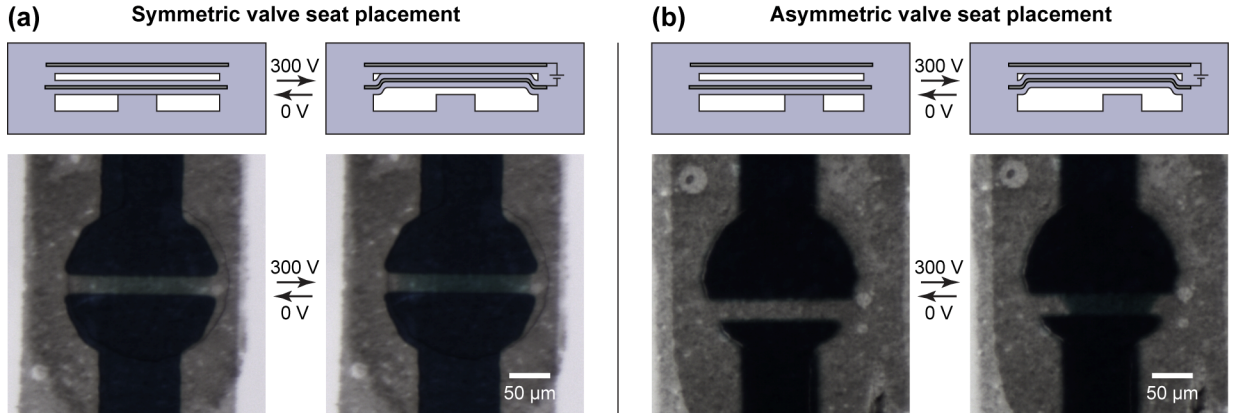

Figure 4.4 Illustrations and micrographs of normally-closed electrostatic microvalves with the barrier of the valve seat placed (a) in the center of the valve chamber, and (b) off-center in the valve chamber.

I characterized a microvalve with a diameter of 200 µm, actuator chamber height of 7 µm, membrane thickness of ~35 µm, and a reagent channel depth of 25 µm. The width of the obstruction in the valve seat was 30 µm. For the case where the obstruction was placed across the center of the valve chamber (Figure 4.4a), the actuation potential was 261 ± 17 V (s.d.). When the obstruction was placed off-center (Figure 4.4b), the actuation potential was lowered to 217 ± 24 V (s.d.). Mohan *et al.* have observed similar trends for normally-closed pneumatic microvalves[14]. Placing the obstruction off-center concentrates stresses on one side of the barrier, thus enhancing crack initiation and propagation. In the case where the barrier is placed in the center, stresses are distributed equally on both edges. I also observed that valves with asymmetric valve seats closed more reliably than valves with the obstruction placed in the middle.

I initially predicted that valves with off-center barriers would be able to withstand pressurization better than the symmetric valves. Külah *et al.*, for instance, showed that

containing pressurized fluid around the periphery by implementing an asymmetric valve seat decreased the load on the membrane, which increased the pressures that could be withstood before leakage. In this study, both symmetric and asymmetric valves could withstand pressures of only several kilopascals. The pressures were too low to accurately distinguish differences between the two designs.

4.3.3 Interfacing microvalves with portable electronic ancillaries

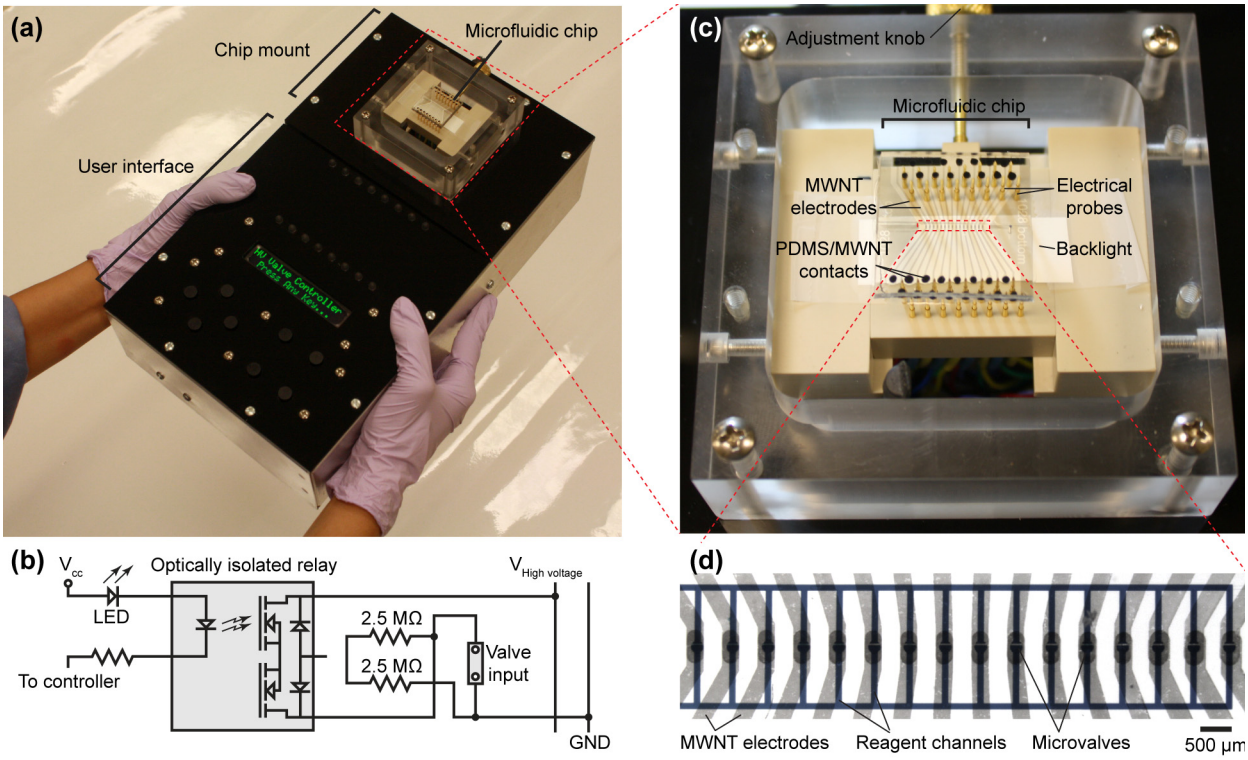

Figure 4.5 (a) A photograph of portable ancillaries for instructing electrostatic microvalves. (b) An electrical circuit diagram of the switching component of the ancillaries. (c) A photograph of the mount used to interface with the microfluidic chip. (d) A micrograph of the microfluidic chip used in this study.

A custom-designed electrical system was constructed to control arrays of normally-closed electrostatic microvalves in a portable format (Figure 4.5a). The system comprised a microprocessor board with program storage, a high voltage switchboard, a mount with arrays of electrical probes to interface with the microfluidic chip, batteries, a battery charger module, a keyboard, a display, and a light emitting diode (LED) array for illuminating the chip. The basic

cellular unit composing the high voltage switchboard is shown in Figure 4.5b. High voltage was generated using a small electronics module (EMCO C06 300VDC power supply), and the voltage was controlled using solid-state relays (Panasonic Electric Works model AQV210E). Passing a current through the LED side of the optically-isolated relay initiated a cascade in the relay that passed high current to the valve. When the current was removed, the switch opened, and residual potential was allowed to bleed off through ~5 MΩ of resistance.

The mount for the microfluidic chip consisted of two arrays of gold contact probes (Spear point; Interconnect Devices, Inc.; Part number 100039-002-958), which were inserted into the PDMS/MWNT electrical contacts integrated on the chip Figure 4.5c). A brass clamp (not shown) was used to press and hold the chip in contact with the spring-loaded pins.

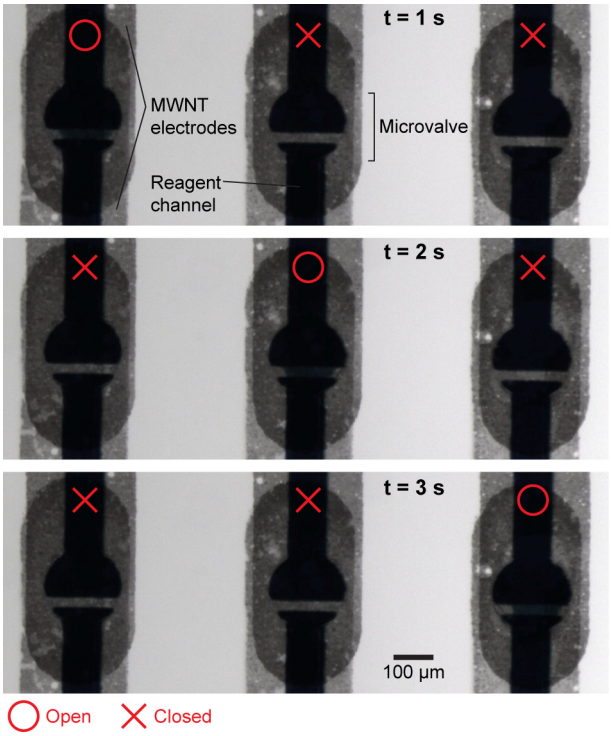

Figure 4.6 A set of three valves activated in sequence with portable electrical ancillaries. The time lapse between states was 1 s.

The initial prototype contained sixteen separate high voltage switches. I designed a test chip containing sixteen independently-operated electrostatic valves (Figure 4.5d) and operated them with the battery-powered ancillaries. Figure 4.6 shows a set of three valves that were actuated consecutively at 1 Hz. The maximum frequency of operation is limited by the physics of the microvalves and not by the electronics. When applying a voltage to the valve, the membrane actuates virtually immediately. The rate-limiting step is the release of the membrane from the roof of the actuator chamber. I was able to operate the microvalves with frequencies up to ~5 Hz, above which the microvalves essentially remained open.

4.4 Conclusions

In this chapter, I demonstrated how aqueous solutions could be directly routed with normally-closed electrostatic microvalves, avoiding many of the challenges encountered with normally-open electrostatic microvalves. I interfaced an array of the polymer-based microvalves with portable electronic ancillaries, which to the best of my knowledge is the first demonstration of such a system.

Currently, the prototype of the ancillaries can operate up to eight hours continuously (without the LED backlight operating). However, future designs could be easily designed to operate more efficiently. Many of the system components were not optimized for energy efficiency. For instance, an LED array was used to signal whether high-voltage switches were on or off. While not necessary, this display was useful for preliminary studies. Additionally, only two battery packs were integrated into the system, while room was available to incorporate more. A second generation design could easily provide the same functionality in half as much space with double the usage time. These ancillaries would also be compatible with the electrostatic actuators shown in Chapter 3.

4.5 References

1. T. Bansal, M.-P. Chang and M.M. Maharbiz, "A class of low voltage, elastomer-metal 'wet' actuators for use in high-density microfluidics" *Lab on a Chip,* 2007, 7, 164-166.

2. M.-P. Chang and M.M. Maharbiz, "Electrostatically-driven elastomer components for user-reconfigurable high density microfluidics" *Lab on a Chip,* 2009, 9, 1274-1281.

3. E. Yıldırım, M.A.S. Arıkan and H. Külah, "A normally-closed electrostatic parylene microvalve for micro total analysis systems" *Sensors and Actuators A: Physical,* 2012, 181, 81-86.

4. T.L. Sounart, T.A. Michalske and K.R. Zavadil, "Frequency-dependent electrostatic actuation in microfluidic MEMS" *Journal of Microelectromechanical Systems,* 2005, 14, 125-133.

5. B.T. Good, S. Reddy, R.H. Davis and C.N. Bowman, "Tailorable low modulus, reversibly deformable elastomeric thiol–ene materials for microfluidic applications" *Sensors and Actuators B: Chemical,* 2007, 120, 473-480.

6. Z.T. Cygan, J.T. Cabral, K.L. Beers and E.J. Amis, "Microfluidic Platform for the Generation of Organic-Phase Microreactors" *Langmuir,* 2005, 21, 3629-3634.

7. L.-H. Hung, R. Lin and A.P. Lee, "Rapid microfabrication of solvent-resistant biocompatible microfluidic devices" *Lab on a Chip,* 2008, 8, 983-987.

8. C.F. Carlborg, T. Haraldsson, K. Oberg, M. Malkoch and W. van der Wijngaart, "Beyond PDMS: off-stoichiometry thiol-ene (OSTE) based soft lithography for rapid prototyping of microfluidic devices" *Lab on a Chip,* 2011, 11, 3136-3147.

9. M. Natali, S. Begolo, T. Carofiglio and G. Mistura, "Rapid prototyping of multilayer thiolene microfluidic chips by photopolymerization and transfer lamination" *Lab on a Chip,* 2008, 8, 492-494.

10. I. Hussain, M. Brust, A.J. Papworth and A.I. Cooper, "Preparation of acrylate-stabilized gold and silver hydrosols and gold−polymer composite films" *Langmuir,* 2003, 19, 4831-4835.

11. Y.N. Tan, J.Y. Lee and D.I.C. Wang, "Aspartic acid synthesis of crystalline gold nanoplates, nanoribbons, and nanowires in aqueous solutions" *The Journal of Physical Chemistry C,* 2008, 112, 5463-5470.

12. J. Zhang, J. Du, B. Han, Z. Liu, T. Jiang and Z. Zhang, "Sonochemical formation of single-crystalline gold nanobelts" *Angewandte Chemie,* 2006, 118, 1134-1137.

13. A. Thangawng, R. Ruoff, M. Swartz and M. Glucksberg, "An ultra-thin PDMS membrane as a bio/micro–nano interface: fabrication and characterization" *Biomedical Microdevices,* 2007, 9, 587-595.

14. R. Mohan, B.R. Schudel, A.V. Desai, J.D. Yearsley, C.A. Apblett and P.J.A. Kenis, "Design considerations for elastomeric normally closed microfluidic valves" *Sensors and Actuators B: Chemical,* 2011, 160, 1216-1223.

Chapter 5
Concluding remarks

5.1 Summary

In Chapter 1 of this dissertation, I laid out the current state of the art in instructing valve-based microfluidic systems. I demonstrated that current systems are severely limited in terms of portability, although portable systems are most urgently needed to address society's need for point-of-care analytical systems. Then, recognizing the importance of *simplicity* in achieving truly transformative technology, I set out to incorporate electrostatic actuation principles into the design of simple membrane-based actuators. Informed by the mathematical model developed in Chapter 2, I developed a soft-lithographic fabrication procedure to produce electrostatic actuators made entirely from PDMS and MWNTs. Due to challenges encountered with electrode screening, I first developed a strategy to *indirectly* control the flow of aqueous solutions by coupling the electrostatic actuators with pneumatic actuators, reported in Chapter 3. Then, in Chapter 4, I developed a normally-closed microvalve design that was capable of *directly* interacting with aqueous fluids. Furthermore, I was able to control the microvalves with battery-operated electrical ancillaries, demonstrating a fully portable microfluidic system.

5.2 Comparison between electrostatic approaches

In one sense, the results presented here move in a linear fashion from the basic pneumatic microvalve design, and then to the intermediate, hybrid pneumatic-electrostatic system, and then ultimately to the fully electrostatic design. This perspective, however, overlooks what I view as a high degree of complementarity between the two electrostatic approaches. I would like to

summarize some salient characteristics of both strategies so that others will be able to decipher which approach is most relevant for their particular application. These characteristics are summarized in Table 5.1.

Table 5.1 Comparison between microfluidic pressure-amplifier circuits and normally closed electrostatic microvalves.

Characteristic	**Actuator**	
	Microfluidic pressure-amplifier circuit	Normally-closed microvalve
Indirect interaction with aqueous fluids	✓	
Direct interaction with aqueous fluids		✓
Normally-open microvalves	✓	
Normally-closed microvalves	✓	✓
Accommodates high pressure	✓	
Pressure source not required		✓
No hydraulic fluid leakage		✓
Portable ancillaries	✓	✓

One of the most important questions from a design point of view is whether the application requires significant pressures to generate flow or obstruct flow. For instance, applications where fluids are mixed only by diffusion might merely require a gate to segregate fluids until mixing is required[1]. These applications would be highly suited for the normally-closed electrostatic microvalves. On the other hand, certain applications may require convective mixing of highly viscous reagents, which could easily require pressures greater than several kilopascals[2]. In this case, the normally-closed design will be insufficient, although the microfluidic pressure-amplifier circuits could generate such pressures.

The pressure-amplifier circuits also benefit from the flexibility of adopting either normally-open or normally-closed configurations. As shown in Section 3.4.2, the number of electrical inputs needed for binary-tree microfluidic multiplexers is minimized as a result of this flexibility.

Also, pressure-amplifier circuits can be used to instruct other pneumatic microfluidic components other than microvalves. Components such as biologically-inspired grippers[3], particle guides[4], etc. could also be integrated with the pressure-amplifier circuits.

The advantages of the normally-closed electrostatic actuators are highlighted in applications where size constraints are important. The footprint of a normally-closed valve is much smaller than that of an entire pressure-amplifier circuit, and the normally-closed valve does not require an external pressure source or reservoir of hydraulic fluid.

In all likelihood, many applications will need to integrate both approaches to achieve the greatest degree of functionality.

5.3 Future directions

In terms of future work, several aspects seem particularly imperative. Firstly, although the materials reported here were chosen for ease of fabrication, they are not necessarily ideal for a number of applications. As mentioned before, PDMS swells in the presence of many solvents[5]. Also, the soft-lithographic approach presented here may not be suitable for mass manufacturing. Ideally, a transition to other elastomers and fabrication processes should be undertaken. Others have investigated a number of intriguing replacements for PDMS, including thermoplastic elastomers[6-8]. These can be processed with methods widely adopted in manufacturing processes, such as injection molding and hot-embossing[9]. One would hope that these materials could be easily incorporated into the design for the electrostatic actuators as well.

Another aspect of the actuators that could use immediate improvement is the interfacing between ancillaries and the electrodes. As it stands, the deposition of PDMS/MWNT electrical contacts on the device is a somewhat crude process. Also, a standardized format would make the technology more accessible to a wider user-base.

Finally, integrating the actuators into a relevant application would surely shed light on improvements that could be made. Likely, much work will also need to be done on engineering the electrical components of the system to both accommodate the electrostatic actuators and any other components that are needed for analysis. By itself, the study of miniaturized optical detection methods is a burgeoning field[10-11], and now is an exciting time when so many analytical components are being reported in compact, portable formats. The next step is to integrate the components to create impactful systems that can serve society.

5.4 References

1. B.R. Schudel, C.J. Choi, B.T. Cunningham and P.J.A. Kenis, "Microfluidic chip for combinatorial mixing and screening of assays" *Lab on a Chip,* 2009, 9, 1676-1680.

2. S.L. Perry, G.W. Roberts, J.D. Tice, R.B. Gennis and P.J.A. Kenis, "Microfluidic generation of lipidic mesophases for membrane protein crystallization" *Crystal Growth & Design,* 2009, 9, 2566-2569.

3. F. Ilievski, A.D. Mazzeo, R.F. Shepherd, X. Chen and G.M. Whitesides, "Soft robotics for chemists" *Angewandte Chemie,* 2011, 123, 1930-1935.

4. S.E. Chung, W. Park, S. Shin, S.A. Lee and S. Kwon, "Guided and fluidic self-assembly of microstructures using railed microfluidic channels" *Nat Mater,* 2008, 7, 581-587.

5. J.N. Lee, C. Park and G.M. Whitesides, "Solvent compatibility of poly(dimethylsiloxane)-based microfluidic devices" *Analytical Chemistry,* 2003, 75, 6544-6554.

6. E. Roy, M. Geissler, J.-C. Galas and T. Veres, "Prototyping of microfluidic systems using a commercial thermoplastic elastomer" *Microfluidics and Nanofluidics,* 2011, 11, 235-244.

7. D. Brassard, L. Clime, K. Li, M. Geissler, C. Miville-Godin, E. Roy and T. Veres, "3D thermoplastic elastomer microfluidic devices for biological probe immobilization" *Lab on a Chip,* 2011, 11, 4099-4107.

8. E. Roy, J.-C. Galas and T. Veres, "Thermoplastic elastomers for microfluidics: Towards a high-throughput fabrication method of multilayered microfluidic devices" *Lab on a Chip,* 2011, 11, 3193-3196.

9. H. Becker and C. Gärtner, "Polymer microfabrication methods for microfluidic analytical applications" *Electrophoresis,* 2000, 21, 12-26.

10. D. Brennan, J. Justice, B. Corbett, T. McCarthy and P. Galvin, "Emerging optofluidic technologies for point-of-care genetic analysis systems: a review" *Analytical and Bioanalytical Chemistry,* 2009, 395, 621-636.

11. D. Psaltis, S.R. Quake and C. Yang, "Developing optofluidic technology through the fusion of microfluidics and optics" *Nature,* 2006, 442, 381-386.